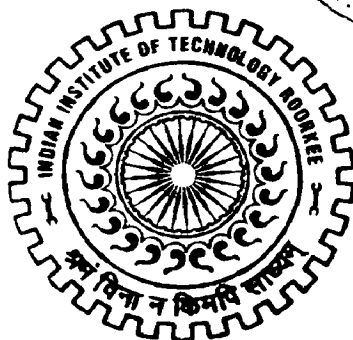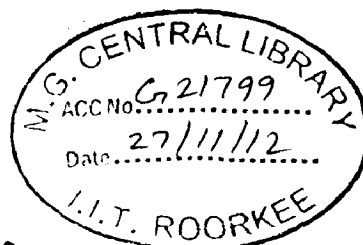# DEVELOPMENT OF NANOCOMPOSITE COATINGS FOR ORTHOPAEDIC IMPLANTS BY MAGNETRON SPUTTERING

A DISSERTATION

*Submitted in partial fulfillment of the
requirements for the award of the degree
of*

MASTER OF TECHNOLOGY
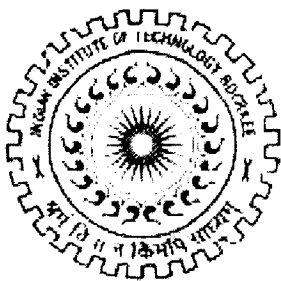
in

NANOTECHNOLOGY

By

SHREYA GOEL

CENTRE OF NANOTECHNOLOGY
INDIAN INSTITUTE OF TECHNOLOGY ROORKEE
ROORKEE-247 667 (INDIA)
JUNE, 2012

Indian Institute of Technology Roorkee

Centre of Nanotechnology

CANDIDATE DECLARATION

I hereby declare that the work being presented in this Dissertation titled "Magnetron Cosputtered ZnO:TiO$_2$ Composite Coatings for Orthopaedic Implants", submitted in partial fulfillment of the requirement for the award of degree of Master in Technology with specialization in Nanotechnology is an authentic record of my own work carried out from August 2011 to June 2012, under the guidance of Dr. R. Jayaganthan and Dr. Ramesh Chandra.

The matter embodied in this dissertation has not been submitted for the award of any other degree.

Date: June 14, 2012

Place: Roorkee
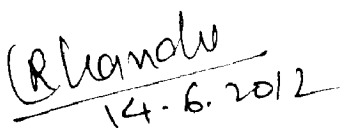
(Shreya Goel)

This is to certify that the statement made by the candidate is correct to the best of my knowledge.

Dr. R. Jayaganthan.

Associate Professor

Department of Metallurgical and Materials Engineering

Indian Institute of Technology Roorkee.

14. 6. 2012

Dr. Ramesh Chandra,

Associate Professsor,

Institute Instrumentation Centre,

Indian Insitute of Technology Roorkee.

ii

Acknowledgement

"Give me a fruitful error any time, full of seeds, bursting with its own corrections. You can keep your sterile truth for yourself". ~ *Vilfredo Pareto*

My dissertation towards the completion of my M.Tech degree at IIT Roorkee has strengthened my faith in Pareto's statement all the more. I would rather tackle a problem, hypothesize and solve a scientific predicament than accept the *status quo*. This thesis is the end of my journey in IIT Roorkee, a journey which has given me erudite teachers, valuable friends and great colleagues, who made this possible and an unforgettable experience.

First and foremost, I would like to express my sincere gratitude and humble regards to my guides and mentors, Dr. R. Jayaganathan, Associate professor, Department of Metallurgical and Materials Sciences and Dr. Ramesh Chandra, Associate Professor and Head, Institute Instrumentation Centre, IIT Roorkee, for their valuable guidance and unfailing support, during the entire course of this project.

I thank all my teachers, who've taught me through these two years, without whose expert guidance, it would not have been possible for me to grasp the nuances of such an intricate subject as Nanotechnology.

I also extend my thanks to all the staff members of Institute Instrumentation Centre and Centre of Nanotechnology, IIT Roorkee, who have always gone out of their way to help students like me, as and when required, during the course of the project.

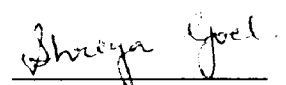I take this opportunity to acknowledge Dr. A.B. Pant, Indian Institute of Toxicology Research, Lucknow and Dr. S.D. Sharma, Hindustan Bioenergy Ltd, Biotech Park Lucknow, for being kind enough to let me carry out a part of my thesis in their labs and providing me all the facilities, as and when needed by me.

Dated: Shreya Goel

Abstract

Orthopaedic implants and prosthetic devices form an imposing bulk among the invasive surgeries performed round the world today. In 1980, biomedical implants were a viable option for patients in need of joint replacement, but the orthopaedic marketplace was unable to create a strong, permanently fixed, cementless implant. As a result of the demand for a better implant, several strategies were adopted and technologies applied to develop an implant which can flawlessly integrate with the surrounding tissue and the developing bone. Most of these efforts were directed at the level of implant surface or implant-tissue interface. Coatings have been designed in an effort to impart the implants with superior osseointegrative and antimicrobial abilities. Drug incorporated or hydroxyapatite coated surfaces and combination of these have become popular. However, with increasing instances of instability and delamination of such coatings from the surface of the implants and reports of antibiotic resistance among microorganisms, especially those responsible for post-operation infections in orthopaedic devices, has resulted in newer and more sophistaicated technology being put to use. A novel approach would be to combine inorganic compounds with superior biocompatibility and antibacterial powers. Titanium oxide is a biocompatible and bioactive compound, capable of inducing the formation of apatite, when immersed in physiological fluid. Zinc oxide, besides the importance of zinc ions in the formation of bone and teeth, is also a potent antimicrobial. Thus, a composite coating of these can provide a plausible solution to the problems faced by the orthopaedic implants of the present day.

The present work aims at the development of a bioactive, biocompatible and antimicrobial coating for orthopaedic implants and prostheses. This has been accomplished by reactive magnetron cosputtering of titanium and zinc oxides, to form thin films on silicon substrates, which were then investigated for their microstructural, morphological and biological properties.

v

TABLE OF CONTENTS

CONTENTS   **PAGE NO.**

Chapter 1: Introduction

Chapter 2: Synthesis and Characterization Techniques

Chapter 3: Synthesis and Characterization of Titania Coatings

List of Figures

List of Tables

List of Abbreviations

Abbreviation	Full Name
AFM	Atomic Force Microscopy
CaP	Calcium Phosphate
CFU	Colony Forming Units
DC	Direct Current
DSA	Drop shape Analysis
EDX/ EDS	Dispersive X-Ray Spectroscopy
FESEM	Field Emission Scanning Electron Microscopy
FBS	Foetal Bovine Serum
FWHM	Full Width Half Maximum
GA-XRD	Glancing angle X-Ray diffraction
H-Ap	Hydroxyapatite
HBSS	Hank's Balanced Salt Solution
ICP-MS	Inductively Coupled Plasma-Mass spectroscopy
JISZ2801	Japanese Industrial Standard Z2801
MEM	Minimum Essential Medium
MTT	3-(4,5-dimethylthiazol-2-yl)-2,5-diphenyltetrazolium bromide
NADH	Nicotinamide adenine dinucleotide
NADPH	nicotinamide adenine dinucleotide phosphate
PBS	Phosphate Buffered Saline
PPM	Parts Per Million
RMS	Root Mean Square

SAED	Selected Area Electron Diffraction
SBF	Simulated Body Fluid
SEM	Scanning Electron Microscopy
TEM	Transmission Electron Microscope
THR	Total Hip Replacement
TKR	Total Knee Replacement
XRD	X-Ray Diffraction

Chapter 1

Introduction

1.1 Introduction to nanostructured coatings

Nanostructured materials may be defined as those materials whose structural elements— clusters, crystallites or molecules—have dimensions in the 1 to 100 nm range Nanomaterials such as thin films and engineered surfaces have been developed and applied across a wide range of industries for decades. A **thin film** is a layer of material ranging from fractions of a nanometer (monolayer) to several micrometers in thickness.[iii] The ability of controlling surface coatings at the nanoscale is of paramount importance for a large-scale industrial development of nanotechnology. Highly sophisticated surface-related properties, such as optical, magnetic, electronic and catalytic can be obtained via nanostructured coatings. The global market for nanostructured coatings and thin films in 2011 was estimated to be approximately $227.5 million dollars, growing to over $1.4 billion by 2016. "One way" coating systems based on nanomaterials make up the bulk of this market, for example in anti-bacterial; protective and conductive coatings. The fastest growing markets to 2016 will be in interior and exterior household protection, textiles and medical markets, driven by the increased demands for protective and repellent coatings. [1]

The coatings industry is a major industry in the United States and worldwide. Coatings are needed to prevent wear, erosion, and corrosion, and to provide thermal insulation. For both commercial and military applications there is a need for coatings with improved durability and performance. Nanostructured coatings show promise based on initial laboratory trials. Durability improvements of 3 to 5 times can be projected for a number of coating applications. It will be necessary to demonstrate the technical and economic viability of these coatings on a commercial scale. To accomplish demonstration and implementation of this

technology in a timely, cost-effective manner, a disciplined concurrent engineering approach

is recommended. [i]
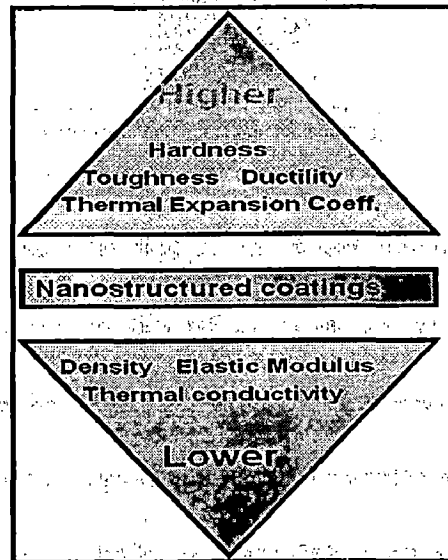
Figure 1: Nanostructured materials: Potential Benefits

The wide spectrum of inorganic thin films can be divided into two categories: active and

passive, depending on their function in a structure or a device. Passive films are coatings

used for cosmetic purposes, or for protection against deleterious chemical reactions, wear etc.

They do not, however, serve a specific catalytic or electronic role. Technologically important

passive thin films include metal carbides and nitrides, used as hard wear resistant coatings,

metal coatings for chemically inert and decorative finishes and oxides as insulators and

diffusion barriers. Electronically and chemically active thin films are used in

microelectronics, sensors and other devices. As examples, alternating thin films of GaAs and

AlGaAs are key components of lasers and optical devices, while ZrO_2 thin films are the

chemically selective components of O_2 sensors. [2]

From the point of view of physics, a *surface* may be defined as "the sudden interruption of

the atomic arrangement". This sudden interruption results in differences between surface and

bulk electronic properties, leading to different physico/chemical behavior between the two

regions of the material. Therefore, from a theoretical standpoint, different modification methods utilized for implant surface engineering may lead to different and unique surface properties [3]
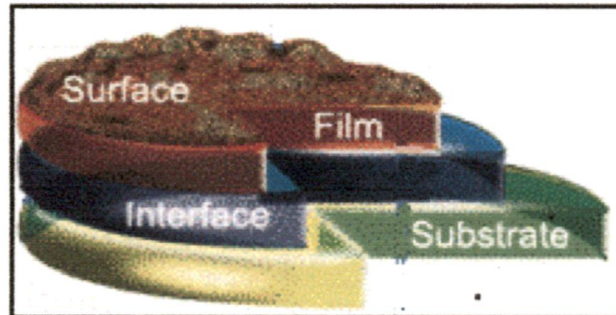
Figure—Schematic of a thin film- substrate system

These different physico/chemical properties can potentially lead to changes in the host-to-implant response. New surface treatments should be tested as new biomaterials. As examples, the alteration of surface topography or the incorporation of bioactive ceramics as coatings have been investigated and utilized on a large scale by implant dentistry practitioners with no or limited surface characterization.[4] The ideal property of orthopaedic or dental implants used to replace missing or diseased bones or teeth is long-term stability. Strategies to accomplish this are based on (1) *enhancing osseointegration* (bone bonding) and (2) *preventing microbial infection* that could cause implant loosening or failure. Combining these two strategies is the challenge toward developing the ideal implant.

1.2 Introduction to Biomedical Coatings

During the past three decades, major advances have been made in developing biomedical materials for use as bone replacements. The first such biomaterials to be developed were tolerated in the physiological environment but were metallic in nature and lacked the ability to encourage bone apposition. As a consequence of this, Hulbert et al. introduced a stable oxide layer on the metallic surfaces in order to activate bone growth [5]. Materials employed

in the manufacture of orthopaedic and dental implants include metals and metal alloys, ceramics, polymers, and composites (e.g., metal/metal ceramic/ceramic, metal/ceramic, and ceramic/polymer). The different metals and metal alloys employed in the commercial manufacture of orthopaedic and dental implants include cobalt–chromium–molybdenum (Co–Cr–Mo) alloy, stainless steel, commercially pure titanium (cpTi), Ti alloy (Ti6Al4V), tantalum [6].

Biomaterials for orthopaedic and dental implants and coatings should meet certain criteria. First of all, they must be *biocompatible and bioinert,* or able to function *in vivo* without eliciting any intolerable immunological response in the body, either locally or systemically. On the other hand, those appropriate biomaterials must be able to withstand the often hostile environment of the body, and show better properties, such as *resistance to corrosion* and degradation, such that the body environment does not adversely affect material performance over the implant' s intended performance lifetime. Furthermore, adequate **mechanical** **properties,** such as *tensile/compressive strength, elastic modulus, good thermic and electric insulation* and *fatigue endurance,* are also critical criteria for the selection of biomaterials to be used as devices intended to replace or reinforce load-bearing skeletal structures. In addition, they must be capable of *reproducible fabrication* and in *desired geometric shapes* to the highest standards of quality control at, of course, a *reasonable cost.* Biomaterials that meet these criteria are fundamental to the practice of orthopaedic surgery and to ensuring the success of implantation [7]. Ideally, a successful orthopaedic or dental implant should have a *long-term skeletal fixation* with the host bone and be free of later complications, especially *resistant to microbial infection.* A considerable number of investigations have focused on

modifying the implant surface, to enhance bone contact or bone anchorage, defined as *osseointegration* [8, 9].

All the above-mentioned conditions are incorporated into the following terms: ***biocompatible, bioinert, and biofunctional***. These properties fill up the ultra thin coating (ultra thin films or nanofilms) as it is expected that ultra thin coatings represent a biophysical system with few free electrons and then the mechanic oscillations of atoms must be smothered.
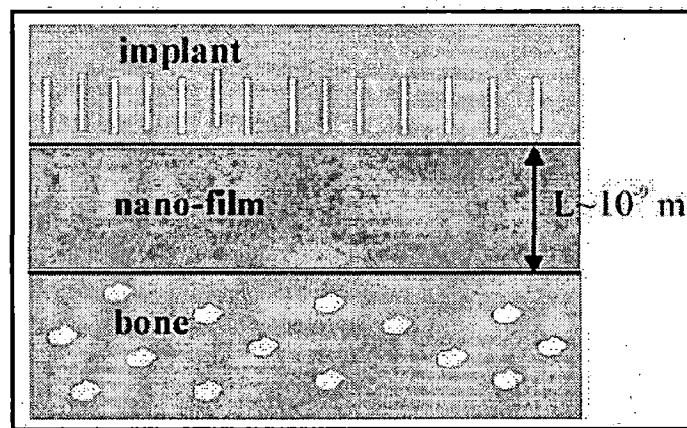
Figure 1.3: Model of nanofilm layer (adapted from [10])

The nano coat should prevent the direct contact between implant and bone. Biomaterials and biomechanical properties are of fundamental importance for the success or failure of dental implants. Biomaterials are "biological substituents" from which "biological spare parts" can be produced. Biomaterials must not act as an antigen but should successfully induce osteogenesis. Over the past sixty years, research has been carried out on the biomaterials and biomechanical design for surgical implants. The result of this research was the discovery that a wide spectrum of materials can replace living tissues, and among those dental implants take one of the more important places on a scale.

In proportion to biochemical electro-chemical interaction of vital tissue and non-vital material, all biomaterials, according to Osborne or according to the level of biocompatibility, can be divided to:

— *Biotolerant materials* (Co, Cr, Mo-alloys, Fe, Cr, Ni-alloys, PMMA)

— *Bioinert materials* (titan CP, tantalum, bioceramics)

— *Bioactive materials* (hydroxapatite, Ca-phosphates) [10].

1.2.1 Osseointegration

The term "osseointegration" was originally introduced by Brannemark (1977) [11], to describe "a close implant–bone contact at the light microscopic level." Such a histological bone-implant contact is considered the prerequisite for implant loading and is critical for initial fixation and long-term clinical success of endosseous dental and orthopedic implants.[12] To achieve secure osseointegration, seven factors must be recognized, depicted schematically in the figure 1.4. The properties affecting the implant surface and hence its interaction with the physiological surroundings are also depicted in figure1.4.

In addition, osseointegration may fail to occur in the absence of primary stability and limitation of micromotion of the implant during healing. To enhance osseointegration, several surface modifications have been developed especially for dental implants. [9]. These modifications can be classified into two general categories:

I. Surface treatments to modify topography and

II. Deposition of bioactive surface coatings, such as by deposition of calcium phosphate coatings.
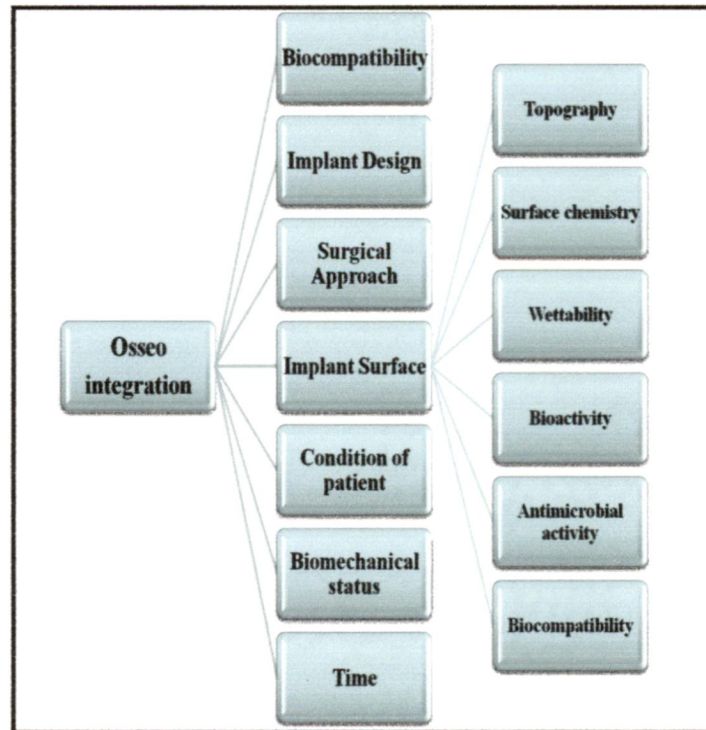
Figure1.4: Factors affecting Osseointegration and Implant surface properties of a bone-implant system

Periods of nonfunctional loading of 3 months are needed for patients with orthopaedic or dental porous implants. Due to the growing demand by patients and health practitioners for faster osseointegration periods, surface modifications of surgical implants have been widely studied. The surface treatments, such as calcium phosphate (Ca-P) coatings, modify both the surface chemistry and topography. The nucleation and growth of Ca-P crystals on implants enhance surface bioactivity by making a chemical bond between the Ca-P film and substrate, which maintains the Ca-P coating and implant fixation. In vivo, a direct bone contact has been observed at the bone–implant interface, without the intervention of a fibrous tissue. This bone apposition is the result of surface calcification of implants due to the super saturation of simulated body fluid (SBF) solutions and titanium surface properties. Several techniques have been applied for the deposition of hydroxyapatite (Hap) coatings such as plasma spray, the most commercially used. However, some techniques run at high temperatures, resulting

in damage to the metallic substrate. A so-called biomimetic process has been developed, and it is based on the heterogeneous nucleation of Ca-P from SBF. Furthermore, biomimetic method reveals the material biocompatibility as it shows the Ca-P formation in vitro. The advantages compared with other coating processes are low process temperature, used in heat sensitive material, production of bioactive bone-like apatite crystals, deposition on and into porous surfaces without affecting the pore morphology, and good film adhesion on substrate [13]. In hard-tissue implants, such as an artificial hip or knee joint, the issue is acceleration of healing to reduce immobilization time for surgery patients. Thus, the role of the coating is to induce bone cell attachment and proliferation on the implant surface.

Immediately after implant placement, a series of events occur between the host and the surface of the implants. [4] The initial host response after implantation is similar to a common bone wound modified by the presence of the implant. When an implant is inserted into a pre-drilled cavity, the blood clot comes into contact with the implant surface and fills the gap between the implant and bone, and then proteins are adsorbed from the blood and tissue fluid. Tissue healing around the implant starts with an inflammatory response. Within the first few days after implantation, mesenchymal cells, pre-osteoblasts, and osteoblasts migrate to colonize the implant surface to produce an extracellular matrix and start mineralization. The reactive new bone formation at the implant-host bone interface consists of three categories of osteogenesis: at the implant surface (contact osteogenesis), within the surgical microgap at sites of neovasculization, and the surgical host bone margin (distance osteogenesis). Three unique environments for the osteoblastic cell can be envisioned; each environment may confer different biologic behaviour to the cells. In other words, the new bone formation can proceed from the host bone to the implant surface and from the implant

surface to the host bone, thereby gradually sealing the gap and causing device integration. As such, surface features that may influence any or all of these rates of bone formation will have the potential to enhance osseointegration. [14]. Because of the dynamic nature of the bone-biomaterial interface as a function of implantation time, endosseous implant biomaterials must have short- and long term biocompatible and biofunctional properties[15]

1.2.2 Antimicrobial activity

For implant materials, the interface biomaterial surface-surrounding tissue represents the real ground where the battle takes place and where accidental contamination can first develop into colonization and, subsequently, into the establishment of a clinically relevant infection. Bacterial adhesion and anchorage on prosthetic surfaces represent an initial crucial step in this process. Figure 1.5
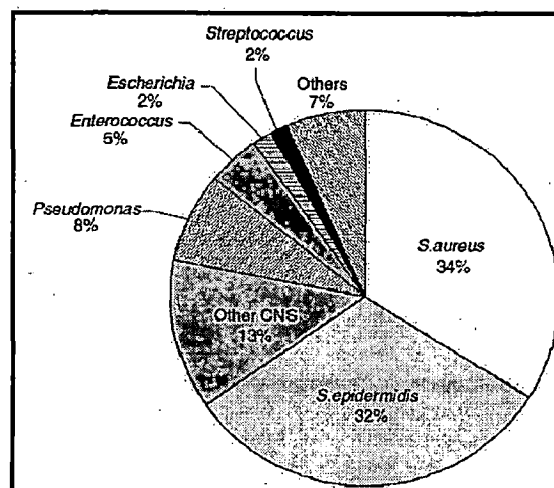
Figure 1.5: Frequency of main pathogenic species among orthopedic clinical isolates of implant-associated infections.(adapted from [16])

Given that current prosthetic bulk materials have already reached best achievable biomechanical performances, the most convenient way to interfere with the early phases of microbial adhesion is a modification of the chemistry or the micro/nanotopology of the out-layer of the device [16]. The numerous possibilities of superficial chemical modifications

include the coating of the device with surfactants [17], proteins such as albumin [18], hydrophilic negatively charged polysaccharides such as hyaluronan and heparin [19, 20], with the scope to generate adhesion resistant or even bacteria repellent surfaces [21]. Peri-operative systemic antibiotics diffuse from the vascular system and blood irrigated tissues to the interface with the implant, at last reaching the material surface. Vice versa material coatings with sustained release of disinfectants, bacteriostatic drugs or antibiotics, reach critical concentrations of active substances directly at the interface of the implant and may even prevent contamination during handling of the implant device. In the long list of the bioactive material surfaces, there are coatings able to release metals, especially zinc, copper and silver ions [22-24], disinfectants such as chlorhexidine or other bactericidal chemicals such as nitric oxide, various antibiotics including gentamicin, minocyclinerifampin, teicoplanin, cefazolin, vancomycin [25,]. Up to now some of these drug-delivering coatings have already demonstrated to be actively preventing infections in vivo and they are currently used especially in critical conditions at high risk of infection development.

In orthopedics as in many other medical fields the vast majority of post-surgical infections is associated to the presence of implant materials, which represent a site of weakness for the host defenses where even bacteria with a low level of virulence can easily establish. Given the enormous and steadily growing diffusion of patients with implant materials a successful control of the rate of postsurgical infections is mandatory. While many past efforts in this direction have mostly relied on containment of environment and personnel contamination and use of perioperative systemic antibiotics, new parallel emerging strategies are currently focussing on reducing the intrinsic vulnerability of the implant materials to microbial colonization. This field of technological innovation represents a main objective in the

orthopedic field, at least equally important as the improvements in terms of biocompatibility of the implant materials. [16]

1.2.3 Biocompatibility

Materials used in medical devices, particularly in those applications in which the device either contacts or is temporarily inserted or permanently implanted in the body, are typically described as biomaterials and have unique design requirements. The National Institute of Health Consensus Development Conference of November 1982 defined a biomaterial as "any substance (other than a drug) or combination of substances, synthetic or natural in origin, which can be used for any period of time, as a whole or as a part of a system which treats, augments, or replaces any tissue, organ, or function of the body". The sterilized device, and by default, the materials of which it is constructed, need to meet basic biocompatibility requirements, generally as defined by the ISO 10993 standards, to be nontoxic, nonthrombogenic, noncarcinogenic, nonantigenic, and nonmutagenic.[27] The material's form and size, how it interfaces with the body, and its required duration of use will determine its required properties. One material property alone is unlikely to lead to a successful and durable device, whereas a lack of a single key property can lead to failure.

Coatings for improved biocompatibility and as carriers for drug delivery have an increasingly important role. Bioactive materials, which tend to use the nature of natural material or mimic natural materials, have applications in orthopedic implants to enhance bone attachment, antimicrobials to mitigate infection, and antithrombotics to mitigate thrombus. The phenomena controlling the bioresponse are basically wound healing in the presence of a sterile medical device. The outcome of this healing process can have profound implications on the success of a device and can depend on material properties such as texture, crystallinity,

wettability, surface chemistry, cytotoxic leachables, and degradation products. [28, 29] These properties determine primarily the interaction between the materials and proteins in the biological environment, and subsequently, the interactions with the cells and tissues. The biologic response to materials, e.g., inflammation and thromboresistance, is an important consideration in the design of medical devices. Chronic inflammatory responses resulting in a thick fibrous capsule and the persistence of white cells, is undesirable and can lead to damage to surrounding tissue and to failure of the device. Leachables can cause local cytotoxicity and result in inflammation. Hypersensitivity reactions can occur to corrosion products and residual monomers, plasticizers, additives such as antioxidants, and degradation products. Cytotoxic leachables and degradation products, which may exhibit systemic effects if the dose is high, may result from the fabrication and sterilization methods used as well as ambient degradation by processes such as hydrolysis and oxidation over time. [30] Contamination by bacteria, endotoxins (the breakdown products of gram-negative bacteria), and particulate debris can have profound effects on inflammatory responses. These responses are generally a matter of handling, processing, and minimizing wear and corrosion in vivo. The lack of bacteriological contamination can be designated as an incoming requirement on materials from a vendor; however, wear and corrosion debris are inherent properties of materials and are a matter for appropriate materials selection. [31]

Biostability refers to the ability of a material to resist biodegradation mechanisms and maintain its properties in situ. Degradation may result from hydrolysis, oxidation, and enzyme catalyzed enhancement of hydrolysis, oxidation, lipid absorption, swelling, and calcification. Biomaterials with enhanced compatibility will combine new materials that have

negligible leachables and exceptional biostability to mitigate adverse biologic responses to leaching of additives and breakdown products. [31]

1.3 Scope of Work

In the light of the literature reviewed, it was found that orthopaedic and dental implants and devices and materials used therein, have some prerequisites to fulfil, in terms of their biocompatibility, osseoinductivity, resistance to microbial infections, mechanical properties, resistance to corrosion, cost effectiveness etc. A closer inspection at the above mentioned traits reveals that most of these properties can be manipulated with effective control of the implant surface. Hence, development of coatings for orthopaedic prostheses is essential to its improvement. Such coatings can serve to satisfy three major requirements of the implants, namely- *osseointegration* or the ability to be incorporated successfully into the growing bone, *biocompatibility* or the ability to allow smooth functioning of the surrounding tissue, non toxicity and non carcinogenicity, and *antimicrobial activity*, or resistance against microbial colonization and infections. Several reports can be found in literature where coatings dressing these issues have been developed. For example, hydroxyapatite coatings have been produced to impart the implant with the necessary osseointegrative property. However, such coatings have mainly been produced by thermal spray techniques, which show reduced stability and enhanced propensity to delaminate in vivo. Silver incorporated coatings have been produced with antibacterial activity to protect the host against post-operation infections. However, silver ions and nanopaticles released in the host produced undesirable colouration of tissues, besides a possibility of producing toxic side effects, beyond a certain concentration. To overcome the drawbacks inherent in the abovementioned coatings, an attempt has been made in this investigation, to produce composite coatings from titania and

zinc oxide, through the process of sputtering. Titania, a biocompatible oxide has inherent osseointegrative capacity while zinc oxide nanoparticles have antimicrobial activity against a broad spectrum of both gram positive and gram negative bacteria, *S. aureus* and *E. coli*. Moreover, zinc ions and nanoparticles, have been shown to be essential to normal development of bones and teeth. A composite coating of both these oxides, should therefore, surmount the three challenges facing the orthopaedic community today.

Thus, this work comprised of two phases. In the first phase titania and zinc oxide thin films were deposited separately by the process of sputtering on silicon substrates and then annealed. Sputtering was chosen as the deposition method of choice owing to its advantages over other techniques, mainly its ability to produce highly uniform and adhesive coatings on the substrate. A detailed morphological analysis and in vitro biocompatibility test of the as deposited and annealed thin films was carried out. Phase two involved reactive cosputtering of titania and zinc oxide thin films on silicon substrate at various deposition temperatures, followed by a detailed morphological, chemical and microstructural analysis of the composite films so formed. In vitro cellular and acellular tests to determine their antimicrobial efficiency and osseointegrative ability were also carried out. Through a detailed investigation of the properties of the ZnO:TiO2 composite thin films, bioactive, biocompatible and antimicrobial coatings for orthopaedic implants have been proposed as a plausible improvement to the anomalies found in the present day bone and dental prostheses.

Chapter 2

Synthesis &

Characterization

Techniques
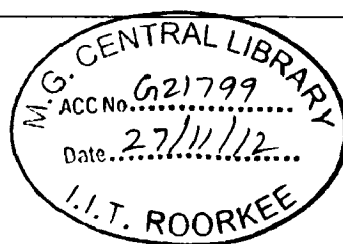
2.1 Thin Films Growth

Thin-film technology is simultaneously one of the oldest arts and one of the newest sciences. Involvement with thin films dates to the metal ages of antiquity. Interest in thin-film formation processes dates at least to the 1920s. During research at the Cavendish Laboratories in England on evaporated thin films, the concept of formation of nuclei that grew and coalesced to form the film was advanced. All phase transformations, including thin-film formation, involve the processes of nucleation and growth. During the earliest stages of film formation, a sufficient number of vapour atoms or molecules condense and establish a permanent residence on the substrate. Many such film birth events occur in this so-called nucleation stage. Although numerous high-resolution transmission electron microscopy investigations have focused on the early stages of film formation, it is doubtful that there is a clear demarcation between the end of nucleation and the onset of nucleus growth. Soon after exposure of the substrate to the incident vapour, a uniform distribution of small but highly mobile clusters or islands is observed. In this stage the prior nuclei incorporate impinging atoms and subcritical clusters and grow in size while the island density rapidly saturates. The next stage involves merging of the islands by a coalescence phenomenon that is liquidlike in character especially at high substrate temperatures. Coalescence decreases the island density, resulting in local denuding of the substrate where further nucleation can then occur. Crystallographic facets and orientations are frequently preserved on islands and at interfaces between initially disoriented, coalesced particles. Coalescence continues until a connected network with unfilled channels in between develops. With further deposition, the channels fill in and shrink, leaving isolated voids behind. Finally, even the voids fill in completely, and the film is said to be continuous. This collective set of

events occurs during the early stages of deposition, typically accounting for the first few hundred angstroms of film thickness. [54, 63]

The many observations of film formation have pointed to three basic growth modes:

I.   **Island (or Volmer-Weber),**

II. **Layer (or Frank-van der Merwe),** and

III. **Stranski-Krastanov,** which are illustrated schematically in Fig. 2.1.

ISLAND

LAYER

STRANSKI-KRASTANOV
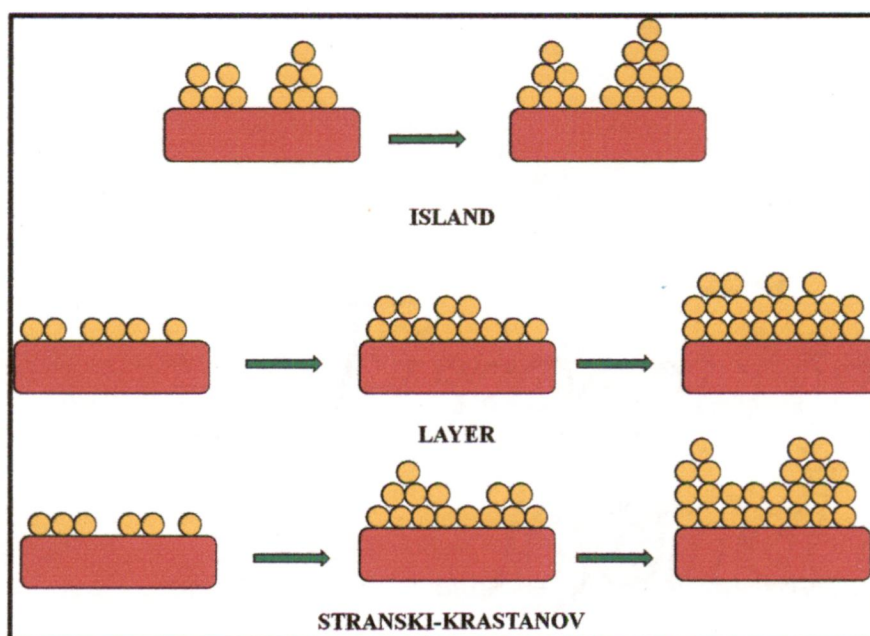
Figure2.1: Basic Modes of Thin film growth

Island growth occurs when the smallest stable clusters nucleate on the substrate and grow in three dimensions to form islands. This happens when atoms or molecules in the deposit are more strongly bound to each other than to the substrate. Many systems of metals on insulators, alkali halide crystals, graphite, and mica substrates display this mode of growth.

The opposite characteristics are displayed during *layer growth*. Here the extension of the smallest stable nucleus occurs overwhelmingly in two dimensions resulting in the formation of planar sheets. In this growth mode the atoms are more strongly bound to the substrate than to each other. The first complete monolayer is then covered with a somewhat less tightly

bound second layer. Providing the decrease in bonding energy is continuous toward the bulk crystal value, the layer growth mode is sustained.

The layer plus island or *Stranski-Krastanov* (S.K.) growth mechanism is an intermediate combination of the aforementioned modes. In this case, after forming one or more monolayers, subsequent layer growth becomes unfavourable and islands form. The transition from two- to three-dimensional growth is not completely understood, but any factor that disturbs the monotonic decrease in binding energy characteristic of layer growth may be the cause. For example, due to film-substrate lattice mismatch, strain energy accumulates in the growing film. When released, the high energy at the deposit-intermediate layer interface may trigger island formation. This growth mode is fairly common and has been observed in metal-metal and metal-semiconductor systems. [55, 56]

2.2 Thin Film Synthesis

Central to thin film technology and research are synthetic methods used to fabricate coatings and thin film materials. These techniques, which differ significantly from the familiar inorganic preparative techniques, can be categorised as either chemical or physical routes. Chemcial techniques include Chemical Vapour Deposition (CVD), sol-gel technique and electrochemical plating. In general, chemical methods rely on decomposition of molecular precursors and the quality of the resulting thin film depends critically on excluding ligand and other contaminants.

In contrast, physical techniques of deposition are based on evaporation and sputtering (PVD) of elemental and multicomponent sources and the subsequent deposition of the material onto a target. The objective of these deposition processes is to controllably transfer atoms from a source to a substrate where film formation and growth proceed atomistically. In evaporation, atoms are removed from the source by thermal means, whereas in sputtering they are dislodged from solid target (source) surfaces through impact of gaseous ions. As such, molecular precursors do not play a role in deposition via these techniques. Some examples of such techniques include: Molecular Beam Epitaxy, Sputtering, Pulsed Laser Deposition etc. [ii] Physical methods of fabricating thin films are very powerful techniques since they allow atomic level of control during film growth.

Some factors that distinguish PVD from CVD are:

1. Reliance on solid or molten sources

2. Physical mechanisms (evaporation or collisional impact) by which source atoms enter the gas phase

3. Reduced pressure environment through which the gaseous species are transported

4. General absence of chemical reactions in the gas phase and at the substrate surface (reactive PVD processes are exceptions).[54]

While, PVD processes have revolutionized the electronics industry with fabrication of semiconductor superlattices etc, they also pose some drawbacks. For example, thermal evaporation techniques like MBE fail to maintain the stoichiometry of the target, where one component of the target may have a higher vapour pressure, resulting in a deposition film with a different composition. Moreover, even PLD faces a disadvantage of non uniformity of thin films over large surface areas. Sputtering as a method of thin film deposition overcomes these obstacles and is termed to revolutionize the synthesis of thin film materials. [iv]

2.2.1 Sputtering

Sputtering is a Physical Vapor Deposition vacuum process used to deposit very thin films onto a substrate for a wide variety of commercial and scientific purposes. Sputtering occurs when an ionized gas molecule is used to displace atoms of a specific material. These atoms then bond at the atomic level to a substrate and create a thin film.

By first creating gaseous plasma and then accelerating the ions from this plasma into some source material (a.k.a. "target"), the source material is eroded by the arriving ions via energy transfer and is ejected in the form of neutral particles - either individual atoms, clusters of atoms or molecules. As these neutral particles are ejected they will travel in a straight line unless they come into contact with something - other particles or a nearby surface. If a "substrate" such as a Si wafer is placed in the path of these ejected particles it will be coated by a thin film of the source material.

Sometimes described as the "fourth state of matter" (the first three being solid, liquid, gas), a gaseous plasma is actually a "dynamic condition" where neutral gas atoms, ions, electrons

and photons exist in a near balanced state simultaneously. An energy source (eg. RF, DC, MW) is required to "feed" and thus maintain the plasma state while the plasma is losing energy into its surroundings. One can create this dynamic condition by metering a gas (e.g. Ar) into a pre-pumped vacuum chamber and allowing the chamber pressure to reach a specific level (eg. 0.1 Torr) and introducing a live electrode into this low pressure gas environment using a vacuum feedthrough.[v] [54, 61]

Critical to the analysis and design of a sputtering process, it is important to understand the interactions between the ions and the surface upon collision 9 presented schematically in the figure 2.2, taken from reference [54]. Each depends on the type of ion (mass, charge), the nature of surface atoms involved, and, importantly, on the ion energy.
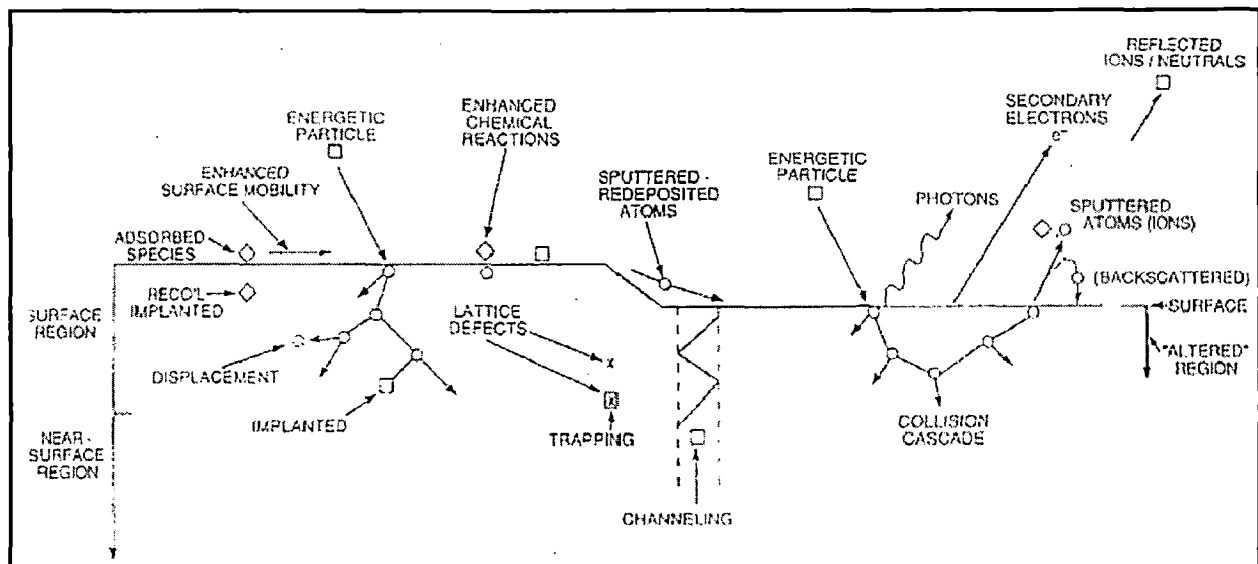
Figure 2.2: Depiction of energetic particle bombardment effects on surfaces and growing thin films.

Sputtering process can be classified into four categories: DC, Rf, Magnetron and Reactive and each category has its own set of variants.

DC Sputtering

Within the sputtering process gas ions out of plasma are accelerated towards a target consisting of the material to be deposited. Material is detached ('sputtered') from the target and afterwards deposited on a substrate in the vicinity. The process is realized in a closed recipient, which is pumped down to a vacuum base pressure\ before deposition starts.

To enable the ignition of plasma usually argon is feed into the chamber up to a pressure between 0.5 to 12Pa. By natural cosmic radiation there is always some ionized Ar+ ions available. In the dc-sputtering a negative potential U up to some hundred Volts is applied to the target. As a result, the Ar-ions are accelerated towards the target and set material free, on the other hand they produce secondary electrons. These electrons cause a further ionization of the gas. The gas pressure p and the electrode distance d determine a break-through voltage UD, from which on a self sustaining glow discharge starts — following the equation

$$UD = A \cdot pd/(ln(pd) + B);$$

with materials constants A and B. The ionization probability rises with an increase in pressure and hence the number of ions and the conductivity of the gas also increase. The break through voltage drops. For a sufficient ionization rate a stable burning plasma results, wherefrom a sufficient amount of ions is available for sputtering of the material [vi][54]

The bombardment of a non-conducting target with positive ions would lead to a charging of the surface and subsequently to a shielding of the electrical field. The ion current would die off. Therefore the dc-sputtering is restricted to conducting materials like metals or doped semiconductors.
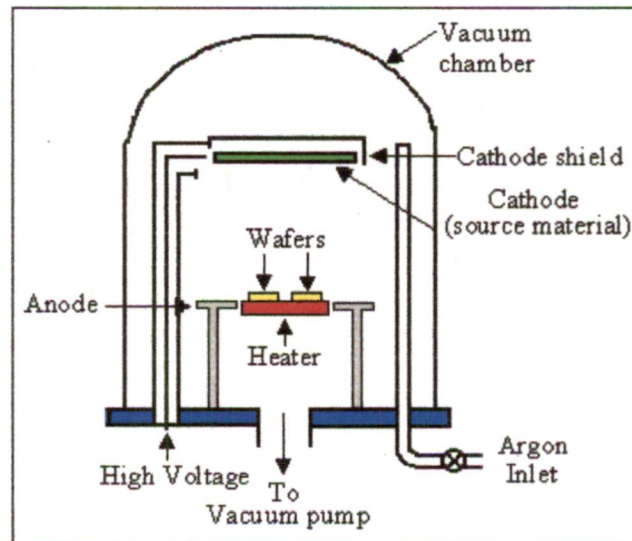
Figure 2.3: Schematic of DC Sputtering chamber (Adapted from [viii])

Parameters affecting DC Sputtering

   I.   Argon Pressure: Optimum sputter rate can be obtained around 100mTorr

  II.   Sputter Voltage: ~ - 2 to -5 kV

 III.   Substrate Temperature

 IV.   Deposition Rate

  V.   Particle Energy. [vii]

Rf Sputtering

RF sputtering was invented as a means of depositing insulating thin films. the accelerating potential cannot be directly applied to the insulator surface. This prevents neutralizing of the positive charge which would accumulate on the surface during ion bombardment. This problem can be overcome by applying a high frequency potential to a metal electrode behind the insulator. Power can be fed into the plasma via the displacement current through the dielectric material, and sputtering can occur because the insulator will now be alternately ion and electron bombarded. The positive charge which accumulates on the surface during the

negative or sputter portion of each cycle will now be neutralized by electrons during the positive part of the cycle. [57, 58]

When an ac signal is applied to the electrodes, below about 50 kHz, ions are sufficiently mobile to establish a complete discharge at each electrode on each half-cycle. Direct current sputtering conditions essentially prevail at both electrodes, which alternately behave as cathodes and anodes. Above 50 kHz two important effects occur. Electrons oscillating in the glow region acquire enough energy to cause ionizing collisions, reducing the need for secondary electrons to sustain the discharge. Secondly, RF voltages can be coupled through any kind of impedance so that the electrodes need not be conductors. This makes it possible to sputter any material irrespective of its resistivity. Typical RF frequencies employed range from 5 to 30 MHz. However, 13.56 MHz has been reserved for plasma processing by the Federal Communications Commission and is widely used. RF sputtering essentially works because the target self-biases to a negative potential. Once this happens, it behaves like a dc target where positive ion bombardment sputters away atoms for subsequent deposition. Negative target bias is a consequence of the fact that electrons are considerably more mobile than ions and have little difficulty in following the periodic change in the electric field. [54]
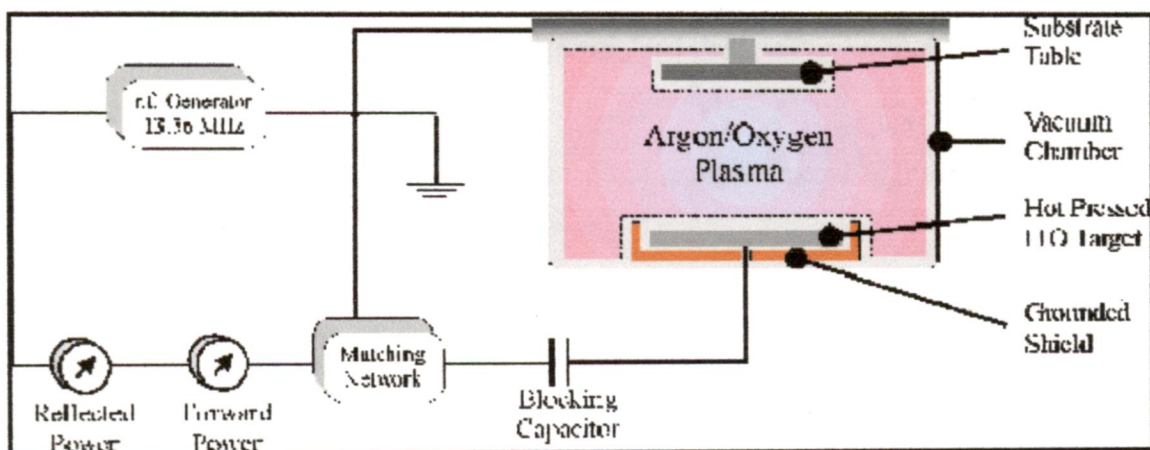
Figure 2.4: Schematic of Rf Sputtering chamber (Adapted from [59])

Magnetron Sputtering

To increase the ionization rate by emitted secondary electrons even further, a ring magnet below the target is used in *the magnetron sputtering*. The electrons in its field are trapped in cycloids and circulate over the targets surface. By the longer dwell time in the gas they cause a higher ionization probability and hence form a plasma ignition at pressures, which can be up to one hundred times smaller than for conventional sputtering. [vi] Higher deposition rates can be realized thereby. On the other hand less, collisions occur for the sputtered material on the way to the substrate because of the lower pressure and hence the kinetic energy at the impact on the substrate is higher. The electron density and hence the number of generated ions is highest, where the B-field is parallel to the substrate surface. The highest sputter yield happens on the target area right below this region. An erosion zone is formed which follows the form of the magnetic field. [60]

When a magnetic field of strength B is superimposed on the electric field ε between the target and substrate, electrons within the dual field environment experience the well-known Lorentz force in addition to electric field force, i.e.,

$$\mathbf{F} = \frac{m\,dv}{dt} = -q(\mathcal{E} + \mathbf{v} \times \mathbf{B})\ ;$$

where q, m and v are the electron charge, mass, and velocity, respectively. [54]

In magnetrons, electrons ideally do not even reach the anode but are trapped near the target, enhancing the ionizing efficiency there. This is accomplished by employing a magnetic field oriented parallel to the target and perpendicular to the electric field. Therefore, the magnetic field lines first emanate normal to the target, then bend with a component parallel to the target surface (this is the magnetron component) and finally return, completing the magnetic

circuit. Electrons emitted from the cathode are initially accelerated toward the anode, executing a helical motion in the process; but when they encounter the region of the parallel magnetic field, they are bent in an orbit back to the target in very much the same way that electrons are deflected toward the hearth in an e-gun evaporator.

Magnetron sputtering is presently the most widely commercially practiced sputtering method. The chief reason for its success is the high deposition rates achieved *(e.g.,* up to 1 pm/min for Al). These are typically an order of magnitude higher than rates attained by conventional sputtering techniques.

Magnetron sputtering is presently the most widely commercially practiced sputtering method. The chief reason for its success is the high deposition rates achieved (e.g., up to 1 pm/min). These are typically an order of magnitude higher than rates attained by conventional sputtering techniques.
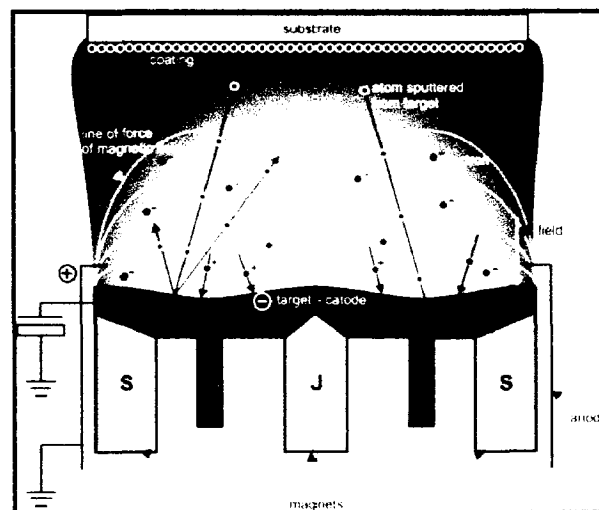
Figure 2.5: Principle of Magnetron Sputtering (Adapted from [ix])

Reactive Sputtering

In reactive sputtering, thin films of compounds are deposited on substrates by sputtering from metallic targets in the presence of a reactive gas, usually mixed with the inert working gas (invariably Ar). Chemical reaction takes place on the target and the substrate. We can adjust

the reactive gas flow, to obtain good stoichiometry and to prevent excess gas incorporation into films. The most common compounds reactively sputtered (and the reactive gases employed) are briefly listed:

1. Oxides (oxygen)-Al,O,, In,O,, SnO,, SO,, Ta,O,

2. Nitrides (nitrogen, ammonia)-TaN, TiN, AlN, Si,N,

3. Carbides (methane, acetylene, propane)-Tic, WC, Sic

4. Sulfides (H,S)-CdS, CuS, ZnS

5. Oxycarbides and oxynitrides of Ti, Ta, Al, and Si

Irrespective of which of these materials is considered, during reactive sputtering the resulting film is either a solid solution alloy of the target metal doped with the reactive element (e.g., $TaN_{0.01}$), a compound (e.g., TiN), or some mixture of the two.[54, 62]
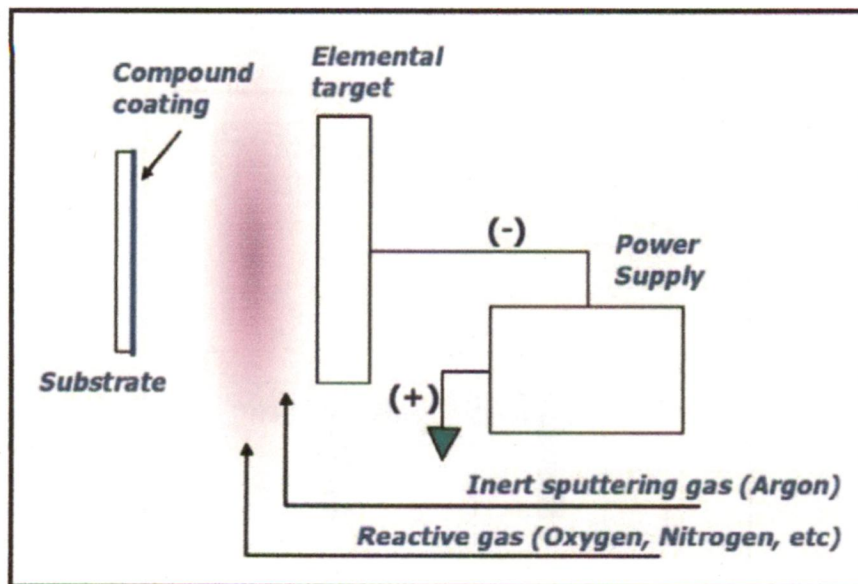
Figure 2.6: Schematic depicting the process of reactive sputtering (adapted from [62])

The choice of whether to employ compound targets and sputter directly or sputter reactively is not always clear. If reactive sputtering is selected, then there is the option of using simple dc diode, RF, or magnetron configurations. Many considerations go into making these choices:

I. Target Purity: It is easier to manufacture high-purity metal targets than to make high-purity compound targets. Since hot pressed and sintered compound powders cannot be consolidated to theoretical bulk densities, incorporation of gases, porosity, and impurities is unavoidable. Film purity using elemental targets is high, particularly since high-purity reactive gases are commercially available.

II. Deposition Rates: Sputter rates of metals drop dramatically when compounds form on the targets. Decreases in deposition rate well in excess of 50% occur because of the lower sputter yield of compounds relative to metals. In dc discharges, sputtering is effectively halted at very high gas pressures, but the limits are also influenced by the applied power. Conditioning of the target in pure Ar is required to restore the pure metal surface and desired deposition rates. Where high deposition rates are a necessity, the reactive sputtering mode of choice is either dc or RF magnetron.

III. Stoichiometry and Properties: Considerable variation in the composition and properties of reactively sputtered films is possible, depending on operating conditions. Colour changes may also accompany varied film stoichiometries. [54]

Reactive sputtering is a viable method for depositing compound films from an elemental of control of the reactive gas has a strong influence on the reactive deposition rate and the film properties. Flow control of the reactive gas, although simpler to implement, invariably produces low deposition rates compared to the deposition rate from the elemental target material. It also produces films with less than optimal properties. Partial pressure control of the reactive gas allows deposition of films in the transition region between the elemental and poisoned states of the target, which leads to higher deposition rates compared to flow control and better film properties. Insulating films can be reactively deposited without the

debilitating effects of arcing as long as the right kind of power (either pulsed dc or mid-frequency ac) is used. Multiple gas reactive sputtering requires partial pressure control of each reactive gas to prevent trapping of the target in a poisoned mode [64]

2.3 Annealing

The term **annealing** refers to a heat treatment in which a material is exposed to an elevated temperature for an extended time period and then slowly cooled. Ordinarily, annealing is carried out to (1) relieve stresses; (2) increase softness, ductility, and toughness; and/or (3) produce a specific microstructure. A variety of annealing heat treatments are possible; they are characterized by the changes that are induced, which many times are microstructural and are responsible for the alteration of the mechanical properties.

Any annealing process consists of three stages:

    I.   heating to the desired temperature,

    II.   holding or "soaking" at that temperature, and

    III. cooling, usually to room temperature.

Time is an important parameter in these procedures. During heating and cooling, there exist temperature gradients between the outside and interior portions of the piece; their magnitudes depend on the size and geometry of the piece. If the rate of temperature change is too great, temperature gradients and internal stresses may be induced that may lead to warping or even cracking. Also, the actual annealing time must be long enough to allow for any necessary transformation reactions. Annealing temperature is also an important consideration; annealing may be accelerated by increasing the temperature, since diffusional processes are normally involved. [65]

During the annealing process, the ZnO atoms gain energy to rearrange in the lattice. As well known, thermal annealing has been used to relieve the film stress and improve the crystal structure. [66]

The amount of process-initiating Gibbs free energy in a deformed metal is also reduced by the annealing process. In practice and industry, this reduction of Gibbs free energy is termed "stress relief". [x] Internal residual stresses may develop in metal pieces in response to the following: (1) plastic deformation processes such as machining and grinding; (2) nonuniform cooling of a piece that was processed or fabricated at an elevated temperature, such as a weld or a casting; and (3) a phase transformation that is induced upon cooling wherein parent and product phases have different densities. They may be eliminated by a stress relief annealing heat treatment in which the piece is heated to the recommended temperature, held there long enough to attain a uniform temperature, and finally cooled to room temperature in air. The annealing temperature is ordinarily a relatively low one such that effects resulting from cold working and other heat treatments are not affected. [65]

Mechanical properties, such as hardness and ductility, change as dislocations are eliminated and the metal's crystal lattice is altered. On heating at specific temperature and cooling it is possible to bring the atom at the right lattice site and new grain growth can improve the mechanical properties. [x] Morphological and microstructural properties as crystallinity, grain size, roughness and characteristics like wettability are affected by annealing time and temperature regime.

2.4 Characterization Techniques

2.4.1 X-Ray Diffraction

In 1919 A.W.Hull gave a paper titled, "A New Method of Chemical Analysis". Here he pointed out that "....every crystalline substance gives a pattern; the same substance always gives the same pattern; and in a mixture of substances each produces its pattern independently of the others. [67]

The X-ray diffraction pattern of a pure substance is, therefore, like a fingerprint of the substance. It is a versatile, non-destructive technique that reveals detailed information about the chemical composition and crystallographic structure of natural and manufactured materials.

X-ray diffraction is based on constructive interference of monochromatic X-rays and a crystalline sample. These X-rays are generated by a cathode ray tube, by heating a filament to produce electrons, accelerating the electrons toward a target by applying a voltage, and bombarding the target material with electrons. When electrons have sufficient energy to dislodge inner shell electrons of the target material, characteristic X-ray spectra are produced. Copper is the most common target material for single-crystal diffraction, with CuK_α radiation = 1.5418Å. These X-rays are filtered to produce monochromatic radiation, collimated to concentrate, and directed toward the sample. The interaction of the incident rays with the sample produces constructive interference (and a diffracted ray) when conditions satisfy ***Bragg's Law***:

$$n\lambda = 2d \sin \theta;$$

where *n* is an integer, λ is the wavelength of incident wave, *d* is the spacing between the planes in the atomic lattice, and θ is the angle between the incident ray and the scattering planes.

This law relates the wavelength of electromagnetic radiation to the diffraction angle and the lattice spacing in a crystalline sample. These diffracted X-rays are then detected, processed and counted. By scanning the sample through a range of 2θangles, all possible diffraction directions of the lattice should be attained due to the random orientation of the powdered material. Conversion of the diffraction peaks to d-spacings allows identification of the mineral because each mineral has a set of unique d-spacings. Typically, this is achieved by comparison of d-spacings with standard reference patterns.
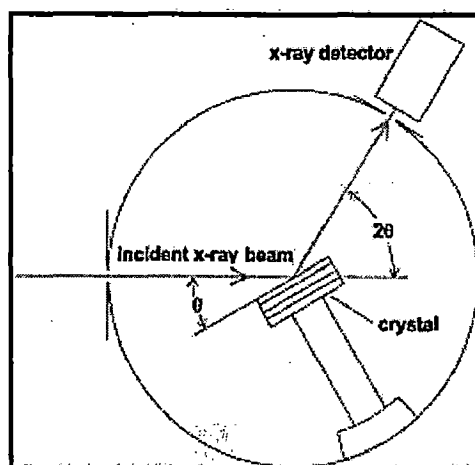
Figure 2.7: Schematic of an X-Ray Diffractometer

XRD patterns can be used to define crystallinity of the material (The crystalline parts give sharp narrow diffraction peaks and the amorphous component gives a very broad peak), the residual stress in films, texture analysis, i.e. determination of the preferred orientation of the crystallites in polycrystalline aggregates. [68, 69]

2.4.2 Field Emission Scanning Electron Microscopy

The scanning electron microscopy is a versatile, non-destructive technique that reveals detailed information about the morphology and the composition of materials. It was Ernest Ruska (1906-1987) who first mentioned the potential for electrons to be used in a microscope. The scanning electron microscope (SEM) uses a focused beam of high-energy electrons to generate a variety of signals at the surface of solid specimens. The signals that derive from electron-sample interactions reveal information about the sample including external morphology (texture), chemical composition, and crystalline structure and orientation of materials making up the sample. In most applications, data are collected over a selected area of the surface of the sample, and a 2-dimensional image is generated that displays spatial variations in these properties. Accelerated electrons in an SEM carry significant amounts of kinetic energy, and this energy is dissipated as a variety of signals produced by electron-sample interactions when the incident electrons are decelerated in the solid sample. These signals include:

Secondary electrons (that produce SEM images; morphology and topography of samples),

Backscattered electrons (illustrate contrast in composition in multiphase samples),

Diffracted backscattered electrons (EBSD that are used to determine crystal structures and orientations of minerals),

Photons (characteristic X-rays that are used for elemental analysis and continuum X-rays), visible light and heat.

In a typical SEM, an electron beam is thermionically emitted from an electron gun fitted with a tungsten filament cathode or lanthanum hexaboride (LaB_6) cathodes . The electron beam, which typically has an energy ranging from 0.2 keV to 40 keV, is focused by one or two

condenser lenses to a spot about 0.4 nm to 5 nm in diameter and scans in a raster fashion over a rectangular area of the sample surface. Thermionic sources have relative low brightness, evaporation of cathode material and thermal drift during operation. A Field Emission Source (FES); also called a cold cathode field emitter, on the other hand, does not heat the filament. The emission is reached by placing the filament in a huge electrical potential gradient. The FES is usually a wire of Tungsten (W) fashioned into a sharp point. The significance of the small tip radius (~ 100 nm) is that an electric field can be concentrated to an extreme level, becoming so big that the work function of the material is lowered and electrons can leave the cathode. [70, 71]

FESEM uses Field Emission Source producing a cleaner image, less electrostatic distortions and spatial resolution < 2nm (that means 3 or 6 times better than SEM).

Energy Dispersive X-Ray Analysis(EDX) is used as add on attachments with FESEM. EDX is an x-ray technique used to identify the elemental composition of a specimen. Its characterization capabilities are due in large part to the fundamental principle that each element has a unique atomic structure allowing unique set of peaks on its X-ray spectrum.
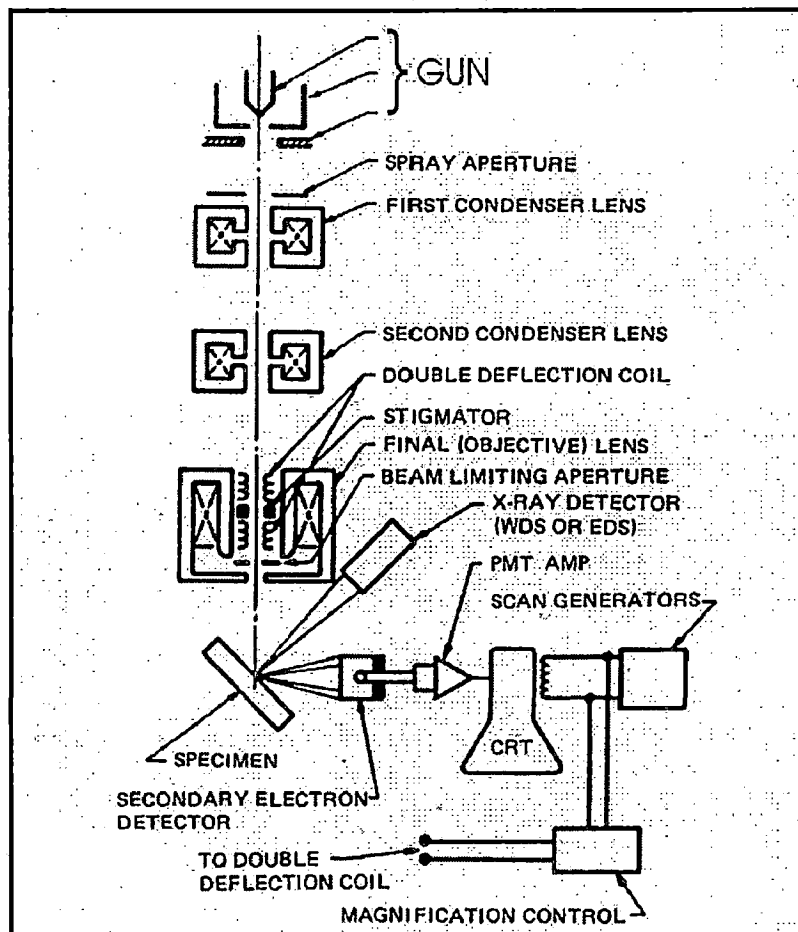
Figure 2.8: Schematic of a Scanning Electron Microscope(Adapted from [xii])

2.4.3 Atomic Force Microscopy

Scanning Probe Microscopy (SPM) is a branch of microscopy that forms images of surfaces using a physical probe that scans the specimen. An image of the surface is obtained by mechanically moving the probe in a raster scan of the specimen, line by line, and recording the probe-surface interaction as a function of position. The remarkable feature of Scanning Probe Microscopes (SPM) is their ability to "view" details at the atomic and molecular level, thus increasing our understanding of how systems work and leading to new discoveries in many fields. These include life science, materials science, electrochemistry, polymer science, biophysics, nanotechnology and biotechnology.

Atomic Force Microscopy (AFM) is a type of SPM which measures the forces acting between a fine tip and a sample. The tip is attached to the free end of a cantilever and is brought very close to a surface. Attractive or repulsive forces resulting from interactions between the tip and the surface will cause a positive or negative bending of the cantilever. The bending is detected by means of a laser beam, which is reflected from the back side of the cantilever.

The AFM can be operated in a number of modes, depending on the application. In general, possible imaging modes are divided into static (also called *contact*) modes and a variety of dynamic (non-contact or "tapping") modes where the cantilever is vibrated.

In the contact regime, the cantilever is held less than a few angstroms from the sample surface, and the interatomic force between the cantilever and the sample is repulsive. In the non-contact regime, the cantilever is held on the order of tens to hundreds of angstroms from the sample surface, and the interatomic force between the cantilever and sample is attractive (largely a result of the long range Van der Waals interactions).

An intermittent and most commonly used mode is the tapping mode. In tapping mode-AFM the cantilever is oscillating close to its resonance frequency. Forces that act between the sample and the tip will not only cause a change in the oscillation amplitude, but also change in the resonant frequency and phase of the cantilever. The advantages of the tapping mode are the elimination of a large part of permanent shearing forces and the causing of less damage to the sample surface, even with stiffer probes.
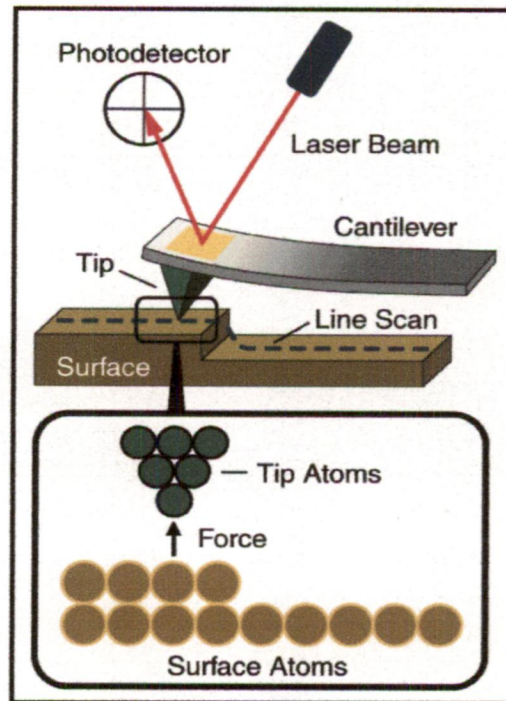
Figure 2.9: Schematic depicting the principle behind Atomic Force Microscopy (Adapted from [73])

The dependence of the van der Waals force upon the distance between the tip and the sample

is shown in fig. 2.13
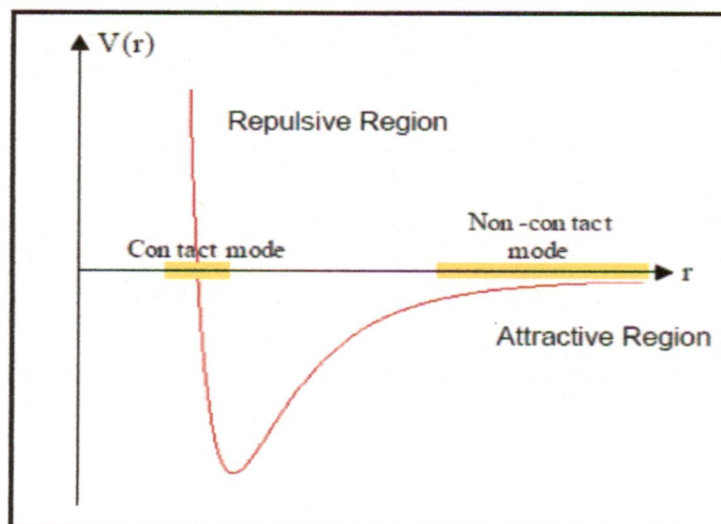
Figure 2.10: Potential Energy Diagram of probe and sample (Adapted from [73])

2.4.4 Transmission Electron Microscopy

The transmission electron microscope (TEM) operates on the same basic principles as the light microscope but uses electrons instead of light. TEMs are capable of imaging at a significantly higher resolution than light microscopes, owing to the small de Broglie wavelength of electrons. [xiii]. A beam of electrons is accelerated to 100 KeV or higher (up to 1MeV) and projected onto a thin specimen (less than 200 nm) by means of the condenser lens system, interacting with the specimen as it passes through. An image is formed from the interaction of the electrons transmitted through the specimen; the image is magnified and focused onto an imaging device, such as a fluorescent screen, on a layer of photographic film, or to be detected by a sensor such as a CCD camera. The greatest advantages that TEM offers are the high magnification ranging from 50 to 10^6 and its ability to provide both image and diffraction information from a single sample.

For the crystallographer, metallurgist or semiconductor research scientist, current high voltage/high resolution TEMs, utilizing 200 keV to 1 MeV, have permitted the routine imaging of atoms, allowing materials researchers to monitor and design materials with custom-tailored properties.

A TEM contains four parts: electron source, electromagnetic lens system, sample holder, and imaging system. From the top down, the TEM consists of an emission source, which may be a tungsten filament, or a lanthanum hexaboride (LaB_6) source.[18] For tungsten, this will be of the form of either a hairpin-style filament, or a small spike-shaped filament. LaB_6 sources utilize small single crystals. By connecting this gun to a high voltage source (typically ~100-300 kV) the gun will, given sufficient current, begin to emit electrons either by thermionic or field electron emission into the vacuum. The lenses of a TEM allow for

beam convergence, with the angle of convergence as a variable parameter, giving the TEM the ability to change magnification simply by modifying the amount of current that flows through the coil, quadrupole or hexapole lenses. Typically a TEM consists of three stages of lensing. The stages are the condensor lenses, the objective lenses, and the projector lenses. The condensor lenses are responsible for primary beam formation, whilst the objective lenses focus the beam that comes through the sample itself. The projector lenses are used to expand the beam onto the phosphor screen or other imaging device, such as film. The magnification of the TEM is due to the ratio of the distances between the specimen and the objective lens' image plane. Imaging systems in a TEM consist of a phosphor screen, which may be made of fine (10-100 μm) particulate zinc sulphide, for direct observation by the operator. Optionally, an image recording system such as film based or doped YAG screen coupled CCDs. [71]

SPECIMEN PREPARATION is an important aspect of the transmission electron microscopy (TEM) analysis of in material sciences. For most materials, metals and ceramics, a common sequence of preparation techniques is **ultrasonic disk cutting, dimpling, and ion-milling**. A critical aspect of preparing a specimen from the bulk state to a 0.3 mm disk is the ability to rapidly capture the specific area of interest and to preserve it in an unaltered state. **Dimpling** is a preparation technique that produces a specimen with a thinned central area and an outer rim of sufficient thickness to permit ease of handling. This specimen configuration is achieved by the simultaneous rotation of both the specimen and a grinding wheel containing abrasive slurry (typically diamond) whose axes are orthogonal and intersecting. Prior to dimpling, it is desirable to reduce the specimen thickness to approximately 75 to 100 microns. This is achieved through the use of classic metallographic polishing techniques utilizing a precision, planar specimen grinder as shown in Figure 2.16. This device allows the rapid

removal of large amounts of material in a controlled manner while inducing minimal specimen damage.
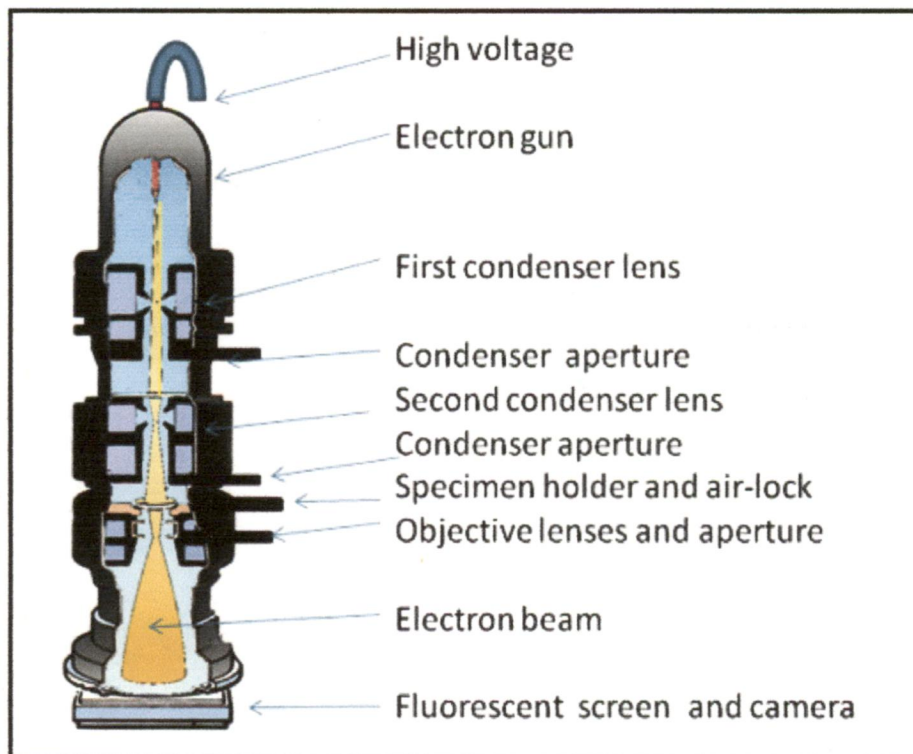
Figure 2.11: Transmission Electron Microscope, showing all its components

Ion milling is traditionally the final form of specimen preparation. In this process, charged argon ions are accelerated to the specimen surface by the application of high voltage. The ion impingement upon the specimen surface removes material as a result of momentum transfer. As a result of low angle, variable-energy ion milling, a large electron transparent area with a uniform thickness is produced. [74]
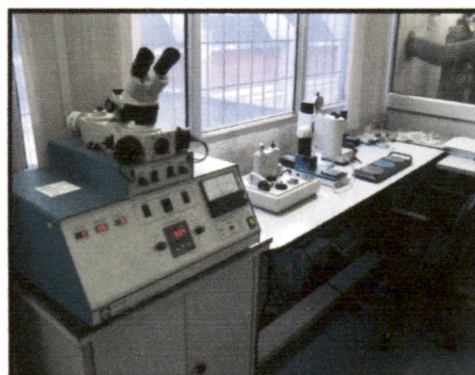
Figure 2.12: Sample Preparation unit with its different units

TEM can be operated in two modes:

I. **Image mode**: In image mode, the condenser lens and aperture will control electron beam to hit the specimen, the transmitted beam will be focused and enlarged by objective and projector lens and form the image in the screen, with recognizable details related to the sample microstructure.

In the *Bright Field* image mode, an aperture is placed in the back focal plane of the objective lens which allows only the direct beam to pass. In this case, the image results from a weakening of the direct beam by its interaction with the sample. Areas in which heavy atoms are enriched, and crystalline areas appear with dark contrast.

In *Dark Field* images, the direct beam is blocked by the aperture while one or more diffracted beams are allowed to pass the objective aperture.

II. **Diffraction mode SAED (Selected Area Electron Diffraction)**: In diffraction mode, an electron diffraction pattern is obtained on the fluorescent screen, originating from the sample area illuminated by the electron beam. The diffraction pattern is entirely equivalent to an X-ray diffraction pattern:

A *single crystal* will produce a spot pattern on the screen; *Poly-crystal* will produce a powder or ring pattern; A *glassy or amorphous material* will produce a series of diffuse halos.

2.4.5 Inductively Coupled Plasma Mass Spectrometry

Inductively Coupled Plasma Mass Spectrometry or ICP-MS is an analytical technique used for elemental determinations. An ICP-MS combines a high-temperature ICP (Inductively Coupled Plasma) source with a mass spectrometer. The ICP source converts the atoms of the elements in the sample to ions. These ions are then separated and detected by the mass spectrometer.

Fig. 2.18 shows a schematic representation of ICP-MS system. Argon gas flows inside the concentric channels of the ICP torch. The Rf load coil is connected to a radio-frequency (Rf) generator. As power is supplied to the load coil from the generator, oscillating electric and magnetic fields are established at the end of the torch. When a spark is applied to the argon flowing through the ICP torch, electrons are stripped off of the argon atoms, forming argon ions. These ions are caught in the oscillating fields and collide with other argon atoms, forming an argon discharge or plasma.[xv]

The ICP-MS analysis of the samples can be divided into four stages: introduction-atomizing, ionization, separation in mass, detection. The sample is typically introduced into the ICP plasma as an aerosol, either by aspirating a liquid or dissolved solid sample into a nebulizer or using a laser to directly convert solid samples into an aerosol. Once the sample aerosol is introduced into the ICP torch, it is completely desolvated and the elements in the aerosol are converted first into gaseous atoms and then ionized towards the end of the plasma. [75]

Once the elements in the sample are converted into ions, they are then brought into the mass spectrometer via the interface cones. The interface region in the ICP-MS transmits the ions traveling in the argon sample stream at atmospheric pressure (1-2 torr) into the low pressure region of the mass spectrometer ($<1 \times 10^{-5}$ torr). The ions from the ICP source are then focused by the electrostatic lenses in the system. Once the ions enter the mass spectrometer, they are separated by their mass-to-charge ratio. The most commonly used type of mass spectrometer is the **quadrupole mass filter**. The result is that an electrostatic filter is established that only allows ions of a single mass-to-charge ratio (m/e) pass through the rods to the detector at a given instant in time. Typical quadrupole mass spectrometers used in ICP-

MS have resolutions between 0.7 - 1.0 amu. Once the ions have been separated by their mass-to-charge ratio, they must then be detected or counted by a suitable detector. The fundamental purpose of the detector is to translate the number of ions striking the detector into an electrical signal that can be measured and related to the number of atoms of that element in the sample via the use of calibration standards. Most detectors use a high negative
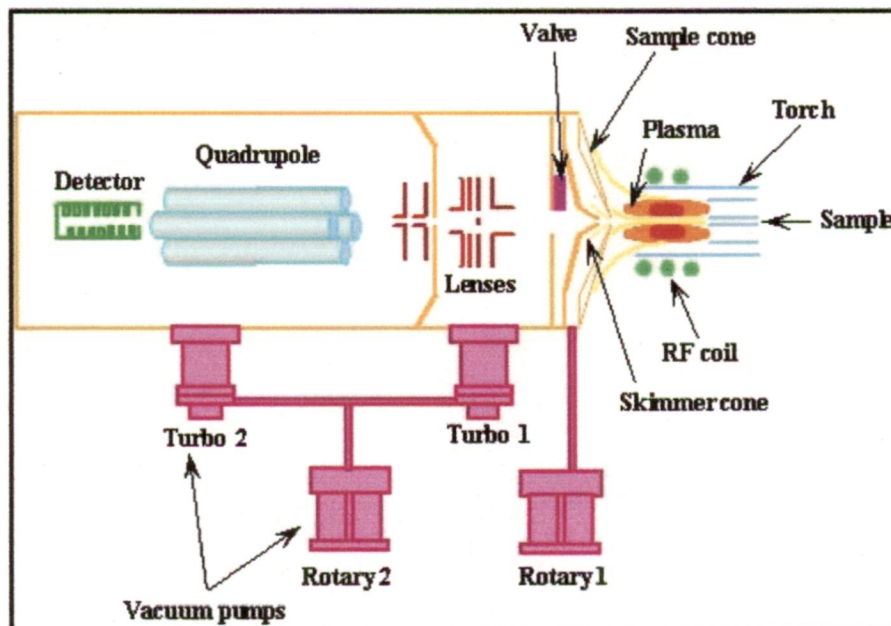
Figure 2.13: Schematic of Inductively Coupled Mass Spectrophotometer (Adapted from [xvi])

voltage on the front surface of the detector to attract the positively charged ions to the detector. Once the ion hits the active surface of the detector, a number of electrons is released which then strike the next surface of the detector, amplifying the signal.

The ICP-MS became essential for the simultaneous analysis of the elements in traces and "ultra-traces" (elements lower than 10^{-6} g/g) and for the determination of the isotopic ratios in rocks, water, sediments, biologic samples. In "routine", it is possible to analyze, in a few minutes, 20 to 30 elements in the most varied materials. In addition, it has an excellent sensitivity, enabling to detect elements present at the level of (1 ppt is a part = 10^{-12} g/g) in a

solution of rock or in water. Without any chemical separation, it allows the analysis of many

elements in trace the level of ppb (10^{-9}g/g).

2.4.6 Contact Angle Goniometer

Microscopic characteristics such as surface roughness, surface energies of the materials

involved, and surface coatings play a role in the wettability of a material for a given fluid.

Quantitatively, a contact angle is the interior angle formed by the substrate being used and

the tangent to the drop interface at the apparent intersection of all three interfaces. This

intersection is called the contact line. Fig. 2.22 illustates the tangent line and the contact

angle of a liquid drop on a surface. Historically a static contact angle on a at surface is

deemed by the Young Equation.[77]
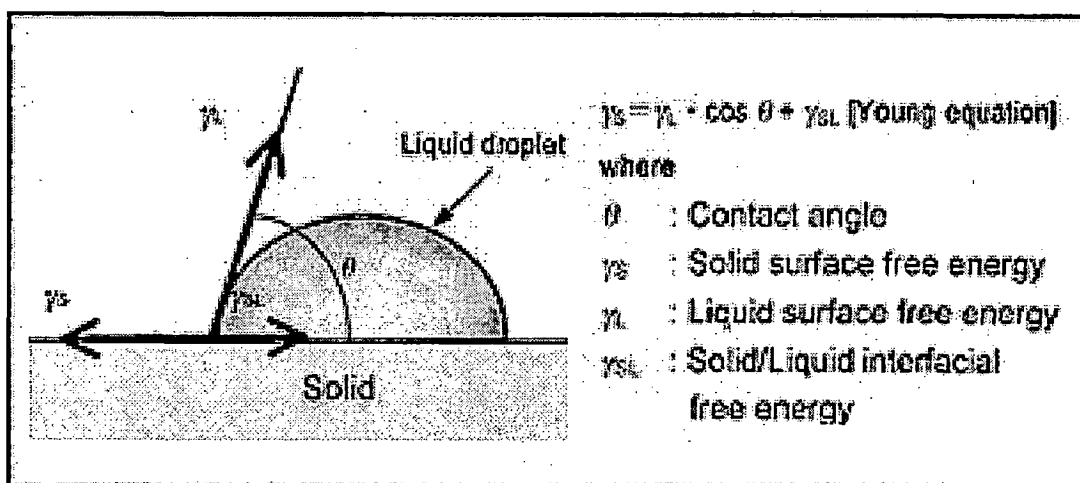
Figure 2.14: Contact angle of a liquid droplet on a surface (Adapted from [xvii])

Contact angle is a simple and yet powerful tool for characterizing three-phase junctions. The

technique of the sessile drop is today the most widely used method to measure this parameter.

In a static contact angle measurement the size of the drop does not alter during the

measurement. However, this does not mean that the contact angle always remains constant;

on the contrary, interactions at the boundary surface can cause the contact angle to change

considerably with time. Depending on the type of time effect the contact angle can increase or decrease with time.

The most complicated, but also the theoretically most exact method for calculating the contact angle is the YOUNG-LAPLACE fitting. In this method the complete drop contour is evaluated; the contour fitting includes a correction which takes into account the fact that it is not just interfacial effects which produce the drop shape, but that the drop is also distorted by the weight of the liquid it contains. After the successful fitting of the YOUNG-LAPLACE Equation the contact angle is determined as the slope of the contour line at the 3-phase contact point. [78]

Calibration is straightforward in that only optical magnification is needed. This can be measured with high accuracy and is easy to trace to national standards.

2.4.7 In Vitro Acellular Testing: Static Immersion Test

Generally, artificial materials implanted into bone defects are encapsulated by a fibrous tissue to be isolated from the surrounding bones. A limited kind of ceramics such as Na_2O-CaO-SiO_2-P_2O_5 glasses called Bioglass, sintered hydroxyapatite and glass-ceramics A-W containing apatite and wollastonite in a MgO-CaO-SiO_2 glassy matrix, however, bond directly to living bone without forcing the fibrous tissue. These bioactive ceramics are already clinically used as important bone repairing materials. Bioactive materials described above, form an apatite layer on their surfaces in the living body and bond to living bone through the apatite layer. This apatite is a carbonate containing hydroxyapatite with small crystallites and defective structure, which is very similar to the apatite in the bone in its composition and structure. Therefore, the bone-producing cell, the osteoblast, can preferentially proliferate and differentiate to produce apatite and collagen on this apatite layer.

As a result, the surrounding bone can come into direct contact with the surface apatite of these materials without intervention of the fibrous tissue. [79] For this reason HA is proposed as a suitable coating material to provide stronger early fixation of uncemented prostheses. Although hydroxyapatite coatings on implants showed long-term survival, there are concerns about their reliability under loads.

Hydroxyapatite coatings can be produced by different methods. Early attempts used plasma spraying, which however resulted in coatings with adhesion problems. Attempts have also been made with physical vapour deposition (PVD) techniques. Both of these methods suffer from the drawback that they are line-of-sight methods, which means that coating of complex implant geometries is technically difficult. The biomimetic way to fabricate apatite coatings on implants overcomes these drawbacks. Biomimetic HA coating is, basically, a solution-based method carried out at ambient temperature mimicking body surroundings. [80] The method allows deposition of CaP coatings on many different objects, such as sponges, cements, metal surfaces or fixation rods [81]. Typically, the substrates with active surfaces are immersed in a simulated body fluid at physiological pH and temperature (approximately 37°C), and an apatite layer will automatically form, crystallize and grow on the surfaces. By varying the immersion conditions, coatings with a wide range of morphologies, thicknesses and composition can be prepared.

The standard way of producing biomimetic coatings has for a long time been based on the simulated body fluid (SBF) solutions described by Kokubo [82]. Recently, in order to improve the coating process, the composition of the solutions used for biomimetic HA coatings has been modified (Table 2.1). Except for the inorganic components, some other organic components, such as protein and lactic acid, have been added into SBF [83].The

immerson temperature has also been expanded to temperatures from 4 to 65 °C [84]. Based on these biomimetic methods, the resulting apatite coatings will be either amorphous calcium phosphate (ACP), octacalcium phosphate (OCP) or hydroxyapatite (HA).

Ion	Na+	K+	Mg2+	Ca2+	Cl-	HPO42-/H2PO4-	SO42-	HCO3-
Blood Plasma	142.0	5.0	1.5	2.5	103.0	1.0	0.5	27
SBF	142.0	5.0	1.5	2.5	148.5	1.0	0.5	4.2
PBS	145.0	4.2	0.49	0.91	143	9.6	-	-
HBSS	141.7	5.7	0.8	1.7	145.6	0.7	0.8	4.2

Table 2.1: Inorganic composition of blood plasma and different simulated body fluids (mM). (Adapted from [84])

2.4.8 In vitro Cellular Testing: Cytotoxicity Analysis

Cytotoxicity testing is a rapid, standardized, sensitive, and inexpensive means to determine whether a material contains significant quantities of biologically harmful extractables. The high sensitivity of the tests is due to the isolation of the test cells in cultures and the absence of the protective mechanisms that assist cells within the body. A mammalian cell culture medium is the preferred extractant because it is a physiological solution capable of extracting a wide range of chemical structures, not just those soluble in water. Antibiotics can be added to the medium to eliminate potential interference from microbial contamination that may be present on the test material and control samples. Results of cytotoxicity tests correlate reasonably well with short-term and long term implant studies. However, they do not necessarily correlate well with other standard tests of biocompatibility that are designed to examine specific end points (such as sensitization) or that use extracts prepared under more rigorous conditions (for example, at 121°C in saline or cottonseed oil). Cytotoxicity test

methods are useful for screening materials that may be used in medical devices because they serve to separate reactive from non-reactive materials, providing predictive evidence of material biocompatibility. The ISO 10993-5 standard, "Guidance on the Selection of Tests," considers these tests so important that they are prescribed for every type of medical device, along with sensitization and irritation testing. Cytotoxicity test methods are also useful for lot-to-lot comparison of materials, for determining whether a potential replacement material is equivalent to that currently being used, and for troubleshooting and exploring the significance of changes in manufacturing processes.

The cytotoxicity assays, and their modifications allow many samples to be analyzed rapidly and simultaneously. Colorimetric and luminescence based assays allow samples to be measured directly in the plate by using a microtiterplate reader or ELISA plate reader. Cytototoxicity assays have been developed which use different parameters associated with cell death and proliferation. One parameter for cell death is the integrity of the cell membrane, which can be measured by the cytoplasmic enzyme activity released by damaged cells. Another parameter used as the basis for colorimetric assays is the metabolic activity of viable cells. Tetrazolium salts are reduced only by metabolically active cells. Thus, 3-(4,5-dimethylthiazol-2-yl)-2,5-diphenyltetrazolium bromide (MTT) can be reduced to a blue colored formazan. Neutral red (3-amino-m-dimethylamino-2-methylphenazine hydrochloride) has been used previously for the identification of vital cells in cultures (DeRenzis and Schechtman, 1973 [85]. This assay quantifies the number of viable, uninjured cells after their exposure to toxicants; based on the uptake and subsequent lysosomal accumulation of the supravital dye, neutral red. Adenosine triphosphate (ATP) that is present in all metabolically active cells can be determined in a bioluminescent measurement. The

bioluminescent method utilizes an enzyme, luciferase, which catalyses the formation of light from ATP and luciferin. The emitted light intensity is linearly related to the ATP concentration. [86]

Measurement of cell viability and proliferation forms the basis for numerous in vitro assays of a cell population's response to external factors. The reduction of tetrazolium salts is now widely accepted as a reliable way to examine cell proliferation. The yellow tetrazolium MTT (3-(4, 5-dimethylthiazolyl-2)-2, 5-diphenyltetrazolium bromide) is reduced by metabolically active cells, in part by the action of dehydrogenase enzymes, to generate reducing equivalents such as NADH and NADPH. The resulting intracellular purple formazan can be solubilized and quantified by spectrophotometric means. [87]
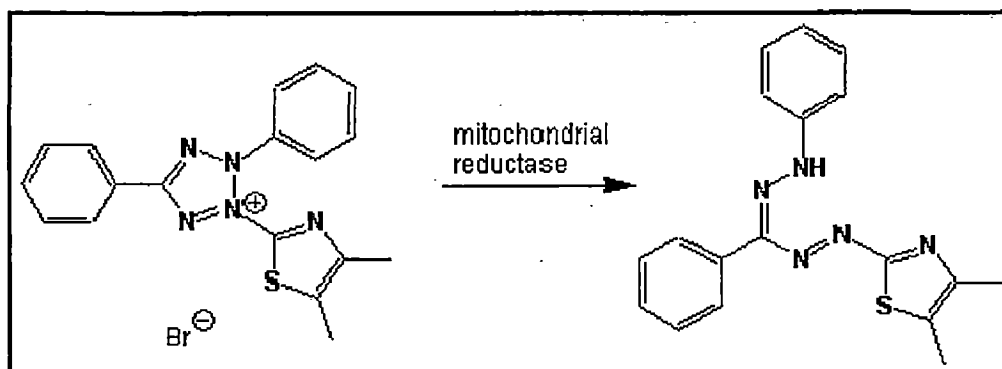
Figure 2.15: MTT Reduction Scheme (Adapted from [xviii])

The MTT Cell Proliferation Assay measures the cell proliferation rate and conversely, when metabolic events lead to apoptosis or necrosis, the reduction in cell viability. [88]

2.4.9 Antimicrobial Efficiency Test

More than 1.5 million primary joint replacements are performed annually worldwide. Aseptic loosening is the most common reason for revision surgery. In addition to this, implant infection is a feared complication after joint replacement. Despite aseptic operation conditions and perioperative antibiotic prophylaxis, infection rates are reported to range between 0.5 and 2% after primary total hip replacement (THR) and approximately 1 to 4%

after primary total knee replacement (TKR) [89] and occur to an even greater extent after revision arthroplasty. [90]

Since *Escherichia coli* and *Staphylococcus aureus* have been reported to be the most important pathogens I biomaterial-associated infections, the anti-bacteria property of the coating was determined by determining the adhesion of these bacteria to the implant surface. The antibacterial efficiency of the thin films was studied, based on references [91] [92], with certain modifications.

The method described in JIS Z 2801

    I.   generates fully quantitative data.

    II.   can be modified to accommodate both biocidal and biostatic effects

    III.   can be modified to accommodate a wide range of microbial species (including certain fungi, algae and protozoa as well as a wide range of bacterial species and viruses)

    IV.   can be modified to allow a wide range of contact times and temperatures to be examined.[93]

Antibacterial activity is measured by quantifying the survival of bacterial cells which have been held in intimate contact for 24 hours at 35°C with a surface that contains an antibacterial agent. The antibacterial effect is measured by comparing the survival of bacteria on a treated material with that achieved on an untreated material.

I.   The test microorganism is prepared, usually by growth in a liquid culture medium.

II.   The suspension of test microorganism is standardized by dilution in a nutritive broth (this affords microorganisms the potential to grow during the test).

III.   Control and test surfaces are inoculated with microorganisms, and then the microbial inoculum is covered with a thin, sterile film or cover slip. Covering the inoculum spreads it, prevents it from evaporating, and ensures close contact with the antimicrobial surface.
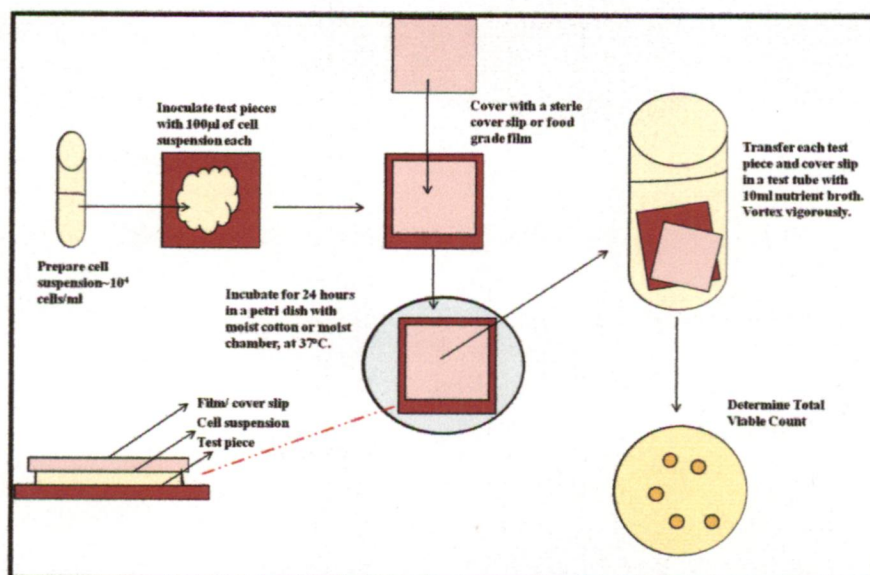
Figure 2.16: Schematic representation of antibacterial efficiency test Summary of the JIS Z 2801 Test:

IV.   A control is run to verify that the neutralization/elution method effectively neutralizes the antimicrobial agent in the antimicrobial surface being tested.

V.   Inoculated, covered control and antimicrobial test surfaces are allowed to incubate undisturbed in a humid environment for 24 - 48 hours.

VI.   After incubation, microbial concentrations on the samples are determined. Reduction of microorganisms relative to initial concentrations and the control surface is calculated.

Chapter 3

Synthesis & Characterization of Titania Coatings

3.1 Introduction to Bioactive Titania coatings

Branemark introduced titanium almost 40 years ago [32] and it quickly grew on to become one of the most favoured and widely used medical implant and prosthetic material. The main factor influencing its success is its high acceptance by the host organism. Titanium is biocompatible, in that it does not cause corrode in the physiological environment, nor does it cause inflammatory reactions. Also, titanium and its alloy form an external superficial passive oxide film that can reach nanometer (nm) thickness and protect against corrosion[33]. The excellent performance of titanium implants has not been understood at the molecular level, and in Parsegian's words, "... *It might be wild luck that makes titanium work so well*".[34]

In case of Ti or Ti alloy (Ti6Al4V) implants, the metal substrate is covered by the always present surface oxide, TiO_2, to which protein molecules from the biologic liquid attach themselves. The nature of the biomolecular layer determines the cell response (proliferation, differentiation) that would eventually lead to bone formation. On the other hand, studies have shown that patients with well-functioning Ti alloy implant have had as much as a threefold increase in the concentration of Ti in their serum, and an accumulation of alloy metal ions over time has shown the potential to cause hypersensitivity, toxicity, and other tissue reactions. Discoloration of the tissue occurs when Ti ions are released into the adjacent tissue of the implant site. This proves to be detrimental to the bone attachment and further bone growth on the implant surface. For this reason, the microarchitecture of the surface (topography, roughness, etc.) and its chemical composition are important determinants of the response of the biologic system to the implant. [35]

Ti implant 1 mm

Bone

1 µm

Titanium Bioliquid Bone

1 nm

Na⁺
Cl⁻
H₂O
Protein

Titanium Titanium oxide Bioliquid
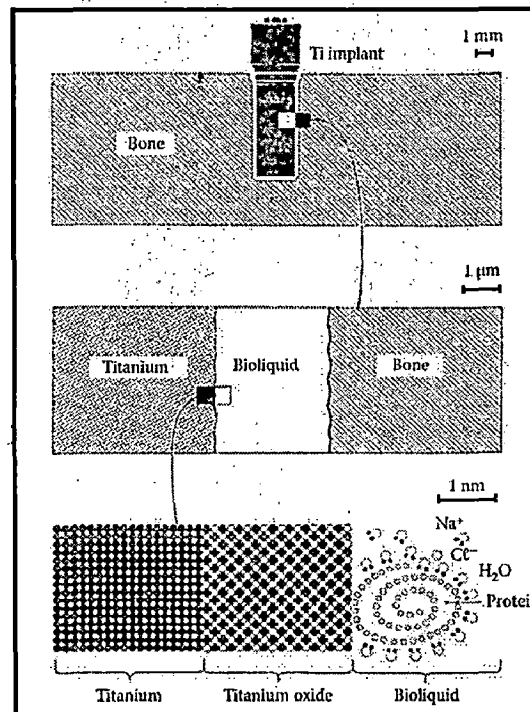
Figure 3.1: Ti implant and bone interface at the tissue, cellular, and atomic levels. (Adapted from [36])

TiO_2, a well known biomaterial has potential applications including as an antibacterial coating for sterilizing biomedical metallic implants, hospital equipments and as self-cleaning surfaces for use in architecture [37]. Nanostructured TiO_2 coated metallic implants have been reported to possess good mechanical properties, high bonding strength to substrates, enhanced photocatalytic activity, bioactivity and biocompatibility due to their nanometer sized surface features which enhances intended surface functions [38, 39].

Structure

Metal oxide surfaces are prime examples of close relationship between structure and reactivity, as local non-stochiometries and geometric defects directly affect the electronic structure. Because of the mixed ionic and covalent bonding, the surface structure in metal oxide systems has an even stronger influence on local surface chemistry than metals and elemental semiconductors. Titanium dioxide crystallizes in three different phases; rutile

(tetragonal, a=b=4.584Å, c=2.953Å), **anatase** (tetragonal, a=b=3.782Å, c=9.502Å) and

brookite (rhombohedrical, a= 5.436 Å, b=9.166 Å and c=5.135 Å). However only rutile and

anatase play any role in the various applications of TiO_2. Their unit cells are shown in fig.3.2.

In both the structures, Ti atom is surrounded by 6 oxygen atoms in a distorted octahedral

configuration. [40]
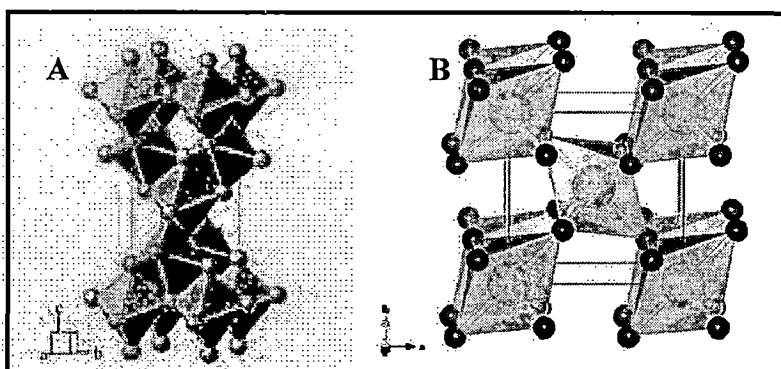
Figure 3.2: Bulk structures of TiO_2, (A) Anatase, and (B) Rutile

Rutile is the thermodynamically most stable face, and the (110) face has the lowest surface

energy and is the most intensely studied surface. TiO_2 surfaces, especially the (110) face of

rutile, have become prototypical model systems in the surface science of metal oxides.

Reduced TiO_2 single crystals are easy to work with experimentally, and their surfaces have

been characterized with virtually all surface-science techniques. Scanning tunneling

microscopy (STM) studies have shown that the surface structure of TiO_2(110) is more

complex than originally anticipated. The reduction state of the sample, i.e. the number and

type of bulk defects, as well as the surface treatment (annealing in vacuum vs. annealing in

oxygen), can give rise to different structures, such as two different reconstructions, a

'rosette' overlayer, and crystallographic shear planes. Single point defects can be identified

with STM and influence the surface chemistry in a variety of ways.[41]

3.2 Experimental details

3.2.1 Synthesis of TiO₂ films on Si(100) substrates

The TiO_2 thin films were deposited by Reactive DC Magnetron sputtering on Silicon Si(100) substrates (10mm x 10mm) from a 99.99% pure titanium target (2' diameter and 5 mm thick). The substrate was cleaned by ultrasonication in acetone for 15 minutes to remove any traces of impurities and then dried in air. The base pressure was better than 2×10^{-6} Torr and the sputtering was carried out in mixed Argon: Oxygen (20:80) atmosphere. The ambient gas pressure during the process was kept at 20 mTorr. Before the actual experiment, the target was pre-sputtered for 15 minutes to remove the native oxide layer formed on the surface. The target-substrate distance 60m, the gun length 250 mm and the deposition time 120 minutes were kept constant for all depositions. Sputtering was carried out at 120W at room temperature. The sputtering parameters for TiO_2 films are listed in Table 3.1

3.2.2 Annealing of TiO₂ thin films

The as deposited TiO_2 thin films were annealed in an open air tubular furnace (Lenton LTF 14/50/240) at temperatures 300°C, 500°C, 700°C, 900°C for one hour at a constant ramp rate of 10°C/minute.

Target	Titanium
Base Pressure	2×10^{-6} Torr
Sputtering Pressure	20 mTorr
Gas Used	Argon+ Oxygen (20:80)
Sputtering Power	120W DC
Substrate temperature	Room temperature
Sputtering Time	120 minutes
Substrate used	Silicon Si(100)

Table 3.1: Sputtering parameters for TiO_2 films

3.2.3 Characterization

3.2.3.1 Microstructural Characterization

The as deposited and the annealed films were characterized by XRD (Bruker AXS, D8 Advance) with $CuK\alpha$ (1.54 Å) radiation for the phase, grain size measurement and texture analysis. The excitation voltage and current were set to 40kV and 30mA respectively, in the diffractometer. The scan rate used was .02°/minute and the scan range was 20° to 80°. The grain size of the films was estimated from the Scherrer's formula (*Cullinity et al. 2001*), given by the equation:

$$t = 0.9\lambda / B\cos\theta,$$

The grain size t is along the surface normal direction, B(crystallite) is the corrected full-width half maximum (FWHM) of a Bragg's peak, λ is the wavelength of X-ray and θ is the Bragg's angle. The grain size was calculated using the preferred orientation of the XRD peaks of the TiO_2 films on the Si substrate.

The surface morphology of the TiO_2 thin films was studied using AFM (NT-MDT, NTegra) in a semicontact (tapping) mode and the root mean square roughness (RMS) of the surface of the sample was calculated from the AFM scans at 3 different spots for each sample.

The wettability of TiO_2 thin films was assessed by measuring the static contact angle between the film surface and water droplet by the sessile drop technique, using Kruss FM40 Easy Drop system. The images were analyzed using the drop shape analysis software.

The chemical analysis of the films was carried out by Dispersive X-Ray Diffraction (EDAX) attachment with the scanning electron microscope (FEI, Quanta). The EDX spectrum was taken at 3000X magnification at 20.0kV, for 20 seconds.

3.2.3.2 In Vitro Cellular Characterization

The biocompatibility of the samples was assessed using the ISO10993-5 test guidelines. L929, an adherent type mouse fibroblast cell line were allowed to grow on the annealed samples for 24-96 hours and assessed for cytotoxicity using standard endpoint- tetrazolium bromide MTT assay.

Protocol:

I. Initiation of culture from frozen cells:

The culture was initiated from a flask of frozen L929 fibroblast cell lines. Frozen vial of L929 cells were taken out from the liquid nitrogen and immediately transferred to a pre warmed (37°C) water bath for thawing. The cells were then transferred to sterile centrifuge tube containing complete medium (MEM + 10% FBS + Antibiotic-Antimycotic solution (1.5 ml/100 ml of medium)) and centrifuged at 600 rpm for 10 minutes at room temperature. The supernatant was discarded & the loosely bound pellet was suspended in 5 ml of complete medium & appropriate numbers of cells were seeded in T-75 tissue culture flask, incubated in a CO_2 incubator (5% CO_2 - 95% air at high humidity) at 37°C. Initially the medium was changed post 24 hr. and subsequently at intervals of 2-3 days till sufficient growth was observed.

II. Cell viability test:

Dye exclusion test: In principle, the cells with damaged membrane allow the trypan blue dye to pass into the cytoplasm whereas undamaged cells are capable of dye exclusion. This dye exclusion method was used to see the cell viability by assessing the loss of membrane integrity. This test was done for every batch of cells before the start of experiments to ascertain that how much cells are viable in the batch specific and batches showing the cell

viability more than 95% were used for the experiments. In brief, well-mixed cell suspension (0.8 ml) was added to a test tube already containing 0.2 ml of trypan blue (0.4%) and mixed the contents by gentle shaking. In continuation, without wasting the time, 20 μl of dye-cell mixture was placed on the edge of both the chambers of the haemocytometer prefixed with the cover slip and allowed the cell suspension to fill the chambers by capillary action. The counting of unstained (viable cells) and stained cells (nonviable cells) in the four large corner squares in both counting chambers was made using a 10X microscope objective. The percent cell viability was calculated by deducting the number of all stained cells from total number of cells counted (stained cells and unstained cells) over the haemocytometer. The only batches showing more than 95% cell viability were used in further experimentation.

Plating of L929 cells: Cells were harvested by trypsinization from the flasks having the high confluency and peletted by centrifugation at 600 rpm for 5 minutes. The pellet was re-suspended in fresh culture medium and clumps were broken if any by a tip of 20 μl by up and down several times. Cells were then counted with the help of coulter electronic cell and particle counter and plated in the frequency of 10,000 cells per well in 100μl of culture medium.

Percent Cell Viability by MTT Assay: The assay was done following the method of Mosmann *et al (1983)* [87] with desired modifications. In brief, titania thin films were placed in the 24 well culture plates and then adequate numbers of cells were seeded. The cells were then allowed to grow for 12-96 h in the CO_2 incubator at 37°C. Tetrazolium (50 μl/well containing 500μl of cell suspension; 5mg/ml of stock in PBS) salt was added 4 h prior to completion the each incubation period. Then, the reaction mixture was carefully taken out and 500 μl of culture grade DMSO (Sigma St Louis, USA) was added to each well by

pipetting up & down several times until the content get homogenized. After 10 minutes, the color was read at 530 nm, using Multiwell Microplate Reader (Bio-Tek, USA). The unexposed sets were also ran parallel under identical conditions & served as basal control, whereas cells treated with manganese (10^{-4} M) were served as positive control.

3.3 Results and Discussion

3.3.1 Influence of annealing temperature on the microstructure and Wettability

The TiO$_2$ thin films deposited by DC Magnetron Sputtering and annealed at various temperatures ranging from 300°C-900°C were analysed by Glancing Angle X-Ray Diffraction (GAXRD) as regards their phase determination and grain size calculation, fig. 3.3. The scan range was kept from 20°-80°, with the scan rate at 2°/ minute and step size 0.02°. The as-deposited films and films annealed upto 700°C show tetragonal anatase phase of TiO$_2$ (2θ= 25.25°) (JCPDS card no. 86-1156). On annealing the film at 900°C, the films show mixed rutile and anatase phases, with rutile phase dominating (2θ= 27.45°) (JCPDS card no. 86-0148).
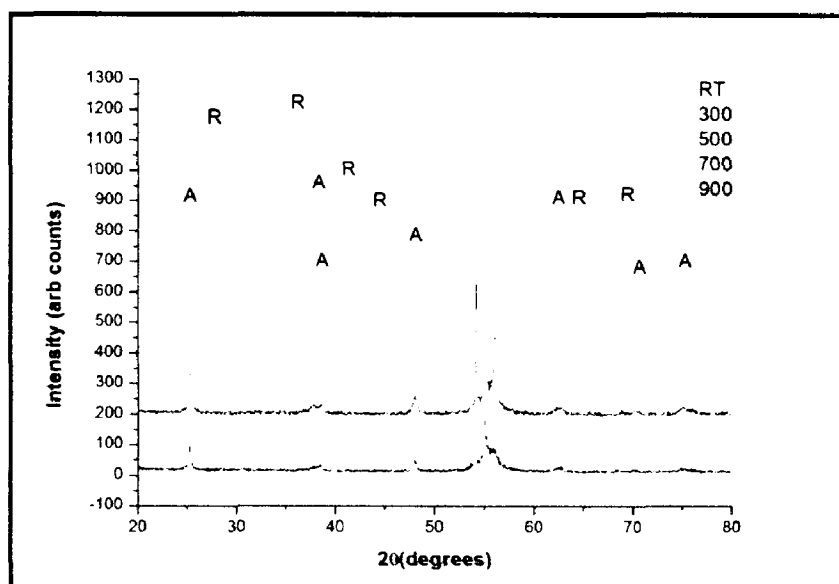
Figure 3.3: XRD pattern of the as-deposited and annealed TiO$_2$ thin films

The crystallite size was calculated according to the Scherrer Formula for each of the as-deposited and annealed films and has been tabulated in the following table 3.2

Deposition temperature (°C)	Phase Structure	Crystallite size (nm)
26	Anatase	25.25
300	Anatase	27.80
500	Anatase	28.56
700	Anatase	44.76
900	Anatase+Rutile	65.18

Table 3.2: Variation of crystallite size and phase structure of TiO₂ thin films with annealing temperature

The following graph, fig. 3.4 depicts the variation of crystallite size with the annealing temperature. As the temperature of annealing increases, the crystallite size increases.
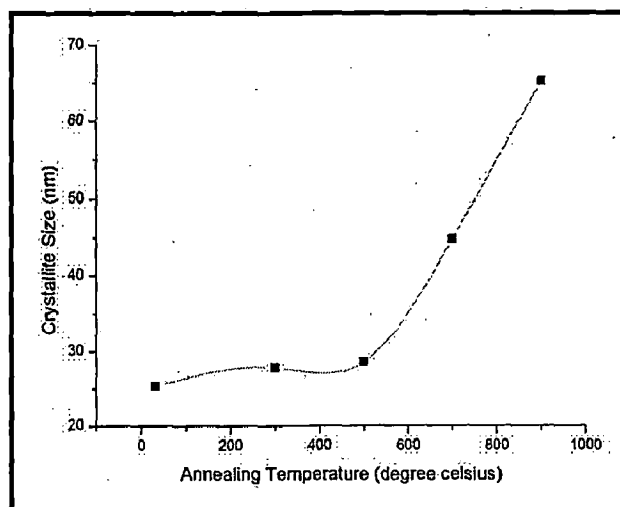
Figure 3.4: Variation in crystallite size of TiO₂ thin films with annealing temperature.

During annealing process, rearrangement of atoms occurs to form fine crystalline structure. The increase in crystallite size is small with increase in annealing temperature, at lower temperatures. However, above 500°C, there is a sharp increase in the size of the crystals formed during sputtering of titania films. Energy supplied during annealing process favours the diffusion of atoms absorbed on the substrate and accelerates the migration of atoms to the favourable energy position. The higher the annealing temperature, the higher will be energy supplied for the atoms rearrangement process. [94, 95]

The chemical analysis of the titania films annealed at different temperatures was performed using SEM-EDX. A typical EDX spectrum for TiO_2 thin films is depicted in the figure 3.5. EDX spectra were acquired from different sites of the as prepared and the annealed samples. Besides the major K silicon peak originating from the substrate, additional peaks were observed, attributed to oxygen K and Ti K as well as Ti L ones (figure 3.5). EDX spectra of all investigated samples have revealed the presence of titanium and oxygen atoms in the thin layers and thus formation of TiO2 thin films was confirmed. On the basis of comparing the intensities of O and Ti K peaks of as-prepared and annealed samples, the effect of annealing on oxygen concentration in thin layers can be determined. Post-deposition annealing has affected the oxygen concentration very slightly, as can be seen from the figure 3.6, where atomic percentages of Ti and O have been plotted as a function of the annealing temperature.
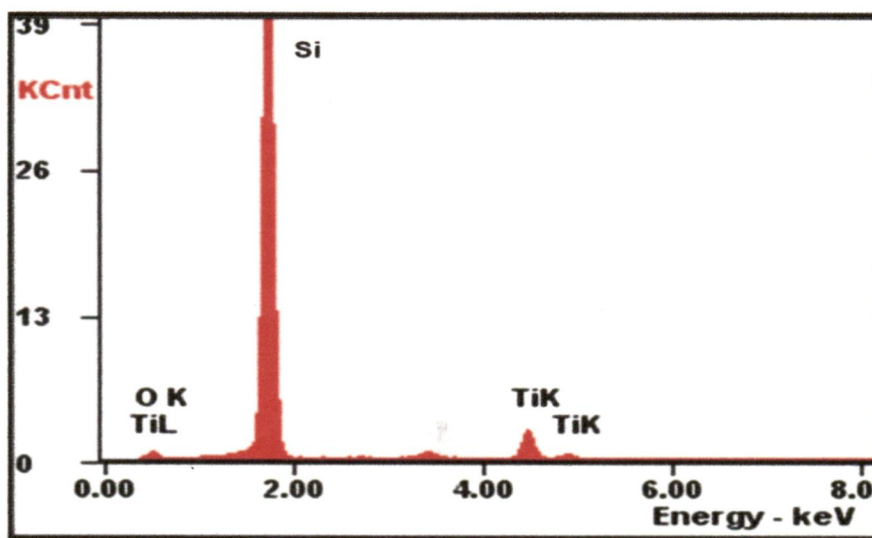
Figure 3.5: Typical EDX spectrum of TiO₂ thin films

Exact determination of Ti:O ratio is not possible since the examined TiO_2 layers are too thin and thus only a small amount of the signal acquired by EDX is attributed to the TiO_2 layer, while a major part of the signal comes from the silicon substrate.

The roughness of the films was analyzed using AFM. The average grain size calculated using AFM was found to be in good agreement with the XRD results. The roughness increases with annealing temperature. The root-mean-square (RMS) average roughness of the TiO_2 surfaces was calculated for a 2 x 2 μm square scan area. The roughness of the as-deposited film (RMS: 3.867 nm) was less than that annealed at 300°C (RMS: 4.72875 nm), which was progressively less than those annealed at higher temperatures.
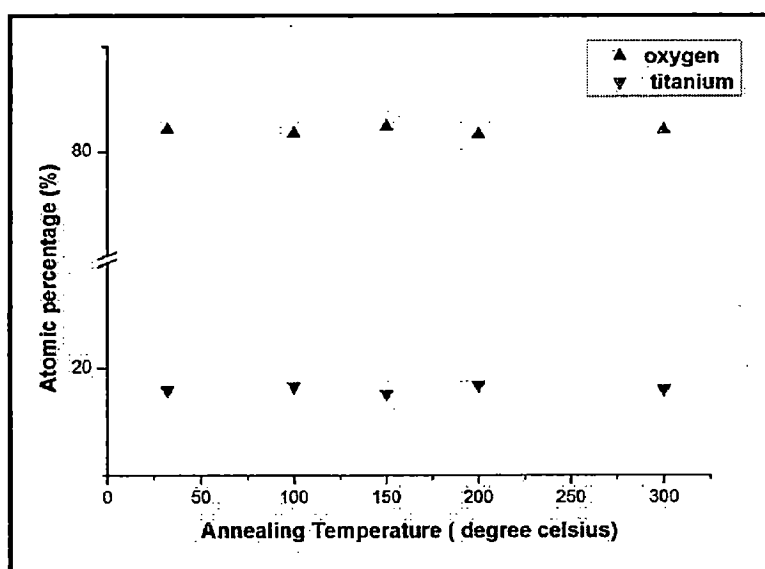
Figure 3.6: Variation of atomic percentages of Ti and O in as deposited and annealed titania films.

The variation of the RMS values with temperature is listed in the table 3.3 and graphically presented in fig. 3.7. The 2D and 3D images of the thin films are presented in the fig. 3.8.

The wettability of the samples was also measured using sessile drop method. Wettability at the surface of an implant material plays a key role in its success as it modulates the protein adsorption and thereby influences cell attachment and tissue integration at the interface. The TiO_2 surfaces show hydrophilic nature, which increases with increasing annealing temperature, as shown in the table 3.3.

Annealing Temperature (°C)	RMS Roughness (nm)	Contact Angle (°)
26	3.86769	75.2±2.15
300	4.72875	71.4±2.15
500	5.50338	62.8±2.15
700	6.32331	61.1±2.15
900	13.3727	42.9±2.15

Table3.3: Variation of Root Mean Square Roughness and Contact Angle of titania thin films with annealing temperature.

The receding values of contact angle with increasing temperature are tabulated graphically in the figure 3.7.
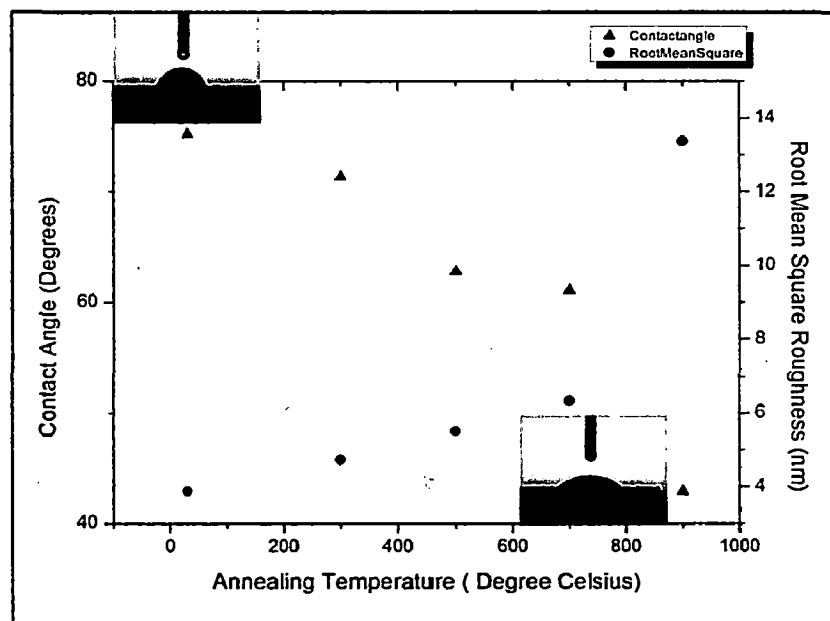
Figure 3.7: Variation of Contact Angle and Root Mean Square Roughness with annealing temperature

Thermo-induced hydrophilicity can be explained in the following three aspects: (1) the cleansing effect, (2) the crystal phase transition. First, the annealing can remove superficial organic contaminants to expose the TiO_2 films to the adsorbent water molecules. Second, the annealing would induce crystal phase transition from amorphous
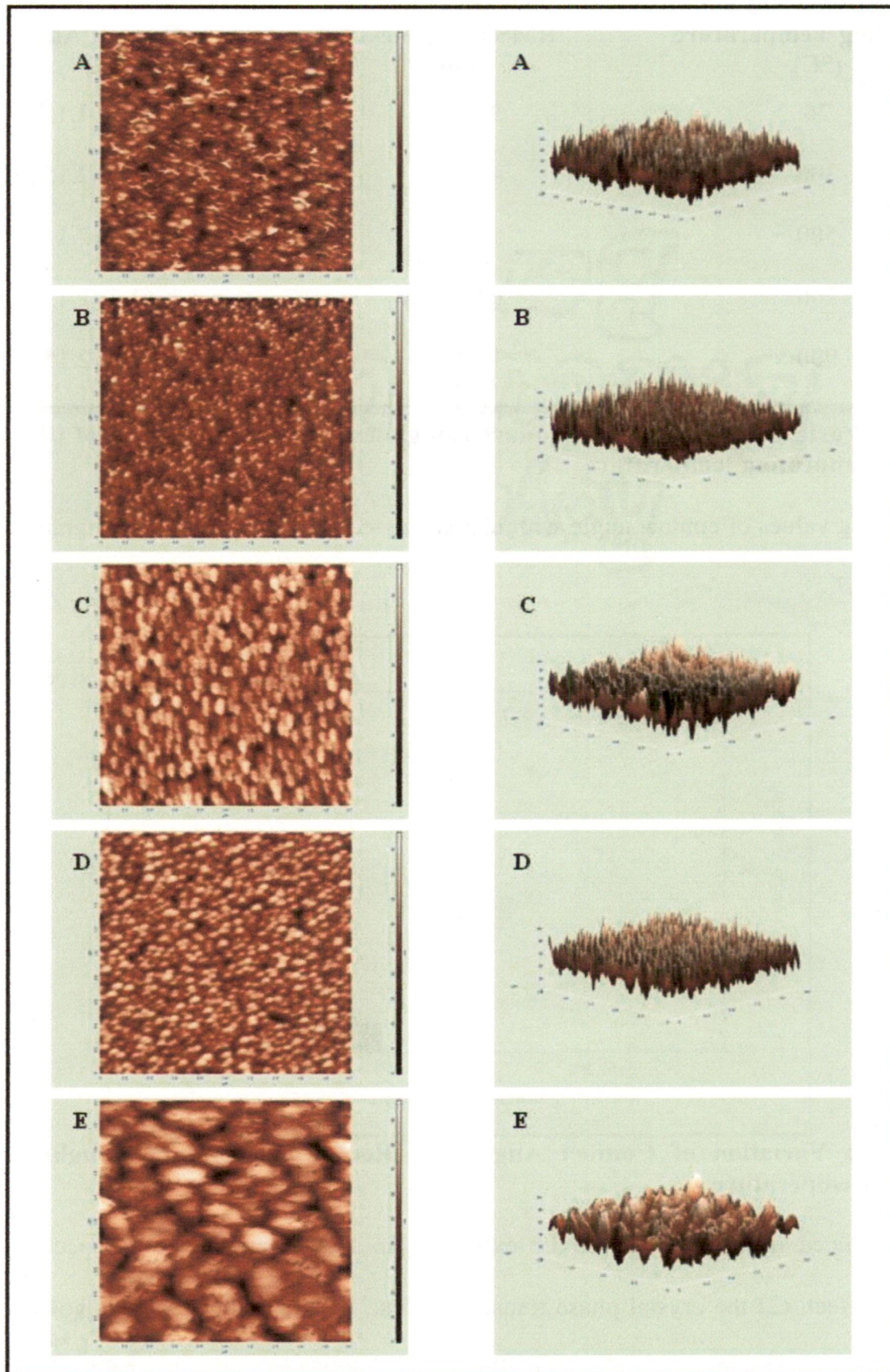
Figure 3.8: 2D and 3D AFM image of TiO$_2$ thin films at different annealing temperatures., (A) Room Temperature, (B) 300°C, (C) 500°C, (D) 700°C, (E) 900°C.

structure to anatase structure or rutile structure, so that the hydrophilicity of the films gets a dramatic change. [96]

The TiO_2 thin films were then tested for biocompatibility. The in vitro cellular test was carried out using L929 fibroblast cell line according to the ISO10993-5 test guidelines. Cells were allowed to grow on test material for the period of 24-96 h and assessed for cytotoxicity using standard endpoint- tetrazolium bromide MTT assay. All the test samples were found to be non-cytotoxic to mouse fibroblast cells- L929 when exposed for a period of 24-96 h. However, in first 12 h of exposure, cells showed a cytostatic response i.e., physiological stress, which recovers by 24 h onwards. In general, TiO_2 thin films were found to be safe to biological material under our experimental conditions. The as-deposited samples and those annealed at lower temperatures, however, demonstrated better response towards the fibroblasts. The readings were performed in triplicate. The results of the in vitro cellular test are depicted in the following figure 3.9.
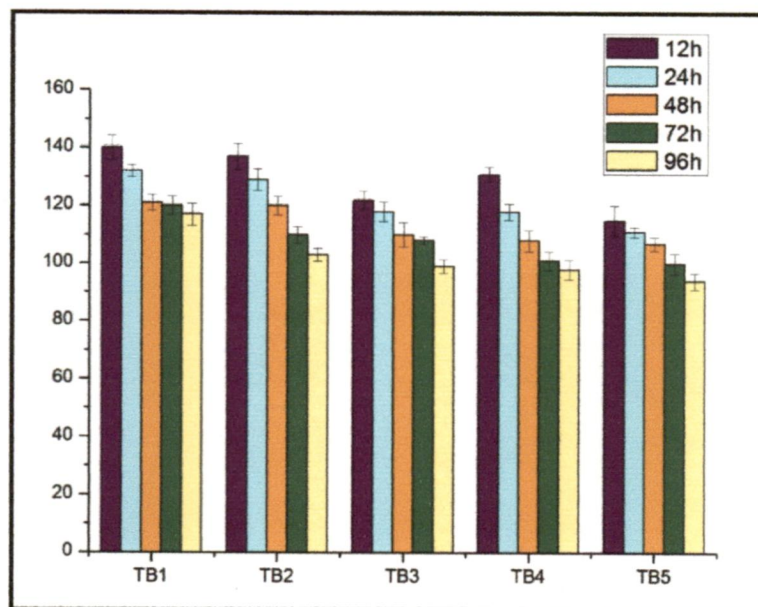
Figure 3.9: In vitro cellular test of the as deposited and annealed TiO_2 thin films annealed at different temperatures (TB1: as deposited; TB2: annealed at 300°C; TB3: annealed at 500°C; TB4: annealed at 700°C and TB5: annealed at 90°C), using the L929 fibroblast cell cultures.

Chapter 4

Synthesis &

Characterization of ZnO

Coatings

4.1 Introduction to Antimicrobial ZnO coatings

Hip or knee replacements, fracture fixation, ligament and tendon reconstruction and other surgical implant procedures have in recent years become valid and extremely common procedures to restore the function of affected joints, fractured bone segments and impaired limbs. In the US alone, total hip and knee arthroplasties currently accounts for over half a million interventions each year. [42] In light of this enormous population of patients with orthopedic implants, even a currently low risk of infection, estimated to be in the range of 0.5–5% for total joint replacements (less than 1–2% in institutions with highly trained surgeons), has to be considered very relevant for its serious consequences. During the first 2 years following the interventions of total knee arthroplasty, infections have variously been reported as the second main cause of revision just after instability. [43, 44]

Simple debridement procedures with retention of prosthesis and chemotherapy with antimicrobial agents are treatments that are not always effective on infections that are already established. Sometimes prosthesis removal and replacement, when not even joint fusion, represent the only salvage option to definitively eradicate severe infections. These drastic interventions bear obvious implications in terms of attendant patient trauma, prolonged hospitalization as well as in terms of health and social costs. Furthermore, following revision surgery there is also a significantly high risk (up to 10%) of a recidive and implant replacement, which has additionally to be taken into consideration. In the strategy for the prevention of infections, much has been done to improve the operating standards, minimize the possibility of contamination during surgery, reduce the establishment of infection by peri-operative antibiotic prophylaxis, and confine pathogenic strains by patient isolation. Along these directions further improvements can still be made, but little advancements in terms of

decreased infection rates are being expected in return of this type of efforts. As a consequence, over the last 15 years, increasing attention has progressively been focused on the epidemiology and the pathogenesis of the infections, especially those associated to implant materials, in order to build knowledge and gain better control over this phenomenon. [16]

Antibacterial agents can be divided into two categories according to their chemical composition: inorganic and organic agents. Many shortcomings of organic antibacterial agents have limited their application, such as low heat resistance, high decomposability and short life expectancy. As a result, inorganic antibacterial agents have received more and more recognition in the antibacterial product market. Among the inorganic antibacterial agents, silver containing materials are representatives. For a long time, discoloration caused by the reduction of silver ions to metallic silver has been considered a common problem for antibacterial agents containing silver ions [6]. As an alternative, certain new types of non-silver-containing inorganic antibacterial agents, based on zinc oxide whisker (ZnOw) and nanoparticles have been introduced, which theoretically will not cause discoloration. [46]

Crystalline ZnO is a semiconductor and a piezoelectric material with a gap energies of about 3.3 eV, which is very close to that of TiO2 anatase. ZnO NPs are believed to be nontoxic, biosafe, and biocompatible and have been used in many applications in daily life, such as drug carriers and in cosmetics and fillings in medical materials. ZnO NPs are versatile in that they have achievable applications in biosensors, biogenerators, bioelectrodes, electroluminescent devices and ultraviolet laser diodes. Zinc oxide (ZnO) is listed as "generally recognized as safe" (GRAS) by the U.S. Food and Drug Administration (21CFR182.8991).

Structure and properties

ZnO is a II–VI compound semiconductor whose ionicity resides at the borderline between the covalent and ionic semiconductors. The crystal structures shared by ZnO are wurtzite, zinc blende, and rocksalt (or Rochelle salt) as schematically shown in Figure 4.1
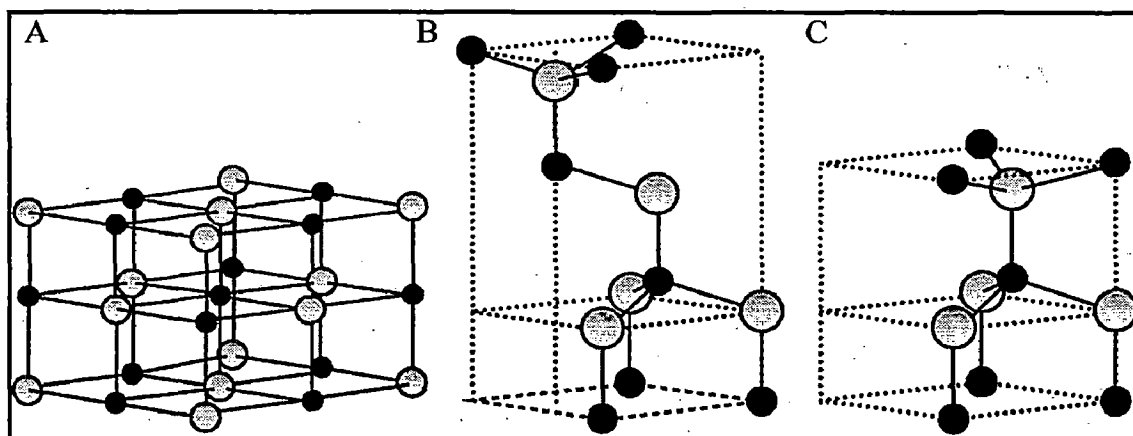
Figure 4.1: Stick and ball representation of ZnO structures, (A) cubic Rock Salt, (B) cubic Zinc Blende, and (C) hexagonal Wurtzite., Grey sphere- zinc; black-oxygen atoms.

The lattice constants mostly range from 3.2475 to 3.2501Å for the a-parameter and from 5.2042 to 5.2075Å for the c-parameter. The c/a ratio varies in a slightly wider range, from 1.593 to 1.6035.

ZnO is widely used in thin-film form deposited on non-native substrates. Therefore, the material quality, actually properties in general, of the ZnO films depends on the properties of the substrates used. Especially, the lattice parameters and thermal expansion coefficients of these substrates are extremely important since reduction of strain and dislocation density in ZnO thin films is the main objective, and substrates with parameters similar to those of ZnO are favourable in this context. [45]

Mechanism:

ZnO nanoparticles have been shown to have a wide range of antibacterial activities against both Gram-positive and Gram-negative bacteria, including major foodborne pathogens

like *Escherichia coli* O157:H7, *Salmonella,Listeria monocytogenes,* and *Staphylococcus aureus* [47, 48]. Nano-sized particles of ZnO have more pronounced antimicrobial activities than large particles, since the small size (less than 100 nm) and high surface-to-volume ratio of nanoparticles allow for better interaction with bacteria. Recent studies have shown that these nanoparticles have selective toxicity to bacteria but exhibit minimal effects on human cells [49].

To make better use of ZnO nanoparticles in healthcare and to assist in the development of powerful, but nontoxic, antimicrobial derivatives, it is necessary to understand the mechanism of action of ZnO nanoparticles against bacteria, but to date, the process underlying their antibacterial effect is not clear. However, a few studies have suggested that the primary cause of the antibacterial function might be from the disruption of cell membrane activity. Another possibility could be the induction of intercellular reactive oxygen species, including hydrogen peroxide (H_2O_2), a strong oxidizing agent harmful to bacterial cells. [47] It has also been reported that ZnO can be activated by UV and visible light to generate highly reactive oxygen species such as OH^-, H_2O_2, and O_2^{2-}. The negatively charged hydroxyl radicals and superoxides cannot penetrate into the cell membrane and are likely to remain on the cell surface, whereas H_2O_2 can penetrate into bacterial cells. [50] The generation of highly reactive species such as OH^-, H_2O_2 and O_2^{2-} is explained as follows. Since ZnO with defects can be activated by both UV and visible light, electron-hole pairs (e^-h^+) can be created. The holes split H_2O molecules (from the suspension of ZnO) into OH^- and H^+. Dissolved oxygen molecules are transformed to superoxide radical anions ($\cdot O_2^-$), which in turn react with H^+ to generate ($HO_2 \cdot$) radicals, which upon subsequent collision with electrons produce hydrogen peroxide anions (HO_2^-). They then react with hydrogen ions to

produce molecules of H_2O_2. The generated H_2O_2 can penetrate the cell membrane and kill the bacteria. [50]

$$ZnO + h\nu \longrightarrow e^- + h^+; \ h^+ + H_2O \longrightarrow \cdot OH + H^+.$$

$$e^- + O_2 \longrightarrow \cdot O_2^-; \ \cdot O2 + H^+ \longrightarrow HO_2 \cdot$$

$$HO_2 \cdot + H^+ + e^- \longrightarrow H_2O_2$$
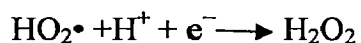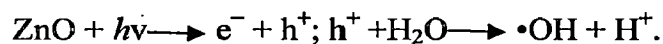
Since, the hydroxyl radicals and superoxides are negatively charged particles, they cannot penetrate into the cell membrane and must remain in direct contact with the outer surface of the bacteria; however, H_2O_2 can penetrate into the cell. [51]

4.2 Experimental details

4.2.1 Synthesis of ZnO films on Si(100) substrates

The ZnO thin films were deposited by Reactive Rf Magnetron sputtering on Silicon Si(100) substrates (10mm x 10mm) from a 99.99% pure zinc target (2' diameter and 5 mm thick). The substrate was cleaned by ultrasonication in acetone for 15 minutes to remove any traces of impurities and then dried in air. The base pressure was better than 2×10^{-6} Torr and the sputtering was carried out in mixed Argon: Oxygen (20:80) atmosphere. The ambient gas pressure during the process was kept at 20mTorr. Before the actual experiment, the target was pre-sputtered for 15 minutes to remove the impurities on the surface. The target-substrate distance 60mm, the gun length 250mm and the deposition time 120 minutes were kept constant for all depositions. Sputtering was carried out at 80W at room temperature. The sputtering parameters for ZnO films are listed in Table 4.1

Target	Zinc
Base Pressure	2×10^{-6} Torr
Sputtering Pressure	20 mTorr
Gas Used	Argon+ Oxygen(20:80)
Sputtering Power	80W
Substrate temperature	Room temperature
Sputtering Time	120 minutes
Substrate used	Silicon Si(100)

Table 4.1: Sputtering parameters for ZnO films

4.2.2 Annealing of ZnO thin films

The as deposited ZnO thin films were annealed in an open air tubular furnace (Lenton LTF 14/50/450) at temperatures 300°C, 500°C, 700°C, 900°C for one hour at a constant ramp rate of 10°C/minute.

4.2.3 Characterization

4.2.3.1 Microstructural Analysis

The as deposited and the annealed films were characterized by XRD (Bruker AXS, D8 Advance) with CuKα (1.54 Å) radiation for the phase, grain size measurement and texture analysis. The excitation voltage and current were set to 40kV and 30mA respectively, in the diffractometer. The scan rate used was 0.02°/minute and the scan range was 20° to 80°. The grain size of the films was estimated from the Scherrer's formula (*Cullity et al. 2001*), given by the equation:

$$t = 0.9\lambda / B\cos\theta,$$

The grain size t is along the surface normal direction, B(crystallite) is the corrected full-width half maximum (FWHM) of a Bragg's peak, λ is the wavelength of X-ray and θ is the Bragg's angle. The grain size was calculated using the preferred orientation of the XRD peaks of the ZnO films on the Si substrate.

The surface morphology of the ZnO thin films was studied using AFM (NT-MDT, NTegra) in a semicontact (tapping) mode and the root mean square roughness (RMS) of the surface of the sample was calculated from the AFM scans at 3 different spots for each sample.

The wettability of TiO_2 thin films was assessed by measuring the static contact angle between the film surface and water droplet by the sessile drop technique, using Kruss FM40 Easy Drop system. The images were analyzed using the drop shape analysis software.

The chemical analysis of the film was carried out by Dispersive X-Ray Diffraction (EDAX) attachment with the scanning electron microscope (FEI, Quanta). The EDX spectrum was taken at 3000X magnification at 20.0kV, for 20 seconds.

4.2.3.2 In Vitro Cellular Test

The biocompatibility of the samples was assessed using the ISO10993-5 test guidelines. L929, an adherent type mouse fibroblast cell line were allowed to grow on the annealed samples for 24-96 hours and assessed for cytotoxicity using standard endpoint- tetrazolium bromide MTT assay.

Protocol:

III. **Initiation of culture from frozen cells:**

The culture was initiated from a flask of frozen L929 fibroblast cell lines. Frozen vial of L929 cells were taken out from the liquid nitrogen and immediately transferred to a pre warmed (37°C) water bath for thawing. The cells were then transferred to sterile centrifuge tube containing complete medium (MEM + 10% FBS + Antibiotic-Antimycotic solution (1.5 ml/100 ml of medium)) and centrifuged at 600 rpm for 10 minutes at room temperature. The supernatant was discarded & the loosely bound pellet was suspended in 5 ml of complete medium & appropriate numbers of cells were seeded in T-75 tissue culture flask, incubated in a CO_2 incubator (5% CO_2 - 95% air at high humidity) at 37°C. Initially the medium was changed post 24 hr. and subsequently at intervals of 2-3 days till sufficient growth was observed.

IV. **Cell viability test:**

Dye exclusion test: In principle, the cells with damaged membrane allow the trypan blue dye to pass into the cytoplasm whereas undamaged cells are capable of dye exclusion. This dye exclusion method was used to see the cell viability by assessing the loss of membrane integrity. This test was done for every batch of cells before the start of experiments to ascertain that how much cells are viable in the batch specific and batches showing the cell

viability more than 95% were used for the experiments. In brief, well-mixed cell suspension (0.8 ml) was added to a test tube already containing 0.2 ml of trypan blue (0.4%) and mixed the contents by gentle shaking. In continuation, without wasting the time, 20 μl of dye-cell mixture was placed on the edge of both the chambers of the haemocytometer prefixed with the cover slip and allowed the cell suspension to fill the chambers by capillary action. The counting of unstained (viable cells) and stained cells (nonviable cells) in the four large corner squares in both counting chambers was made using a 10X microscope objective. The percent cell viability was calculated by deducting the number of all stained cells from total number of cells counted (stained cells and unstained cells) over the haemocytometer. The only batches showing more than 95% cell viability were used in further experimentation.

Plating of L929 cells: Cells were harvested by trypsinization from the flasks having the high confluency and peletted by centrifugation at 600 rpm for 5 minutes. The pellet was re-suspended in fresh culture medium and clumps were broken if any by a tip of 20 μl by up and down several times. Cells were then counted with the help of coulter electronic cell and particle counter and plated in the frequency of 10,000 cells per well in 100μl of culture medium.

Percent Cell Viability by MTT Assay: The assay was done following the method of Mosmann *et al (1983)* [87] with desired modifications. In brief, ZnO thin films were placed in the 24 well culture plates and then adequate numbers of cells were seeded. The cells were then allowed to grow for 12-96 h in the CO_2 incubator at 37°C. Tetrazolium (50 μl/well containing 500μl of cell suspension; 5mg/ml of stock in PBS) salt was added 4 h prior to completion the each incubation period. Then, the reaction mixture was carefully taken out and 500 μl of culture grade DMSO (Sigma St Louis, USA) was added to each well by

pipetting up & down several times until the content get homogenized. After 10 minutes, the color was read at 530 nm, using Multiwell Microplate Reader (Bio-Tek, USA). The unexposed sets were also ran parallel under identical conditions & served as basal control, whereas cells treated with manganese (10^{-4} M) were served as positive control.

4.1   Results and Discussion

The ZnO thin films deposited by Rf Magnetron Sputtering and annealed at various temperatures ranging from 300°C-900°C were analysed by Glancing Angle X-Ray Diffraction (GAXRD) as regards their phase determination and grain size calculation. The scan range was kept from 20°-80°, with the scan rate at .02°/ minute and step size 0.02°. The as-deposited films show a slightly amorphous and polycrystalline nature. Annealing treatment of the films produces peaks mainly from the (100), (002) and (101) planes of the hexagonal wurtzite ZnO lattice. (JCPDS card no. 80-075). The crystallization of ZnO in the Wurtzite phase is improved, as it results from the increasing of the intensity of the diffraction lines with increasing annealing temperature. The results are in accordance to those published earlier by Li et.al. [66] The corresponding XRD patterns are shown in figure 4.2.
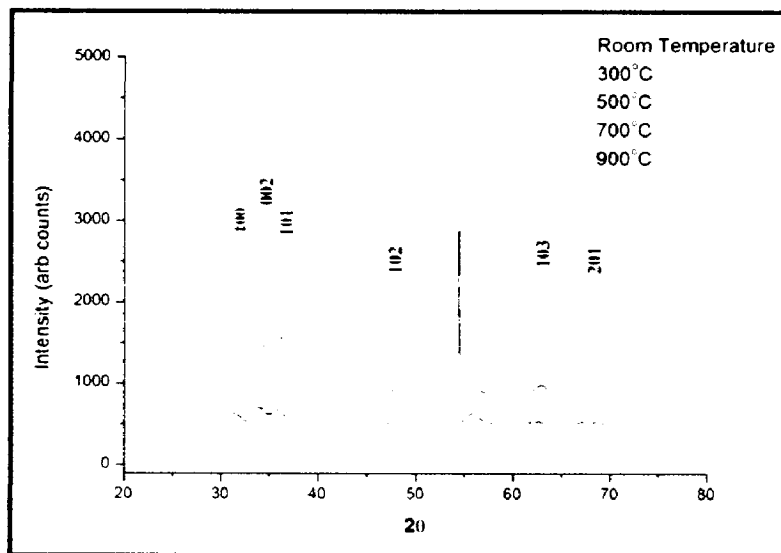
Figure 4.2: X-Ray Diffraction pattern of as deposited and annealed ZnO thin films on Si substrate.

The crystallite size was calculated according to the Scherrer Formula for each of the as-deposited and annealed films and has been tabulated in the following table 4.2

Deposition temperature (°C)	Phase Structure	Crystallite size (nm)
26	Amorphous	--
300	Wurtzite	10.17
500	Wurtzite	13.37
700	Wurtzite	14.15
900	Wurtzite	42.59

Table 4.2: Variation of crystallite size and phase structure of ZnO films with annealing temperature

The following graph, fig. 4.3 depicts the variation of crystallite size with the annealing temperature. As the temperature of annealing increases, the crystallite size increases.
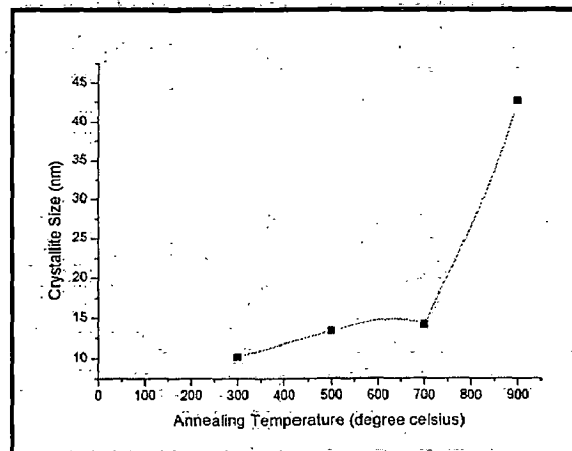
Figure 4.3: Variation in crystallite size of ZnO thin films with annealing temperature

During annealing process, rearrangement of atoms occurs to form fine crystalline structure. The as deposited film with a very small crystallite size, effectively represent amorphous coatings. The increase in crystallite size is small with increase in annealing temperature, at lower temperatures. However, above 700°C, there is a sharp increase in the size of the crystals formed during sputtering of zinc oxide films. Energy supplied during annealing process favours the diffusion of atoms absorbed on the substrate and accelerates the

migration of atoms to the favourable energy position. The higher the annealing temperature, the higher will be energy supplied for the atoms rearrangement process. [95, 96]

The chemical analysis of the zinc oxide films annealed at different temperatures was performed using SEM-EDX. A typical EDX spectrum for ZnO thin films is depicted in the figure 4.4. EDX spectra were acquired from different sites of the as prepared and the annealed samples. Besides the major K silicon peak originating from the substrate, additional peaks were observed, attributed to oxygen K and Zn K as well as Zn L ones (figure 4.4). EDX spectra of all investigated samples have revealed the presence of zinc and oxygen atoms in the thin layers and thus formation of ZnO thin films was confirmed. On the basis of comparing the intensities of O and Zn K peaks of as-prepared and annealed samples, the effect of annealing on oxygen concentration in thin layers can be determined. Post-deposition annealing has affected the oxygen concentration very slightly, as can be seen from the fig. 4.5, where atomic percentages of Zn and O have been plotted as a function of the annealing temperature.
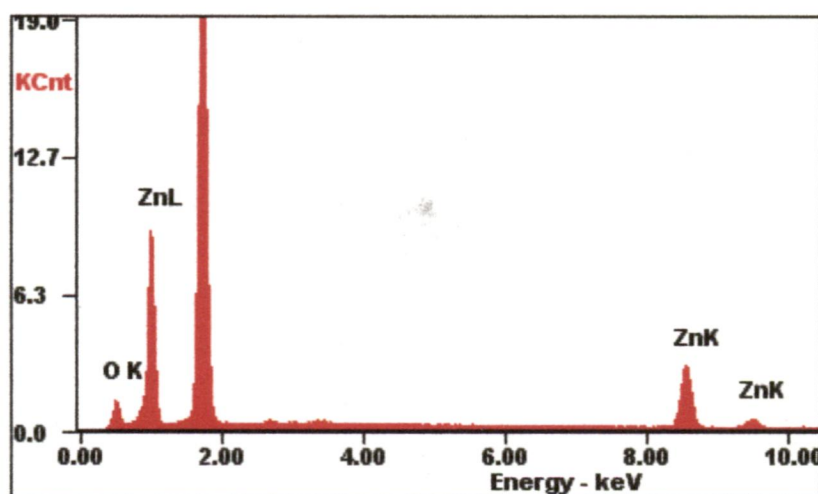
Figure 4.4: Typical EDX spectrum of ZnO thin films
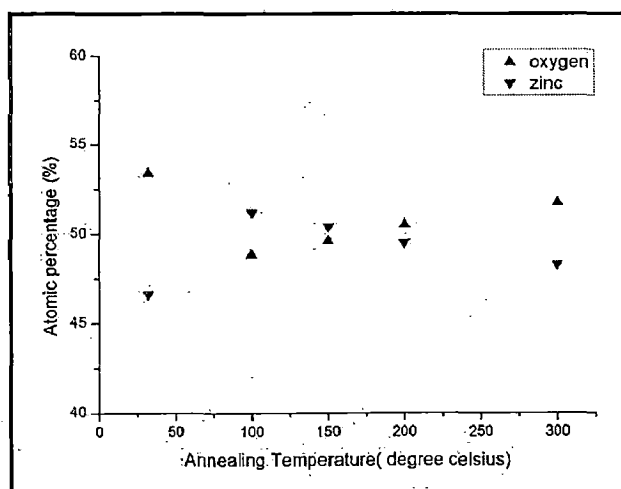
Figure 4.5: Variation of atomic percentages of Zn and O in as deposited and annealed ZnO films.

The roughness of the films was analyzed using AFM. The average grain size calculated using AFM was found to be in good agreement with the XRD results. The roughness increases with annealing temperature. The root-mean-square (RMS) average roughness of the ZnO surfaces was calculated for a 2 x 2 µm square scan area. After acquiring the AFM images, they were subjected to a flattening procedure using the NOVA image processing software. The roughness of the as-deposited film (RMS: 6.50nm) was less than that annealed at 300°C (RMS: 8.50 nm), which was progressively less than those annealed at higher temperatures. The variation of the RMS values with temperature is listed in the table 4.3 and graphically presented in figure 4.6. The 2D and 3D images of the thin films are presented in the figure4.7. The wettability of the samples was also measured using sessile drop method. Wettability at the surface of an implant material plays a key role in its success as it modulates the protein adsorption and thereby influences cell attachment and tissue integration at the interface. The ZnO surfaces show hydrophobic nature.

Annealing Temperature (°C)	RMS Roughness (nm)	Contact Angle (°)
26	6.50	104.2±2.15
300	8.50	103.3±2.15
500	8.90	101.0±2.15
700	9.40	99.9±2.15
900	10.21	99.8±2.15

Table 4.3: Variation of Root Mean Square Roughness and Contact Angle of ZnO thin films with annealing temperature

However, with increasing annealing temperature, the contact angle recedes, as shown in the table 4.3. The receding values of contact angle with increasing temperature are tabulated graphically in the figure 4.6.

Thermo-induced hydrophilicity can be explained in the following three aspects: (1) the cleansing effect, (2) the crystal phase transition. First, the annealing can remove superficial organic contaminants to expose the ZnO films to the adsorbent water molecules. Second, the annealing induces crystal phase transition from amorphous structure to polycrystalline, so that the hydrophilicity of the films gets a dramatic change.

The ZnO thin films were then tested for biocompatibility. The in vitro cellular test was carried out using L929 fibroblast cell line according to the ISO10993-5 test guidelines. Cells were allowed to grow on test material for the period of 24-96 h and assessed for cytotoxicity using standard endpoint- tetrazolium bromide MTT assay. All the test samples were found to be non-cytotoxic to mouse fibroblast cells- L929 when exposed for a period of 24-96 h. However, in first 12 h of exposure, cells showed a cytostatic response i.e., physiological stress, which recovers by 24 h onwards.
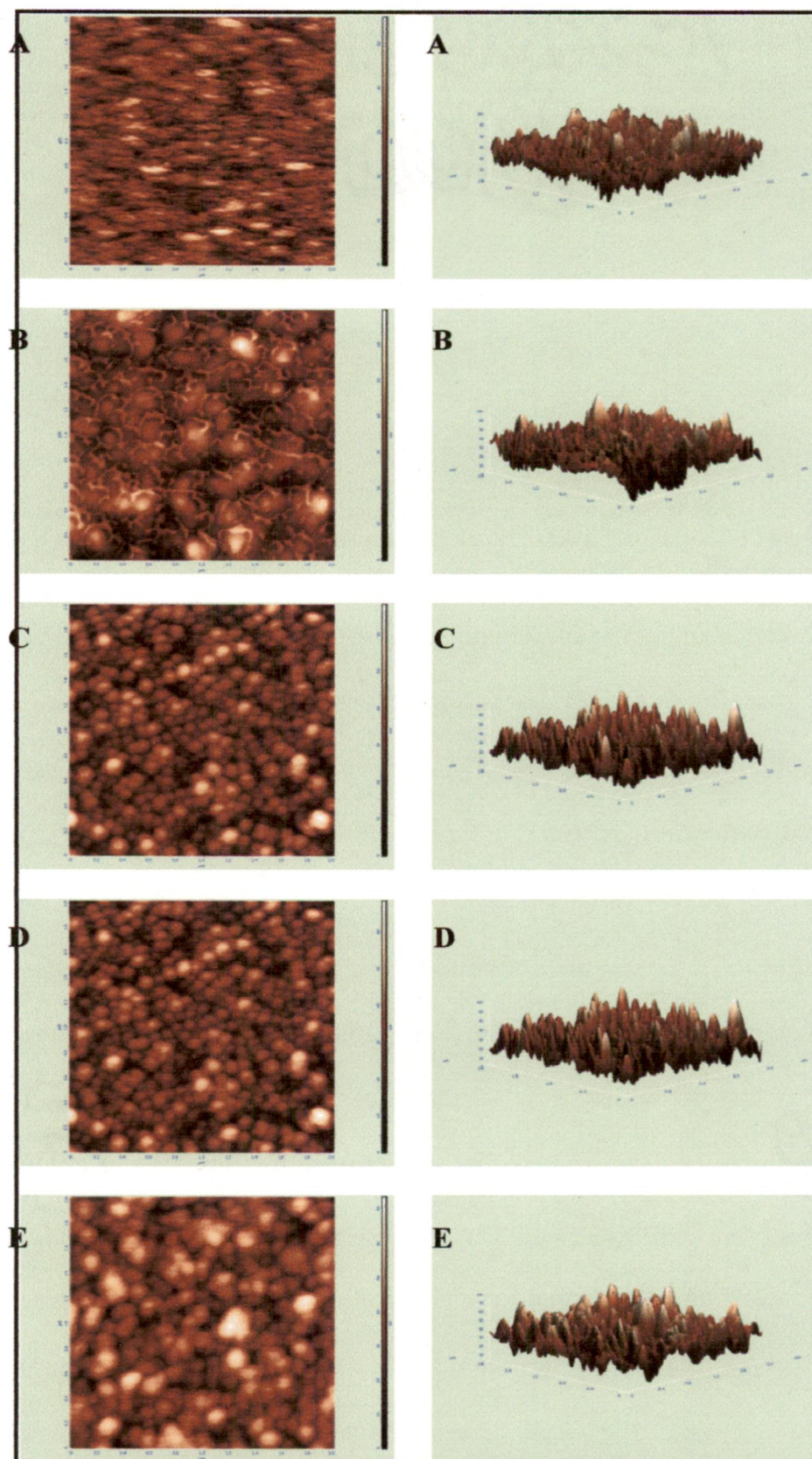
Figure 4.7: 2D and 3D AFM images of the ZnO thin films at different annealing temperatures. (A) Room Temperature, (B) 300C, (C) 500C, (D) 700C, (E) 900C.
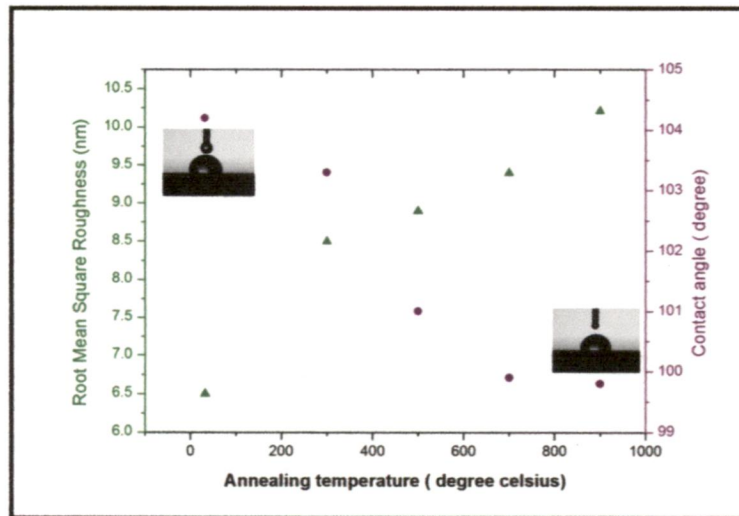
Figure 4.6: Variation of root mean square roughness and contact angle with annealing temperature for ZnO thin films

In general, ZnO thin films were found to be safe to biological material under our experimental conditions. The as-deposited samples and those annealed at lower temperatures, however, demonstrated better response towards the fibroblasts. The readings were performed in triplicate. The results of the in vitro cellular test are depicted in the following fig. 4.7.
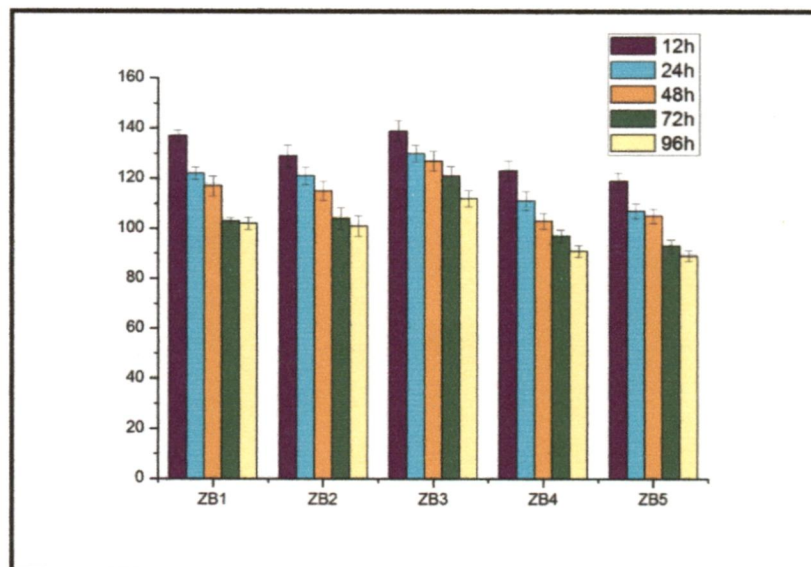
Figure 4.8: In vitro cellular test of the as deposited and annealed ZnO thin films annealed at different temperatures (ZB1: as deposited; ZB2: annealed at 300°C; ZB3: annealed at 500°C; ZB4: annealed at 700°C and ZB5: annealed at 900°C), using the L929 fibroblast cell cultures.

Chapter 5

Synthesis &

Characterization of TiO2-

ZnO Coatings

5.1 Introduction to ZnO: TiO_2 Composite Coatings

Zinc titanates have been used as white color pigment and as catalytic sorbents for the desulfurization of hot coal gases. They have a wide range of applications such as solid oxide fuel cell, sensors, thermoelectric materials, microwave dielectric materials and high performance catalysts. Levy suggested five compounds in the ZnO–TiO_2 system: zinc orthotitanate (Zn_2TiO_4), zinc metatitanate ($ZnTiO_3$), $Zn_3Ti_2O_7$, $ZnTi_3O_7$, and $Zn_4Ti_5O_{14}$. However, only three compounds were confirmed to exist in the later studies: Zn_2TiO_4, $ZnTiO_3$, and $Zn_2Ti_3O_8$. Zn_2TiO_4 has a face-centered cubic crystal structure, with a lattice parameter of $a = 0.8460(2)$ nm (a-form). $ZnTiO_3$ has a rhombohedral structure, with lattice parameters of $a = 0.5078(7)$ nm and $c = 1.3927(1)$ nm, and decomposes to Zn_2TiO_4 and TiO_2 when heated at temperatures of $T \square 945°C$. The existence of metastable $Zn_2Ti_3O_8$ was confirmed in 1961; it also decomposes to Zn_2TiO_4 and TiO_2 at $T \square 945°C$, similar to $ZnTiO_3$. $Zn_2Ti_3O_8$ has a simple cubic structure, with a lattice parameter of $a = 0.8390(5)$ nm, and has been observed to be a low-temperature form of $ZnTiO_3$ that exists at $T \square 820°C$. [52, 53]

Compunds in the system ZnO-TiO_2

Although many intermediate compounds have been discussed in the literature, only the orthotitanate (Zn_2TiO_4) and the metatitanate ($ZnTiO_3$) were encountered as stable phases in this investigation.
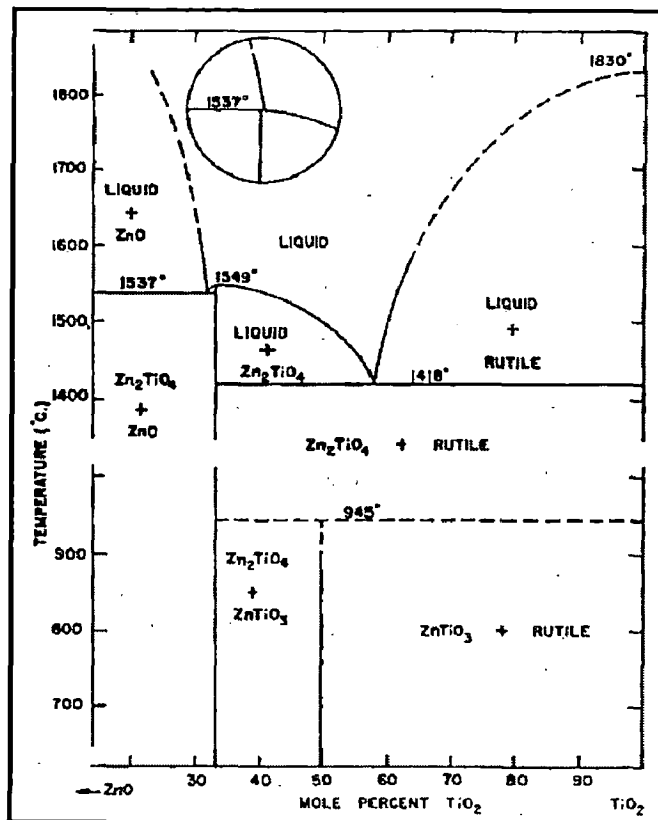
Figure 5.1: The system ZnO-TiO₂ (Adapted from [53])

TiO_2 and ZnO, both are sensitive to formation of lattice defects. Hence, there is also a possibility of formation of solid solutions and compounds in this system. Lattice imperfections could promote interesting solid-state reactions and alter the equilibrium relations between the pure oxides.

Ti doped ZnO coatings have been synthesised by several methods as hydrothermal method, thermal oxidation, CVD, cathodic vacuum arc technique, spray pyrolysis and magnetron sputtering etc. in an attempt to study their structural, optical and electrical properties. Among these methods, sputtering has advantages of good uniformity, high process controllability, and large-area deposition. The properties of TZO films are generally dependent on sputtering parameters such as substrate temperature, working pressure, type of substrate, and ambient gas. The reason why Ti doped ZnO thin films have generated such a large volume of interest

among researchers lies in their use in optoelectronic devices like solar cells, LEDs, flat panel displays, etc. Although Sn-doped In2O3 (ITO) films are also extensively utilized, they still have some disadvantages such as their high cost and their toxicity. ZnO films on the other hand have the absence of toxicity, lower cost, and good thermal stability.

ZnO films with a hexagonal wurtzite structure have a wide optical energy gap (around 3.3 eV) [7]. Although the electrical characteristics of non-doped ZnO films are primarily dominated by electrons generated by oxygen vacancies and Zn interstitial atoms, they are not very stable in the long term. For example oxygen chemisorption or desorption cause the electrical resistivity of non-doped ZnO films can degenerate [8]. Compared with non-doped ZnO films, impurity-doped ZnO films have the advantages of lower electrical resistivity and better stability. In order to create free electrons and enhance ntype conductivity, the doping cation should be smaller than or equal to the diameter of the host ion, and should have a higher valence than the host ion. Impurity-doped ZnO films, with their good electrical and optical properties, are a promising alternative to replace ITO films for transparent electrode applications. the ionic radius of titanium (6.8 A $^\circ$) is smaller than that of zinc (7.4 A $^\circ$), which means that it becomes Ti4+ when Zn2+ is substituted into the ZnO films. This in turn acts as a donor by providing two free electrons.[108-113]

However, to the best of my knowledge, after an extensive literature survey, the use of such ZnO: TiO2 doped thin films for biomedical purposes remains largely unexplored, despite the extremely potent biological properties displayed by both the oxides. Hence it presents a hugely exciting and competitive area.

5.2 Experimental details

5.2.1 Synthesis of ZnO-TiO$_2$ nanocomposite films on Si(100) substrates.

The ZnO-TiO$_2$ nanocomposite thin films were deposited by Reactive Magnetron co-sputtering on Silicon Si (100) substrates (10mm x 10mm) from 99.99% pure zinc and titanium targets (2" diameter and 5 mm thick). The substrate was cleaned by ultrasonication in acetone for 15 minutes to remove any traces of impurities and then dried in air. The base pressure was better than 2×10^{-6} Torr and the sputtering was carried out in mixed Argon: Oxygen (20:80) atmosphere. The ambient gas pressure during the process was kept at 20mTorr. Before the actual experiment, the target was pre-sputtered for 15 minutes to remove the impurities and native oxide layer formed on the surface. The target-substrate distance 60mm, gun length 250mm and the deposition time 120 minutes were kept constant for all depositions. Sputtering was carried out at 80W Rf/ 120W DC power respectively for zinc and titanium targets at various substrate temperatures, room temperature, 100°C, 150°C, 200°C and 300°C. The sputtering parameters for nanocomposite films are listed in Table 5.1

Target	Zinc/Titanium
Base Pressure	2×10^{-6} Torr
Sputtering Pressure	20 mTorr
Gas Used	Argon+ Oxygen (20:80)
Sputtering Power	80W Rf/ 120W DC
Substrate temperature	Room Temperature to 300°C
Sputtering Time	120 minutes
Substrate used	Silicon Si(100)

Table 5.1: Sputtering parameters for ZnO:TiO$_2$ thin films

5.2.2 Characterization

5.2.2.1 Microstructural Analysis

The sputtered films at different substrate temperatures were characterized by XRD (Bruker AXS, D8 Advance) with $CuK\alpha$ (1.54 Å) radiation for the phase identification. The excitation voltage and current were set to 40kV and 30mA respectively, in the diffractometer. The scan rate used was 1°/minute, giving an increment of 0.02° and the scan range was 20° to 70°.

The microstuctures of the film were characterized by FE-SEM (FEI, Quanta 200F) at an acceleration voltage of 20kV. The chemical analysis of the film was carried out by EDX attachment to FE-SEM.

The ZnO:TiO2 thin film, deposited at 100°C was subjected to FEI, Tecnai G^2 Transmission Electron Microscopy (TEM) for further structural analysis and phase characterization. The sample preparation consisted of the following stages: ultrasonic disc cutting, metallographic polishing, till the sample reaches a thickness ~90μ, followed by dimpling, polishing and ion milling.

The surface morphology of the ZnO thin films was studied using AFM (NT-MDT, NTegra) in a semicontact (tapping) mode and the root mean square roughness (RMS) of the surface of the sample was calculated from the AFM scans at 3 different spots for each sample.

The wettability of the films was measured using contact angle measurement device (Kruss FM40 Easy Drop).The contact angle measurements were carried out by the Drop Shape Analysis software by sessile drop method. The contact angles were measured at 3 different spots for each sample

5.2.2.2 In Vitro Biological Tests

The bioactivity, biocompatibility and antimicrobial properties were determined for the ZnO-TiO2 nanocomposite thin films deposited at different substrate temperatures.

5.2.2.2.1 In vitro Acellular Test: Biomimetic Apatite Deposition

Bioactivity or apatite forming ability of the films was studied by static immersion test in Hank's Balanced Salt Solution (HBSS), T-2010, Himedia, India). The films were immersed in 25 ml of SBF at 37°C in an incubator for a period of 14 days. The immersion solution was drawn out at regular periods, specifically on days 1, 4, 7, 10 and 14 and analyzed for concentration of Ca^{2+} and P^{3-}ions by ICP-MS (--), by calibration with high purity standards of Ca^{2+} and P^{3-} ions, prepared in miliQ water. . The Zn^{2+} and Ti^{2+} ion release was measured by ICP-MS using standards of high purity, prepared in miliQ water. The concentrations of the standards were kept at 10ppb, 50ppb and 100ppb for calibration purposes. The samples were appropriately diluted to make them amenable to the highly sensitive ICP technique. The concentration of Ca^{2+} and P^{3-} ions decreases owing to the formation of hydroxyapatite layer on the film surface, while that of Zn^{2+} and Ti^{2+} ions increases with time. XRD was used for phase identification of the apatite layer and its morphology and chemical composition were analyzed by FE-SEM and EDX respectively.

5.2.2.2.2 In Vitro Antimicrobial Efficiency Test

To check for the antimicrobial properties of the nanocomposite coatings of Zno-TiO2, antibacterial susceptibility test was carried out for each sample. Bacterial strains *E.coli* (gram negative) and *S.aureus* (gram positive) were used.

Test samples are not generally disinfected or sterilised prior to testing. The level of natural contamination of the samples is so low compared to the number of cells exposed to the

samples during the test that sterilization is not necessary. However, the samples were disinfected by dipping in 70% isopropyl alcohol.

Stock cultures of *E.coli* and *S.aureus* are maintained by inoculating one loop onto a Nutrient Agar (or equivalent medium) and incubating at 37°C for 48 hours before storing at 4-10°C. Before using the culture in a test, it was allowed to grow for at least 24 hours in a fresh nutrient broth of agar.

Protocol:

I. From a stock culture, a sterile flask containing Nutrient Agar or equivalent medium was inoculated and incubated for 18 hours at 37°C while shaking.

II. From this culture, 1 ml was removed and disperse in 9ml of sterile water; vortexed.

III. To determine the actual number of viable of organisms in the exposure solution, nine serial 1:10 dilutions were made of the cell suspension in the previous section. Plated 100μl of the last three dilutions: 10^{-7}, 10^{-8}, 10^{-9}. Incubated inverted for 48 hours at 37°C. Following incubation, the colony formation units (CFU) were counted and calculated the CFU/ml. This number is the actual number of viable cells/ml exposed to the samples.

IV. The samples were then kept in moist chambers, formed of sterile petri dishes, containing sterile moist absorbent cotton or blotting paper. The petri dishes were autoclaved at 121°C for 20 minutes , prior to being used.

V. 100μl of the bacterial suspension, containing about 10^4 CFU/ml was applied to each thin film coated as well as uncoated Si substrate.

VI. The bacterial suspension was then covered carefully, with a sterile coverslip, to ensure the liquid spreads to the edges of the sample, without overflowing, thus ensuring good contact between the film and the bacterial suspension and to prevent it from evaporating.

VII. The exposed samples were then incubated in 90-100% humidity, provided by the moist chamber, at 37°C for 24 hours.

VIII. To determine the number of bacteria killed from the exposure to the ZnO/TiO_2 composite films, the plaque and film "sandwich" were washed with 10ml of nutrient broth. The cover film was lifted up with forceps and the wash medium was pipetted repeatedly over them to suspend as many cells as possible. 100μl of the solution was plated onto a nutrient agar plate (10^0 dilution) and made three serial 1:10 dilutions from this solution, plating 100μl of each dilution. This was repeated for all thin film samples and Si controls for both *E. coli* and *S. aureus*. The inoculated plates for each sample, were incubated, inverted, at 37°C for 24 hours.

IX. Following incubation, the plates were counted for CFU. Only CFU between 25 and 300 are considered accurate.

X. The antimicrobial efficiency was calculated from the following formula—

Antimicrobial Efficiency $\varepsilon= \dfrac{(A- B) \times 100}{A}$ **%**

A= number of viable bacteria with uncoated (standard) silicon substrate

B=number of viable bacteria with $ZnO: TiO_2$ coated substrates.

5.2.2.2.3 In Vitro Cytotoxcity Characterization

The biocompatibility of the samples was assessed using the ISO10993-5 test guidelines. MG-63 (Human osteocyte cell line) and L929 (Mouse skin fibroblast cell line) were allowed to grow on the coated and uncoated Si samples for 24-96 hours and assessed for cytotoxicity using standard endpoint- tetrazolium bromide MTT assay.

I.   Culture initiation:

Frozen vials of cells were taken out from the liquid nitrogen and immediately transferred to a pre warmed (37°C) water bath for thawing. The cells were then transferred to sterile centrifuge tubes containing 10 ml complete medium (DMEM + 10% FBS + Antibiotic-Antimycotic solution (1.0 ml/100 ml of medium) and centrifuged at 600 rpm for 10 minutes at room temperature. The supernatant was discarded & the loosely bound cell pellet was suspended in 5 ml of complete medium & appropriate numbers of cells were seeded in T-75 tissue culture flask, incubated in a CO_2 incubator (5% CO_2 - 95% air at high humidity) at 37°C. Initially the medium was changed at an interval of 24 h and subsequently in a gap of 2-3 days till sufficient growth was observed. Both the cell types used in the study were between passages 15 to 28.

II.   Cell viability test:

Dye exclusion test: In principle, the cells with damaged membrane allow the trypan blue dye to pass into the cytoplasm whereas undamaged cells are capable of dye exclusion. This dye exclusion method was used to see the cell viability by assessing the loss of membrane integrity. This test was done for every batch of cells before the start of experiments to ascertain that how much cells are viable in the batch specific and batches showing the cell viability more than 95% were used for the experiments. In brief, well-mixed cell suspension (0.8 ml) was added to a test tube already containing 0.2 ml of trypan blue (0.4%) and mixed the contents by gentle shaking. In continuation, without wasting the time, 20 μl of dye-cell mixture was placed on the edge of both the chambers of the haemocytometer prefixed with the cover slip and allowed the cell suspension to fill the chambers by capillary action. The counting of unstained (viable cells) and stained cells (nonviable cells) in the four large corner

squares in both counting chambers was made using a 10X microscope objective. The percent cell viability was calculated by deducting the number of all stained cells from total number of cells counted (stained cells and unstained cells) over the haemocytometer. The only batches showing more than 95% cell viability were used in further experimentation.

Plating of L929 cells: Cells were harvested by trypsinization from the flasks having the high confluency and peletted by centrifugation at 600 rpm for 5 minutes. The pellet was re-suspended in fresh culture medium and clumps were broken if any by a tip of 20 µl by up and down several times. Cells were then counted with the help of coulter electronic cell and particle counter and plated in the frequency of 10,000 cells per well in 100µl of culture medium.

Percent Cell Viability by MTT Assay: The assay was done following the method of Mosmann *et al (1983)* [87] with desired modifications. In brief, titania thin films were placed in the 24 well culture plates and then adequate numbers of cells (1×10^5) were seeded. The cells were then allowed to grow for 12-96 h in the CO_2 incubator at 37°C. Tetrazolium (50 µl/well containing 500µl of cell suspension; 5mg/ml of stock in PBS) salt was added 4 h prior to completion the each incubation period. Then, the reaction mixture was carefully taken out and 500 µl of culture grade DMSO (Sigma St Louis, USA) was added to each well by pipetting up & down several times until the content get homogenized. After 10 minutes, the color was read at 530 nm, using Multiwell Microplate Reader (Bio-Tek, USA). The uncoated Si wafers were also ran parallel under identical conditions and served as basal control, whereas cells treated with manganese (10^{-4} M) served as positive control.

5.3 Results and discussion

Nanocomposite thin films of ZnO: TiO_2 were deposited by Magnetron Co-Sputtering of Ti and Zn targets respectively, in Ar+O_2 ambience at various substrate temperatures. The coatings formed thus, were characterised for their structural and biological properties.

5.3.1 Microstructural and Morphological Characterization

The nanocomposite titanate films were first characterized using Glancing Angle XRD for phase determination. The XRD pattern of the zinc titanate films, deposited at different substrate temperatures is shown in figure 5.2. The films deposited at substrate temperatures ranging from room temperature (~ 26°C) to 200°C showed a hump like region in the scan range $28.1° \leq 2\theta \leq 38.5°$, suggesting amorphous nature of the films. The peak of the hump showed a lateral shift towards higher 2θ, with increasing substrate temperatures. At deposition temperature of 300°C, two small peaks appear, indicating the formation of titanate phases $ZnTiO_3$, (104), (110) (JCPDS card no. 14-0033). A small hump like region was also observed in the scan range $60.0° \leq 2\theta \leq 63.1°$, peaking off at ~62°. Amorphous or glassy materials have a structure that exhibits only short-range order or regions where a predictable placement of atoms occurs. However, within a very few atom spacings, this order breaks down, and no long-range correlation in the geometric positioning of atoms is preserved. Production of amorphous films requires very high deposition rates and low substrate temperatures. The latter immobilizes or freezes adatoms on the substrate where they impinge and prevents them from diffusing and seeking out equilibrium lattice sites. [54]

The ZnO: TiO_2 films were then annealed at 1000°C to determine if any phase separation occurs at higher temperatures. At low substrate temperatures, $ZnTiO_3$ results in amorphous films.
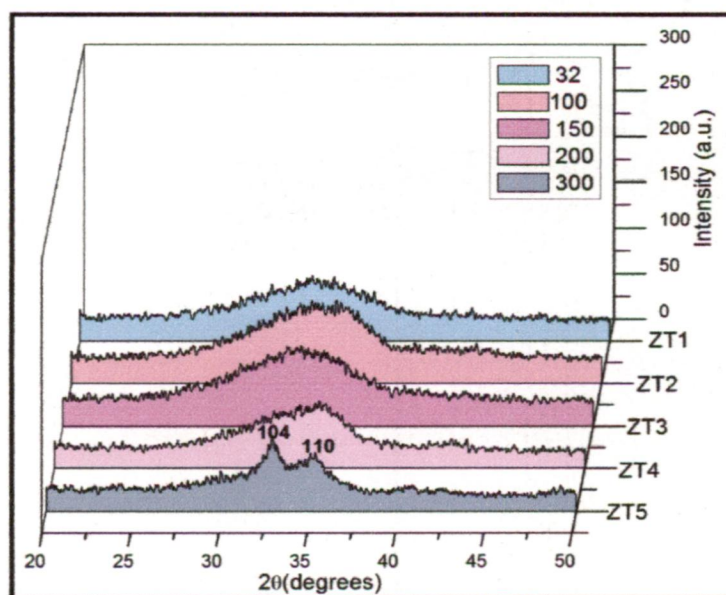
Figure 5.2: X-ray Diffraction pattern for ZnO:TiO₂ films deposited at different substrate temperatures by Magnetron Co-Sputtering from Zn and Ti targets at 80W Rf and 120W DC respectively.

Annealing at high temperatures ~1000°C, peaks corresponding to Zn_2TiO_4, ZnO and TiO_2 (both anatase and rutile phases) are observed. It can be inferred that at such high temperatures, $ZnTiO_3$ dissociates into Zn_2TiO_4, ZnO and TiO_2 components. The film, after annealing treatment, shows high crystallinity. This amorphous-crystalline transformation apparently proceeds in a manner first suggested by Ostwald in 1897. According to the so-called Ostwald rule, a system undergoing a reaction proceeds from a less stable to a final equilibrium state through a succession of intermediate metastable states of increasing stability. [54] The following fig.5.3 is an X-Ray Diffraction pattern showing the peaks obtained after annealing the titanate film at 1000°C.

The morphology and chemical composition of the films were studied using Field Emission Scanning Electron Microscopy (FESEM). FESEM analysis of the film revealed the formation of nanflower like structures, scattered throughout the film surface. A closer examination

revealed that each nanoflower is an assembly of nanorod like structures, which appear to grow from beneath the surface of the film.
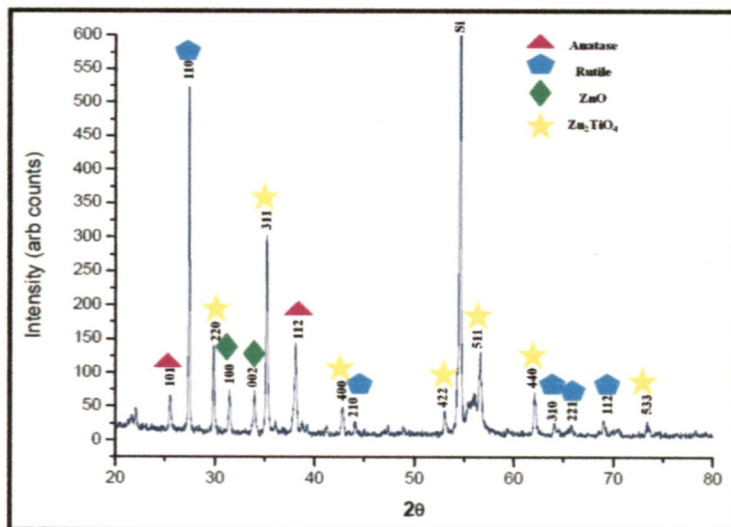
Figure 5.3: X-Ray Diffraction pattern of the zinc titanate film deposited at room temperature and annealed at 1000°C

Moreover, such morphology appears to follow a distinct trend. The formation of the structures is seen to be influenced by the substrate temperature. Films deposited at room temperature, show sparse bud-like outgrowths on the film surface, even high magnification of 16000X (Fig. 5.4(A)). As the temperature increases to 100-150°C, the nanorods grow, reaching about 50nm in diameter and various lengths. These nanorods cluster together to form nanoflower like nanostructures ~10μm in diameter. The number of nanoflowers also increases, as seen my scanning electron micrographs, even at lower magnifications of 800X and 8000X (Fig. 5.4(B, C). However, as the temperature is further increased to 200 and 300°C, the nanorod formation is inhibited, with the films deposited at 300°C, showing bud-like outgrowths only. To the best of my knowledge, such morphology, by the process of sputtering, and its apparent dependence on temperature has not been reported before. Nanorod formation can be attributed to Stranski -Krastanov mode of thin film growth, which is intermediate between layer-by-layer and island growth modes of thin film formation. The

nanorod formation might occur due to strain produced in the film during co-sputtering of titania and zinc oxide, leading also to amorphous films. Such nanorod-nanoflower formation may act as a stress relieving mechanism for the film. In general, the origin of compressive stress generally comes from two kinds of defects, one is lattice dislocation resulting from the difference of the thermal expansion coefficient and lattice mismatch between Si and ZnO, and the others are grain boundaries and intrinsic point defects coming from the course of crystal growth.

To further investigate the morphology and phase of the nanorod arrays or nanoflowers formed on the co-sputtered thin films, transmission electron microscopy was used. $ZnO-TiO_2$ film, deposited at 100°C was prepared by disc grinding, ion milling and dimpling and then analysed under Tecnai G^2 TEM operated at 200kV. Transmission Electron Micrographs also revealed the formation of nanorod like structures, about 50nm in diameter (fig. 5.5). The nanoflowers in the film appear to have disintegrated into individual petals or nanorods during sample preparation. SAED pattern of the petals distinctly show hazy rings, indicative of the amorphous nature of the nanoflower formed. However, further investigations are required to confirm the structure of the nanorods formed. Each nanorod may be a single crystal, while the diffraction pattern generated shows diffuse rings, characteristic of amorphous materials. Hence, improved TEM analysis and TEM sample preparation might help in confirming the nature of nanoflowers and film formed.
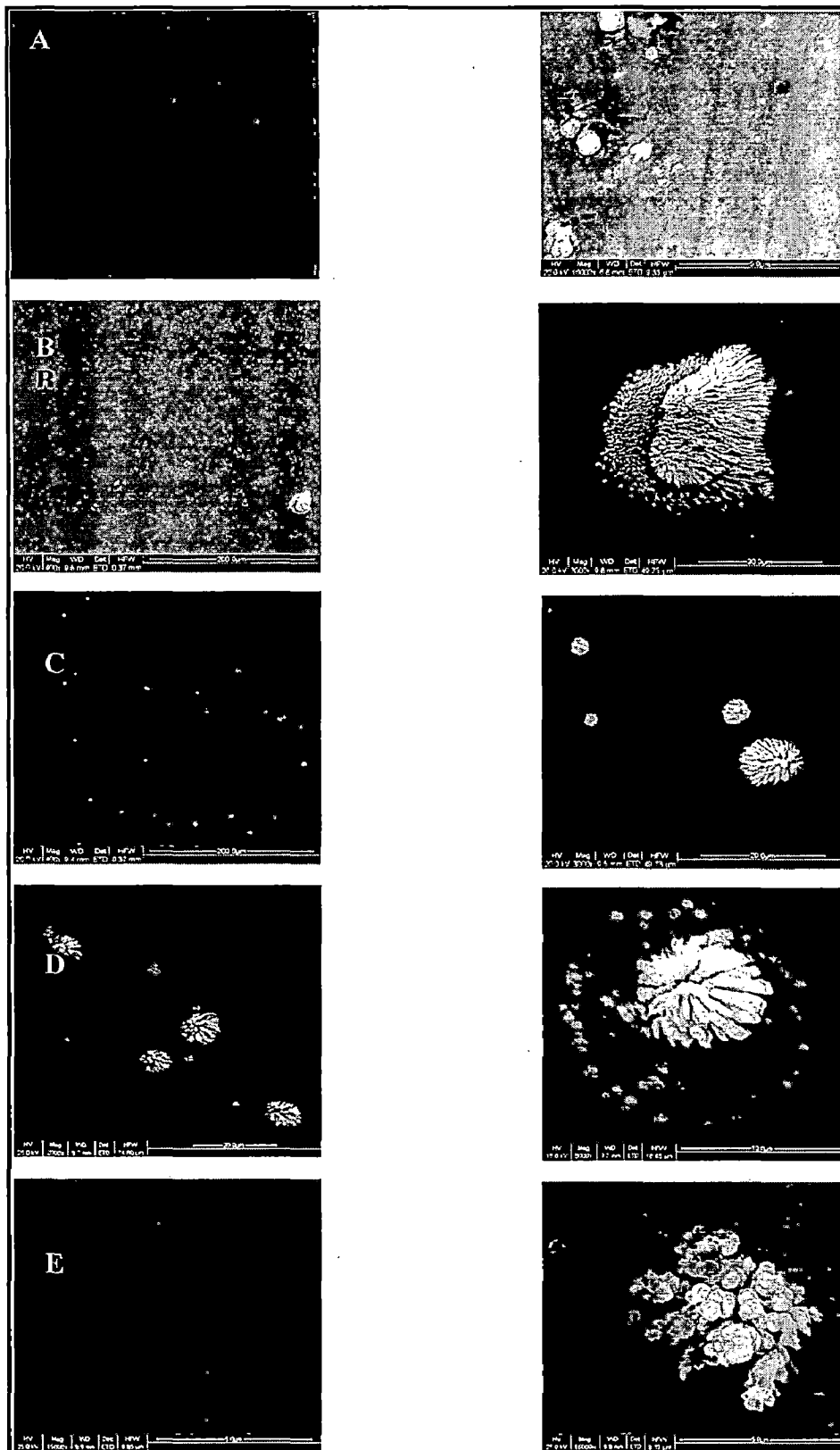
Figure 5.4: Scanning Electron micrographs of ZnO:TiO$_2$ composite coatings deposited at (A) Room temperature, (B) 100°C, (C)150°C, (D) 200°C and (E) 300°C.
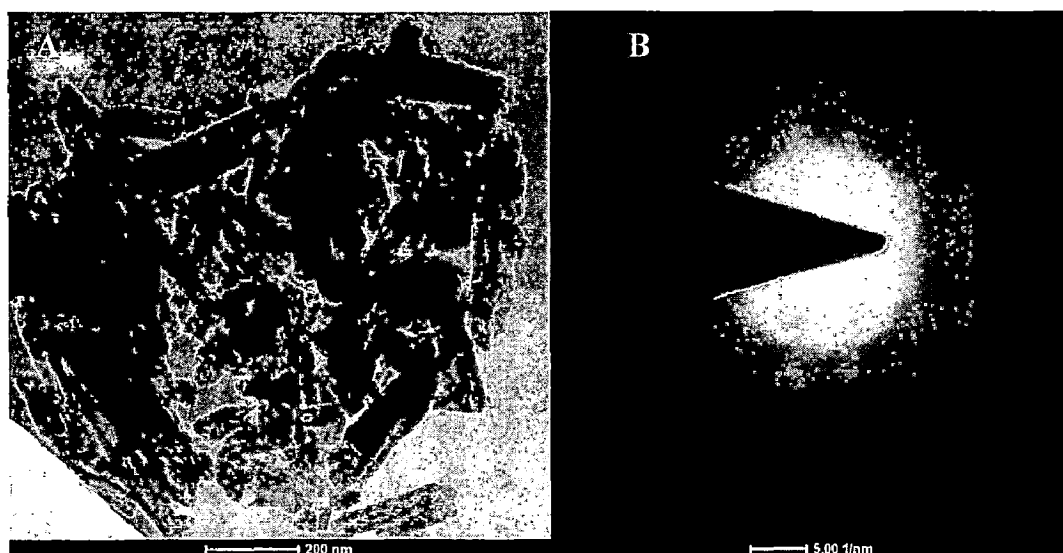
Figure 5.5: (A) Transmission Scanning Micrograph of ZnO : TiO$_2$ co-sputtered thin film at 150°C, showing the disintegrated petals or nanorods of a nanoflower. (B) SAED pattern of the nanofilms.

The morphology of the film was also studied using Atomic Force Microscopy (AFM). The AFM images were then analysed using NT-MDT software to determine the approximate grain size of the film as well as the root mean square (RMS) roughness. Fig. 5.6 represents a 3D AFM image of the film, showing a cluster of nanorods, forming a nanoflower like structure. The area around the nanoflower seems to be deeply etched. This further validates the growth of nanorod like structures, as a means of stress relief, from beneath the film. The scan area is 10μ x 10μ.
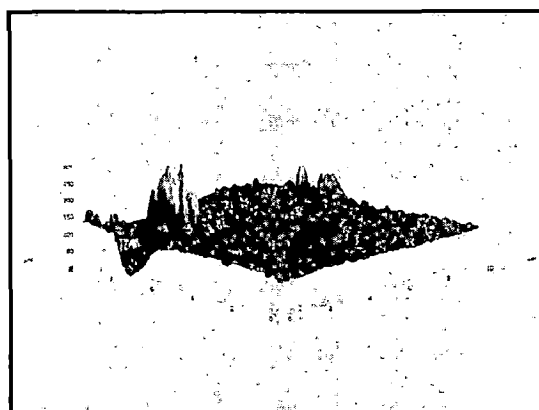
Figure 5.6: 3D Atomic Microscoscopy Image of thin film deposited at 200°C showing the formation of nanoflower like arrays of nanorods. The scan area is 10μ x 10μ.

The AFM images of the zinc titanate films, deposited at different substrate temperatures are shown in fig. 5.8. The root-mean-square (RMS) average roughness of the surfaces was calculated for a 2 x 2 μm square scan area. The roughness of the films first recedes and then increases with increasing substrate temperature. This trend correlates with the number and morphology of the nanorod arrays formed on the film. The films at 100°C and 150°C, which show enhanced nanoflower - nanorod arrays result in lower roughness in the film. The results have been tabulated in figure 5.7.
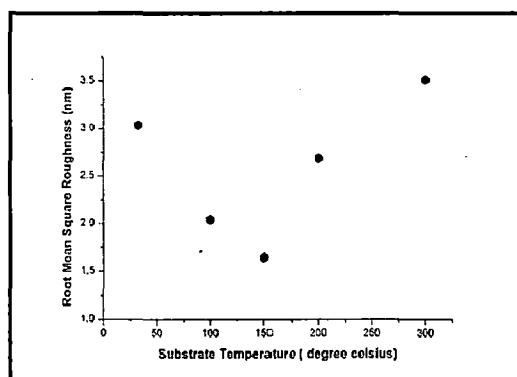
Figure 5.7: Variation of RMS Roughness of zinc titanate films with substrate temperature.

The wettability characteristics of the zinc titanate films were measure by the Sessile Drop Method, using a contact angle measuring device. Their affinity for both water and Hanks' Balanced Salt Solution (HBSS), with composition similar to simulated body fluid (SBF), was determined by calculating the contact angle formed by the water or HBSS droplet with the film surface. The measurements were taken at 3 positions on the film and results were averaged. The films show better affinity with HBSS as compared to water, as evidenced by the lower contact angles. Also, the contact angle first recedes and then increases with increasing substrate temperature, following a trend similar to that followed by the film roughness. It can be concluded from here that strain and roughness in the films seems to play an important role in their interaction with water and other fluids as SBF. The trend can be

noted from the table 5.2, which shows the measured mean values of the contact angles measured with both water and SBF (HBSS) and the corresponding graph is presented in fig. 5.9. Hydrophobicity decelerates interaction between the implant surface and the aqueous biosystem. Surface wettability control is extremely interesting from the point of view of osseointegration mechanisms, because during surgical procedures, the biomaterial will encounter blood. Almost immediately after contact with blood, the implant surface will be covered with plasma proteins that become absorbed onto the surface. Both the degree and type of absorption of plasma proteins is directly dependent on the wettability of the surface. Cell adhesion to the orthopaedic implant is a crucial phase in osseointegration. Cells from surrounding tissues, blood vessels and bone are essential to the repair of the injured tissue. Hydophilicity or surface wettability has a pivotal role in cell attachment and adhesion. It is intrinsically related to the chemical composition and roughness of the surface, as evidenced by the EDX and AFM results, respectively.

Substrate temperature (°C)	Contact Angle (water) (°)	Contact Angle (SBF) (°)
26	85.9±6.21	64.7 ±9.94
100	74.4±6.93	34.6±1.30
150	79.3±4.16	40.4±12.61
200	80.5±3.55	44.1±2.65
300	79.2±3.30	46.5±5.07

Table 5.2: Variation of contact angle of the film with substrate temperature with water and SBF
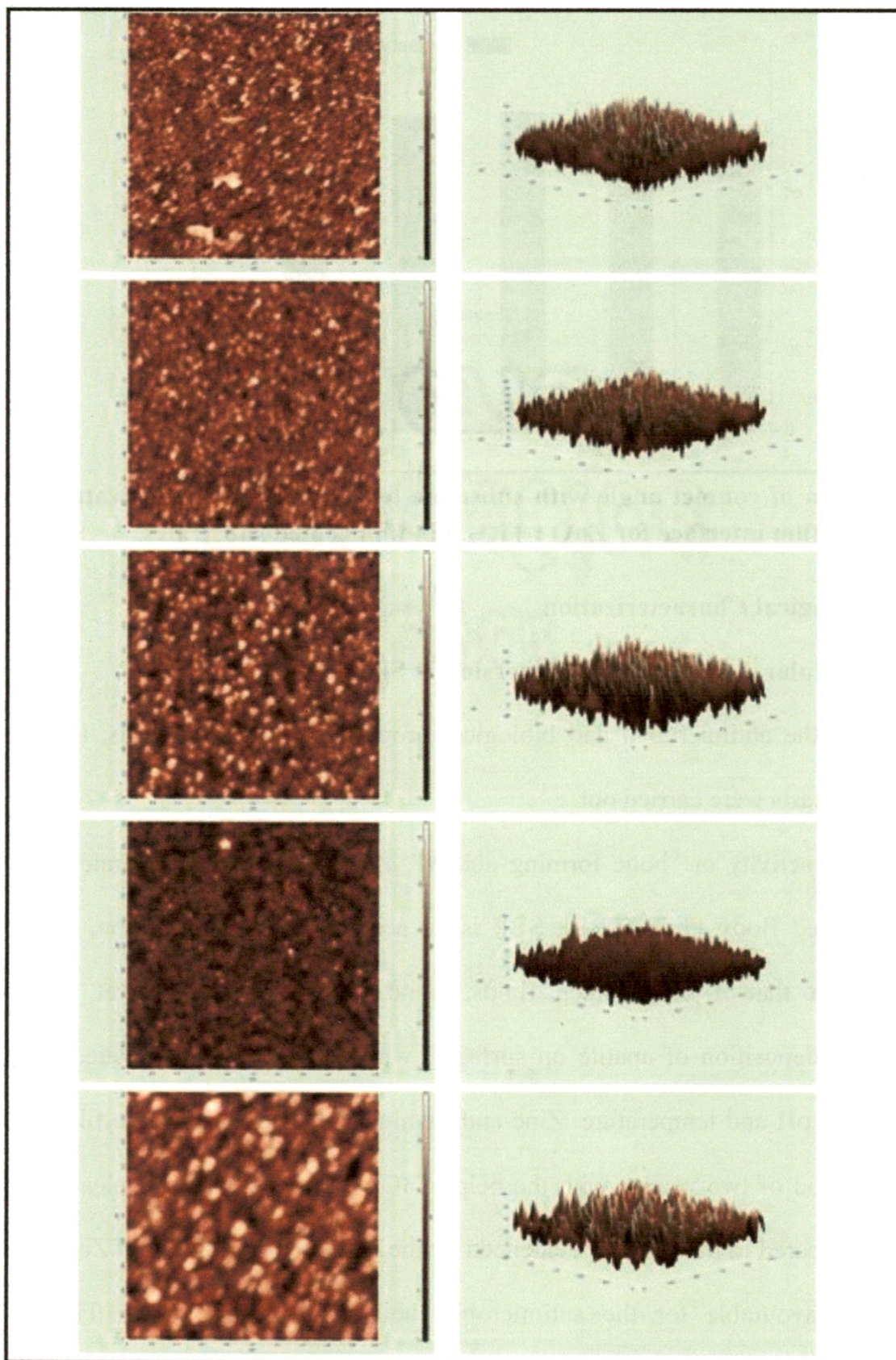
Figure 5.8: 2D and 3D images of zinc titanate films at (A) Room temperature, (B) 100°C, (C)150°C, (D) 200°C and (E) 300°C.
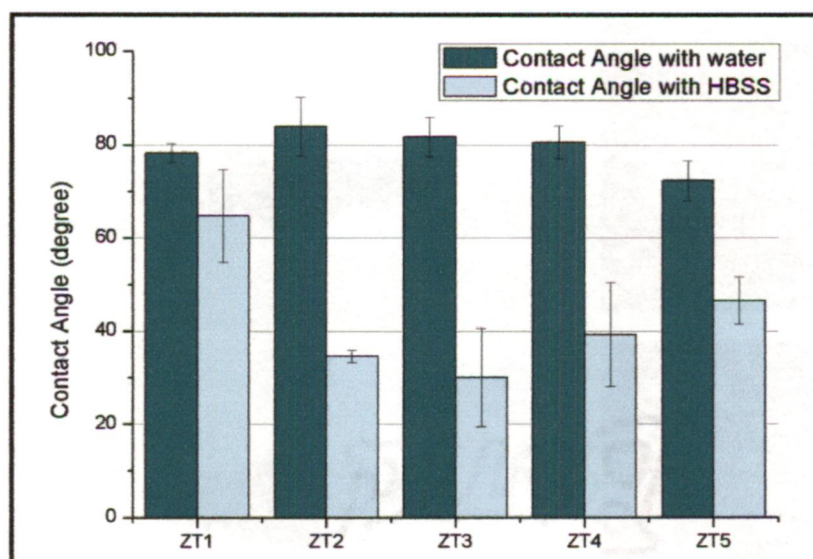
Figure 5.9: Variation of contact angle with substrate temperature for both water-film and SBF like HBSS-film interface for ZnO : TiO$_2$ thin film coated substrates.

5.3.2 In Vitro Biological Characterization

5.3.2.1 In Vitro Acellular Testing: Static immersion in Simulated Body Fluid

In order to evaluate the antimicrobial and biological properties of the thin films, in vitro acellular and cellular tests were carried out.

To establish their bioactivity or "bone forming ability", ZnO:TiO$_2$ coated substrates were immersed in Simulated Body Fluid (SBF). SBF is an acellular artificial solution, with a composition similar to that of physiological fluids, found in the body. Kokubo et. al.[79] reported biomimetic deposition of apatite on surfaces, when immersed in simulated body fluid at physiological pH and temperature. Zinc and titanium ion release from the film was measured over a period of two weeks, with the help of ICP-MS analysis. Zinc release was more prominent, compared to titanium, as evidenced by the higher concentration of Zn^{2+} ions than Ti^{4+}. This is favourable for the antimicrobial activity of the coatings. Ti^{4+} ion concentration reaches a maximum of about 0.095 ppm in two weeks, which is lower than the average daily uptake of titanium by the human body under normal conditions (~0.8 mg/day).

The Ti and Zn ion concentrations have been mapped for each coating over a period of 14 days and are shown in figs. 5.10 and 5.11. Composite coatings, sputtered at room temperature, show maximum accumulated concentration of Ti ions in HBSS, which can be intuitively attributed to the comparatively poor adhesion of the coating to the substrate at lower temperatures. However, counter intuitively, Zn ion release is minimum for coatings deposited at room temperature and maximum for those deposited at 300°C.
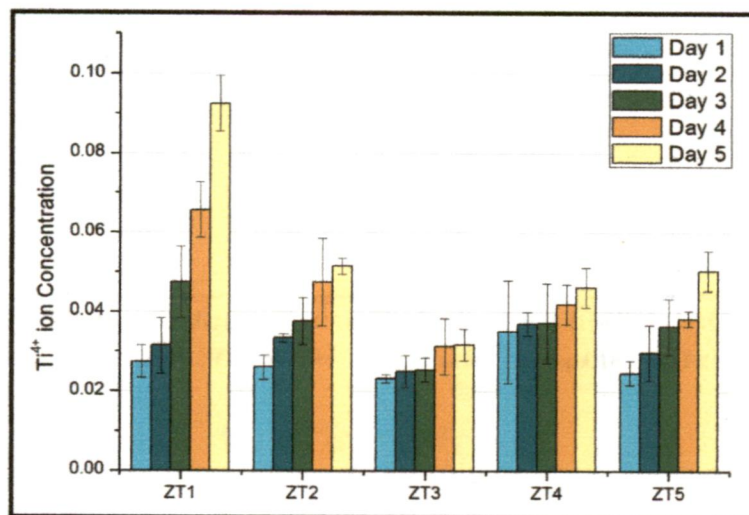
Figure 5.10: Release of Ti ions in HBSS from ZnO: TiO$_2$ composite and TiO$_2$ thin films over a period of 14 days
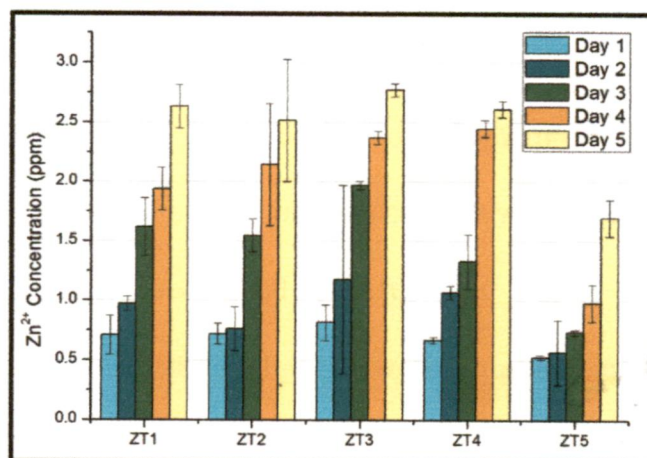
Figure 5.11: Release of Zn ions in HBSS from ZnO: TiO$_2$ composite and ZnO thin films over a period of 14 days

Figure 5.12 shows the XRD pattern for the apatite formation on films deposited at different substrate temperature.

The apatite formation ability increases with increase in the deposition temperature. Peaks corresponding to an apatite- like compound, calcium phosphate hydroxide (JCPDS Card No. 83-1889) also appear in the diffractogram.
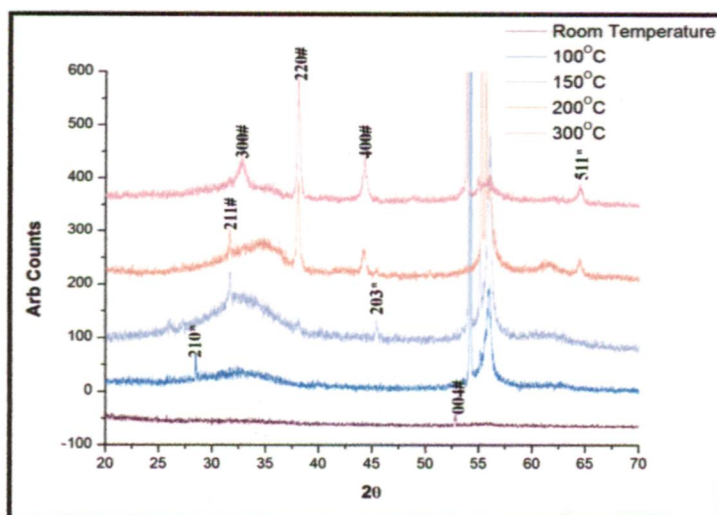
Figure 5.12: X-Ray Diffraction pattern of hydroxyapatite layer deposited on ZnO:TiO2 films post 14 day immersion in SBF. (#- Hydroxyapatite, *- Calcium Phosphate Hydroxide)

The morphology of the hydroxyapatite layer formed on the surfaces was observed, using scanning electron microscope and the images are presented in fig. 5.13

5.3.2.2 In Vitro Antimicrobial Efficiency Test

Microbial infections are one of the major problems facing implantology today, resulting in implant failures, additional medical costs and post operative re-surgeries. Moreover, emergence of microbial strains, with resistance to most antibiotics has made it important to look further. Zinc and Silver nanoparticles have been stipulated to have enhanced antimicrobial effects, even in strains showing high resistance to organics antibiotics, while affecting the human tissues minimally. Hence, a successful orthopaedic coating must incorporate a form of antimicrobial, effective against a wide range of potentially pathologic microbes, especially *S. aureus* and *E. coli*, the most common causes of orthopaedic implant infections. With this in mind, the ZnO: TiO_2 composite coated silicon substrates were

evaluated for their antimicrobial efficiency, taking cues from the Japanese Industrial Standard Test, JIS Z2801, for solid plate samples.

All the films showed good antimicrobial efficiency against both *S. aureus* and *E. coli*, though the activity against *S. aureus* was found to be more potent, as can be seen in figure 5.14. The uncoated Silicon wafers were used as controls and the antimicrobial efficiency calculated using the formula:

Antimicrobial Efficiency $\varepsilon = \dfrac{(A-B) \times 100}{A}$ %

Where A= number of viable bacteria uncoated (standard) silicon substrate

B=number of viable bacteria with ZnO/TiO_2 coated substrates.

Figs.5.14 and 5.15 (a and b) show the results of viable bacteria in the exposure solution, after 24 hours incubation with $ZnO: TiO_2$ composite thin films. The viable bacterial count was significantly reduced on coated substrate, when compared to uncoated silicon wafers, for both *S. aureus* and *E. coli* bacteria. The images shown are for 10^{-1} dilution, plated onto nutrient agar medium.
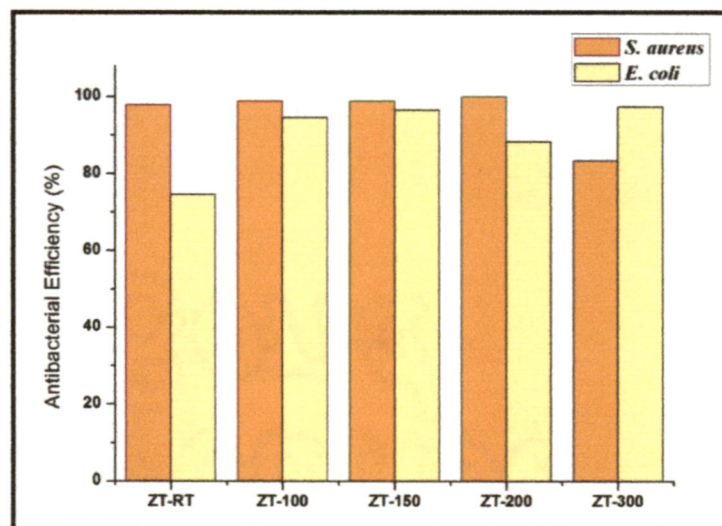
Figure 5.14: Graphical representation of the antibacterial activities against *S. aureus* and *E. coli.* of ZnO : TiO2 thin films, deposited at room temperature (ZT-RT), 100°C (ZT-100), 150°C (ZT-150), 200°C (ZT-200) and 300°C (ZT-300).
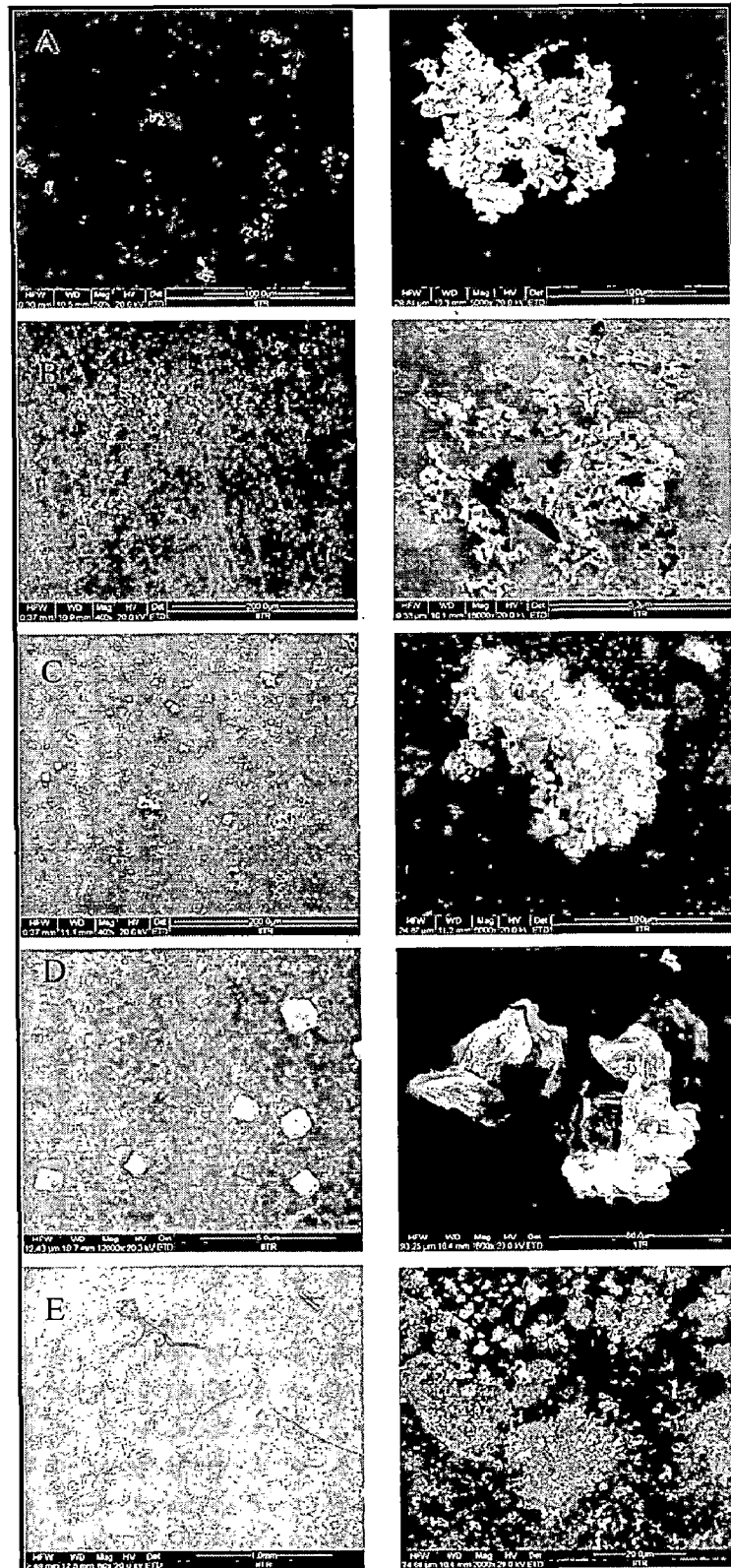
Figure 5.13 : FESEM images showing the formation of hydroxyapatite layer on ZnO:TiO$_2$ coated substrates after 14 day immersion in SBF at 500X and 5000X, for deposition at (A) Room Temperature, (B) 100°C, (C) 150°C, (D) 200°C and (E) 300°C

5.3.2.3 In Vitro Cytotoxicity Test
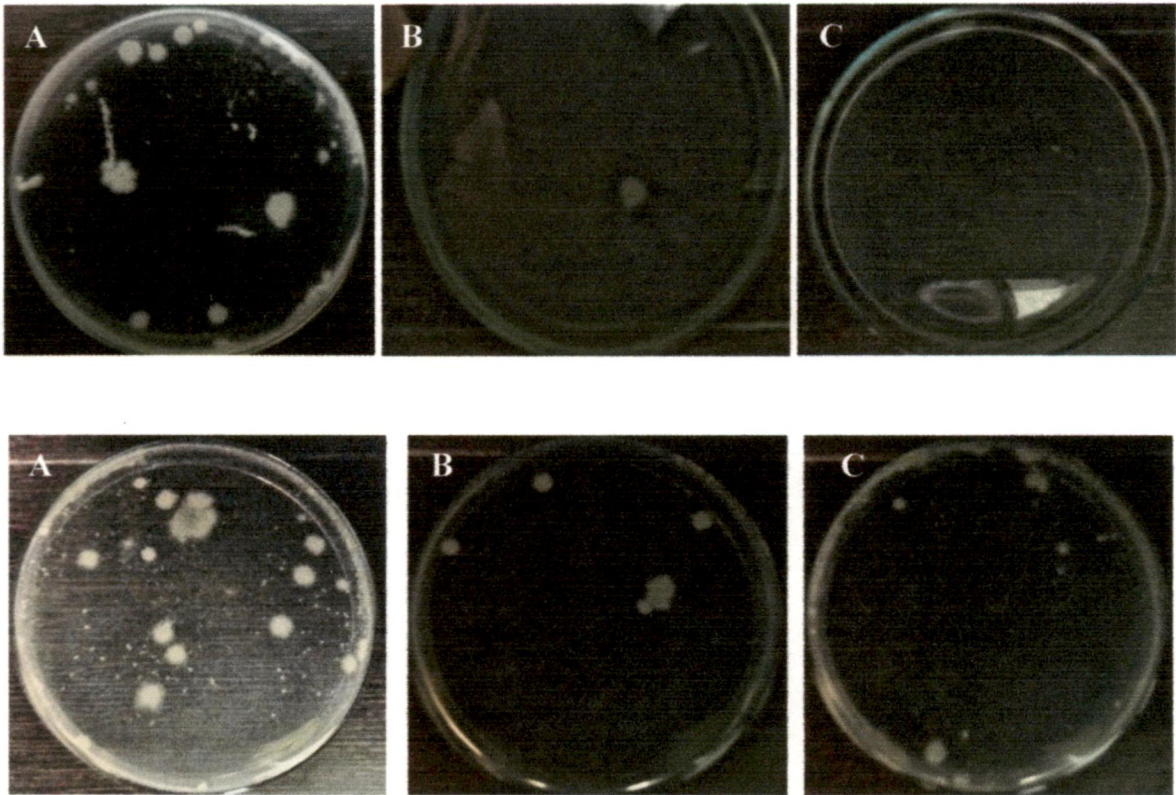
Figure 5.15: Representative photo of viable (a) *S. aureus* **and (b)** *E. coli* **plated on nutrient agar after 24 hour incubation (10^{-1} dilution). (A) Uncoated silicon substrate, (B) substrate coated with ZnO:TiO$_2$ film deposited at 150°C, and (C) at 300°C.**

5.3.2.3 In Vitro Cytotoxicity Test

Both the cell lines used in the study i.e., MG-63 (Human osteocyte cell line) and L929 (mouse skin fibroblast) have shown no sign of significant toxicity following the exposure to the test materials. There was no statistically significant loss of specific morphology, no rounding, no vacuole formation or spindle shaped structures, no blabbing or apoptotic swelling observed in the cells. Cells of experimental group were as healthy as in the control group and proliferation of cells was also quite normal. The cells retained all the healthy features without any toxicity sign and symptoms along with normal proliferation till the end of extended period i.e., 96 h.

MTT assay: The highlights of the data of cytotoxicity study are summarized in Fig. 5.17 (a and b) Similar to the morphological examinations, there was no admissible alterations in the percent cell viability in both the cell lines used i.e., L929 and MG-63 in any time interval. The mean+ SE values were less than 8% in general, which also shows that there was no significant deviation in the values obtained from different sample peaces and experimental groups.
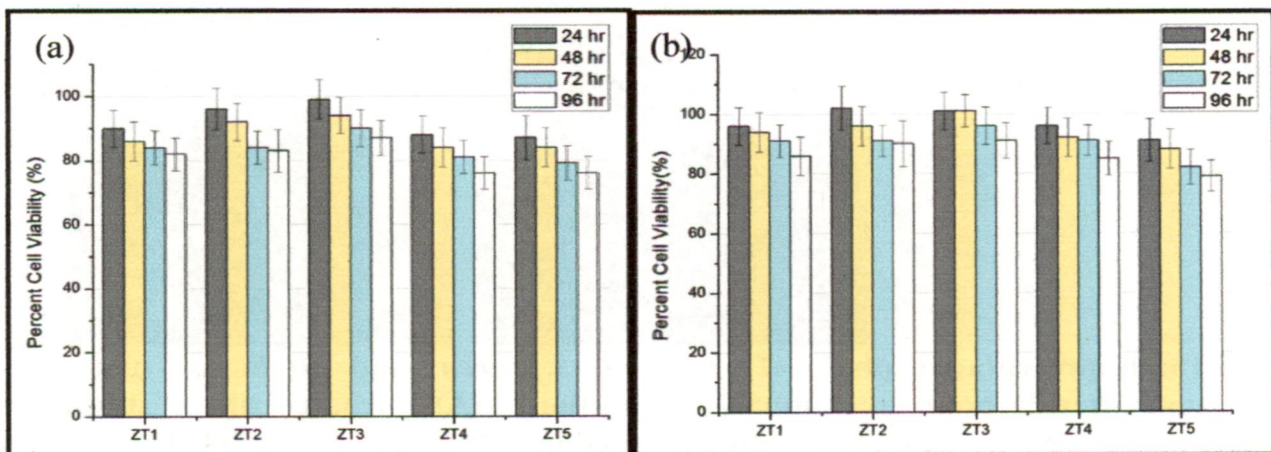
Figure 5.16: Graphical representation of the compatibility of the cosputtered TiO2-ZnO thin films with (a) MG63 human osteoblast and (b) L929 mouse fibroblast cell lines.

Chapter 6

Conclusion

6.1 Conclusion

The ideal property of orthopedic or dental implants used to replace missing or diseased bones or teeth is long-term stability. Strategies to accomplish this are based on (1) enhancing osseointegration (bone bonding) and (2) preventing microbial infection that could cause implant loosening or failure.

"Bioactivity," the property that allows the material to directly bond with bone, was first observed and described by Hench et al. [99], with silica-based bioactive glasses. In vitro, bioactivity is demonstrated by the formation of carbonate apatite on the surfaces of materials after immersion in serum [100, 101] or in simulated body fluid [102]. In vitro cell culture studies showed greater cell proliferation and differentiation (gene expression of markers for bone formation) of bone-forming cells on surfaces coated with apatite [103, 104] In vivo, bioactivity is shown by the formation of the nanocrystals of carbonate apatite associated with the bioactive material [100]. The long-term failure rate of dental implants, reported to be between 5% and 10%, is associated with presence of certain bacteria population [105.]. With regard to orthopedic implants, microbial infection caused by bacterial adhesion and colonization is also a major concern [106]. Bacterial adhesion and colonization is also a problem with orthodontic bracket guided tissue regeneration membranes [107]

Combining these two strategies is the challenge toward developing the ideal implant. With this aim, composite coatings containing TiO_2, with its ability to induce the formation of hydroxyapatite and derivatives, from a solution similar to that found in physiological conditions and ZnO, with its antimicrobial activity, were designed, via the process of sputtering. The composite coatings were deposited on silicon(100) substrate successfully at various deposition temperatures from room temperature upto 300°C. The films largely

showed amorphous nature, as confirmed by XRD spectra, due to the formation of different phases of titanate compounds, each of which tries to orient itself in a particular crystallographic direction. This was confirmed by the high temperature (1000°C) annealing treatment of the film where phase separation occurs and the XRD spectrum shows peaks corresponding to Zn_2TiO_4, TiO_2 (anatase and rutile) and ZnO.

FESEM and AFM analysis of surface morphology revealed the formation of nanoflower like nanorod arrays on the surface of the thin films. The nanorods were composed of both zinc and titanium components, as determined by EDX analysis. The formation of such nanostructures can be thought of as a stress releasing mechanism of the film. Cosputtering of zinc and titanium oxides may result in lattice mismatch or difference in the thermal expansion coefficient between the two oxides and the substrate, leading to build up of strain. Thus, by switching to Stranski-Krastanov mode of film formation, small 3D islands begin to form and grow onto form nanorod like structures, arrayed into the form of nanoflowers. However, further investigation is required into the mechanism of nanoflower formation. Also, the nanorod formation seems to be highly temperature dependent, with films deposited at 100°C and 150°C, showing the formation of more number of and denser nanorods and nanorod arrays, compared to those deposited at room temperature or higher, 200°C and 300°C. The roughness of the films shows similar trend, decreasing first with temperature, upto 150°C and then increasing beyond it.

Contact angle measurements of the $ZnO:TiO_2$ composite thin films were carried out to determine their interaction with water and HBSS (with composition similar to that of body fluid). Films deposited at 100°C showed maximum affinity for water, which increased for HBSS. This is favourable to the precipitation of apatite like crystals from the physiological

solution onto the implant surface, adhesion of cells and absorption of bone forming factors and proteins. Surface features, like wettability and roughness govern to a great extent, the interaction process observed by mammalian cells and bacteria with the implants, including polymers and metals. [98]

The films were then immersed in HBSS for a period of two weeks and showed the formation of apatite layer on the surface, as confirmed by XRD and SEM analysis. This ability is essential to better osseointegration of implants. The $ZnO:TiO_2$ composite films also showed good antibacterial ativity ($\square$ 70%) against both *S. aureus* and *E. coli*, the major microorganisms responsible for post operative infections in orhopedic implants.

Overall, our studies indicate that the thin films deposited at 150°C demonstrate optimal properties, as manifested from their minimal Ti^{4+} and maximum Zn^{2+} ion release, excellent wettability with HBSS, deposition of hydroxyapatite crystals on the surface in vitro, inhibition of bacterial growth as well as compatibility with human osteoblast MG63 cell lines. Thus, in the present work, co-sputtered nanocomposite films, and those deposited at 150°C substrate temperature in particular, provide a multipurpose biocompatible, bioactive and antimicrobial coating for surface engineering of orthopaedic implants and devices.

Besides the cosputtered ZnO:TiO2 coatings, TiO_2 and ZnO coatings on silicon (100) substrates were individually synthesised by DC and Rf Magnetron Sputtering and annealed at various temperatures upto 900°C and their morphological and cytotoxicity properties studied successfully. XRD spectra showed the formation of polycrystalline films, whse crystallinity increases with an increase in the annealing temperature. Titania films also showed phase change at 900°C, where anatase phase changes to rutile, a more dense and stable form of TiO_2. EDX analysis shows no major change in the elemental composition of the films even at

higher annealing temperatures. However, AFM and contact angle measurements show increasing roughness and corresponding receding contact angle values for the surfaces, with an increase in the annealing temperature.

The TiO2 and ZnO films were also assessed in vitro for biocompatibility with mammalian cell lines, L929, to ensure that the coatings do not elicit any unfavourable or toxic response from the cells, when implanted into the body. All the coatings demonstrated the ability to harbour cells on the surface, without any unfavourable reaction.

Thus, in the light of the above results, a plausible surface coating for orthopaedic and dental implants is be proposed, which shall be biocompatible, bioactive or osseoinductive as well as antimicrobial, for better interaction of the implant with the body, during surgical procedures and later. Inexpensive components, ease of synthesis, lack of any harmful chemicals either during the manufacture or processing and ability to be mass produced, makes $ZnO:TiO_2$ composite thin films, an ideal candidate for biomedical devices and orthopaedic implants.

List of Publications (Work done as a part of M.Tech Dissertation)

1. **Goel S**, Dubey P, Jayaganthan R, Pant AB, Chandra R. Sputter deposited Antibacterial and Biocompatible Nanocomposite TiO_2-ZnO Coatings for Orthopaedic Implants. (Submitted in the **Journal of Biomedical Materials Research-A**. Wiley Publishers Ltd.) (2012)).

List of Publications (from Internship at the University of Wisconsin-Madison)

1. Hong H, **Goel S**, Zhang Y, Cai W. "Molecular imaging with nucleic acid aptamers". Current Medicinal Chemistry, 2011, 18, 4195-4205. (PMCID: PMC3205285)

2. Hong H., **Goel S.**, Cai W., "In vivo Imaging of protein-protein interactions"-Book Chapter in Protein-protein Interactions. InTech Open Access Publisher (In Press).

3. Hong H, Yang K, Zhang Y, Engle JW, Feng L, Yang Y, Nayak TR, **Goel S**, Bean J, Theuer CP, Barnhart TE, Liu Z, Cai W. In vivo targeting and imaging of tumor vasculature with radiolabeled antibody-conjugated nano-graphene. ACS Nano, 2012, Epub. (NIHMSID # 356436).

References

1. Opportunities in Nanostructured Coatings: A Market Assessment to 2015, Electronics.ca Research Network, (2011).

2. Liu Chunming and Lieber Charles M., Thin film synthesis of solids, Wiley, (1994).

3. Kittel Charles, Introduction to Solid State Physics, Wiley, (1995).

4. Lemons JE., Biomaterials, biomechanics, tissue healing, and immediate-function dental implants. J Oral Implantol 30:318–324, (2004).

5. Hulber, S.F., Cooke, F., Klawitter, J.J., Attachment of prostheses to the musculoskeletal system by tissue ingrowth and mechanical interlocking, Journal of Biomedical Materials Research Symposium 4, 1-23 (1973).

6. Ratner, BD, Hoffman AS, Schoen FJ, et al., Biomaterials Science: An Introduction to Materials in Medicine, Elsevier Academic Press, (2004).

7. Wang Yongsheng, Sol–Gel Derived Hydroxyapatite Coatings on Metallic Implants: Characterization, In Vitro and In Vivo Analysis, In: Biological and Biomedical Coatings Handbook: Applications, Sam Zhang, Editor, CRC Press, (2011).

8. Zimmerli W, Trampu Z, Ochsner PE., Prosthetic joint infections, N Engl J Med 351:1645–1654, (2004)

9. Albrektsson T, Wennerberg A., Oral implant surfaces: Part 1. Review focusing on topographic and chemical properties of different surfaces and in vivo responses to them, International Journal of Prosthodontology, 17:536–543, (2004).

10. Vladan D. Mirjaniã, Radmila R. Arbutina , Jovan P. Šetrajãiã, Ljubiša D. Dÿambas, Physical Properties of Thin films on Implant Materials, Proc. Nat. Sci, Matica Srpska Novi Sad, 118, 121—126, (2010).

11. Brånemark P-I, Hansson BO, Adell R, Breine U, Lindström J, Hallén O, Öhman A., Osseointegrated implants in the treatment of the edentulous jaw, Stockholm: Almqvist and Wiksell, 132 pp, (1977).

12. LeGeros, RZ, Coelho PG, Holmes D, Dimaano F, LeGeros DP, orthopaedic and Dentala Surface Implant and Coatings, In: Biological and Biomedical Coatings Handbook: Applications, Sam Zhang, Editor, CRC Press, 301-333, (2011).

13. Waléria Silva de Medeiros, Marize Varella de Oliveira, Luiz Carlos Pereira, and Mônica Calixto de Andrade, Bioactive Porous Titanium: An Alternative to Surgical Implants, Artificial Organs, 32(4):277–282,(2008).

14. Y. Yang, N. Oh, Y. Liu, W. Chen, S. Oh, M. Appleford, S. Kim, K. Kim, S. Park, J. Bumgardner, W. Haggard, and J. Ong, Enhancing Osseointegration Using Surface-Modified Titanium Implants, JOM, 71-76, (2006).

15. Coelho PG, Lemons JE., Physico-chemical characterization and in vivo evaluation of nanothickness bioceramic depositions on alumina-blasted acid-etched Ti–6Al–4V implant surfaces, J Biomed Mater Res 90:351–361, (2009).

16. Davide Campoccia, Lucio Montanaroa, Carla Renata Arciola, The significance of infection related to orthopedic devices and issues of antibiotic resistance, Biomaterials;27, 2331–2339, (2006).

17. Vacheethasanee K, Marchant RE., Surfactant polymers designed to suppress bacterial (Staphylococcus epidermidis) adhesion on biomaterials, J Biomed Mater Res, 50(3):302–12,(2002).

18. An YH, Stuart GW, McDowell SJ, McDaniel SE, Kang Q, Friedman RJ, Prevention of bacterial adherence to implant surfaces with a crosslinked albumin coating in vitro, J Orthop Res,14(5):846–9, (1996).

19. Pavesio A, Renier D, Cassinelli C, Morra M., Anti-adhesive surfaces through hyaluronan coatings, Med Device Technol, 8(7) 20–1, 24–7, (1997).

20. Arciola CR, Radin L, Alvergna P, Cenni E, Pizzoferrato A, Heparin surface treatment of poly(methylmethacrylate) alters adhesion of a Staphylococcus aureus strain: utility of bacterial fatty acid analysis, Biomaterials,14(15):1161–4, (1993).

21. An YH, Blair BK, Martin KL, Friedman RJ, Macromolecule surface coating for preventing bacterial adhesion. In: Handbook of bacterial adhesion. Principles, methods and applications, An YH, Friedmann RJ, editors, Totowa, NJ: Humana Press Inc, p. 609–25, (2000).

22. Véronique B. Schwartz, Franck Thétiot, Sandra Ritz, Sabine Pütz, Lars Choritz, Alexandros Lappas, Renate Förch, Katharina Landfester, Ulrich Jonas, Antibacterial Surface Coatings from Zinc Oxide Nanoparticles Embedded in Poly(N-isopropylacrylamide) Hydrogel Surface Layers, Adv. Funct. Mater., (2012).

23. Borkow G, Gabbay J. Putting copper into action: copper impregnated products with potent biocidal activities. FASEB J; 18(14):1728–30. (2004).

24. W. Chen, Y. Liu, H.S Courtney, M. Bettenga, C.M. Agrawal, J.D. Bumgardner, J.L. Ong, In vitro anti-bacterial and biological properties of magnetron co-sputtered silver-containing hydroxyapatite coating, Biomaterials 27, 5512–5517, (2006).

25. Stigter M, Bezemer J, de Groot K, Layrolle P. Incorporation of different antibiotics into carbonated hydroxyapatite coatings on titanium implants, release and antibiotic efficacy. J Control Release; 99(1):127–37, (2004).

26. Lin TL, Lu FM, Conroy S, Sheu MS, Su SH, Tang L., Antimicrobial coatings: a remedy for medical device-related infections. Med Device Technol; 12(8):26–30, (2001).

27. Helmus, M. N. editor, Biomaterials in the design and reliability of medical devices. Kluwer Academic/Plenum Publishers and Landes Bioscience, New York and Georgetown, TX. (2003).

28. Andrade, J. D., Nagaoka, S., Cooper, S., Okano, T., and Kim S. W., Surfaces and blood compatibility: current hypotheses, Transactions of the Society of Artificial Internal Organs 33, 75-84, (1987).

29. Brash J. L., Exploiting the current paradigm of blood-material interactions for the rational design of blood-compatible materials. J Biomater Sci Polym Ed 11 1135-46, (2000).

30. Takahara, A., Hergenrother, R. W., Coury, A. J., and Cooper, S. L., Effect of soft tissue chemistry on the biostability of segmented polyurethanes. II. In vitro hydrolytic degradation and lipid sorption, J Biomed Mater Res 26, 801-818, (1992)..

31. Michael N. Helmus, Donald F. Gibbons and David Cebon, Biocompatibility: Meeting a Key Functional Requirement of Next-Generation Medical Devices, Toxicol Pathol 2008 36: 70-80, (2008).

32. Albrektsson T.,, Branemark PI., Hansson A., and Lindstrom J., Osseointegrated titanium implants, Requirements for Ensuring a Long-Lasting, Direct Bone-to-Implant Anchorage in Man, Acta orthop. scand. Informahealthcare.com 52, 155-170, (1981).

33. Grosgogeat B, Boinet M, Dalard F, Lissac M., Electrochemical studies of the corrosion behaviour of titanium and the Ti–6Al–4V alloy using electrochemical impedance spectroscopy. Bio-Med Mater Eng 14:323–331, (2004).

34. Parsegian VA., Molecular forces governing tight contact between cellular surfaces and substrates. J. Prosthet. Dent., 49, 838–842, (1983).

35. Nikita Zaveri, Gerald D. McEwen, Ramji Karpagavalli, Anhong Zhou. J., Biocorrosion studies of TiO_2 nanoparticle-coated Ti–6Al–4V implant in simulated . biofluids. Nanopart Res, 12:1609–1623, (2010).

36. Kasemo B, Lausmaa J, Biomaterial and implant surfaces: a surface science approach. Int J Oral Maxillofac Implants 3:247–259.1988).

37. Rana S, Rawat J, Sorensson MM, Misra RDK, Antimicrobial function of Nd3þ-doped anatase titania-coated nickel ferrite composite nanoparticles: a biomaterial system. Acta Biomater ;2:421-32, (2006).

38. Li B, Liu X, Meng F, Chang J, Ding C. Preparation and antibacterial properties of plasma sprayed nano titania/silver coatings.MaterChem. Phys; 118:99-104, (2009).

39. Necula BS, Fratila-Apachitei LE, Zaat SAJ, Apachitei I, Duszczyk J., In vitro antibacterial activity of porous TiO_2-Ag composite layers against methicilinresistant Staphylococcus aureus, Acta Biomater; 2:3573-80, (2009).

40. Ulrike Diebold, The surface science of titanium dioxide, Surface Science reports 48; 53-229, (2003).

41. U. Diebold, Structure and properties of TiO2 surfaces: a brief review, Appl. Phys. A 76, 1–7 (2002).

42. Popovic JR, Kozac LJ, National hospital discharge survey: annual summary, 199,. Vital and health statistics. National Center for Health Statistics, US Government Printing Office; (2000).

43. Gioe TJ, Killeen KK, Grimm K, Mehle S, Scheltema K., Why are total knee replacements revised? Analysis of early revision in a community knee implant registry, Clin Orthop Relat Res (428):100–6, (2004).

44. Trampuz A, Osmon DR, Hanssen AD, Steckelberg JM, Patel R., Molecular and antibiofilm approaches to prosthetic joint infection. Clin Orthop Relat Res (414):69–88, (2003).

45. Hadis Morkoç and Ümit Özg€ur, General Structure of ZnO, In: Zinc Oxide: Fundamentals, Materials and Device Technology. Wiley-VCH Verlag, (2009).

46. Fang M, Chen JH, Xu XL, Yang PH, Hildebrand HF, Antibacterial activities of inorganic agents on six bacteria associated with oral infections by two susceptibility tests, International Journal of Antimicrobial Agents 27 513–517, (2006).

47. Jones, N., B. Ray, K. T. Ranjit, and A. C. Manna, Antibacterial activity of ZnO nanoparticle suspensions on a broad spectrum of microorganisms, FEMS Microbiol. Lett. 279:71-76, 92008).

48. Liu, Y., et al. , Antibacterial activities of zinc oxide nanoparticles against Escherichia coli O157:H7. J. Appl. Microbiol. 107:1193-1201, (2009).

49. Reddy, K. M., et al., Selective toxicity of zinc oxide nanoparticles to prokaryotic and eukaryotic systems. Appl. Phys. Lett. 90:2139021-2139023, (2007).

50. Xie Y, He Y, Irwin PL, Jin T, and Shi X, Antibacterial Activity and Mechanism of Action of Zinc Oxide Nanoparticles against Campylobacter jejuni, Appl Environ Microbiol; 77(7): 2325–2331, (2011).

51. Padmavathy Nagarajan and Vijayaraghavan Rajagopalan, Enhanced bioactivity of ZnO nanoparticles—an antimicrobial study, Sci. Technol. Adv. Mater. 9 035004 (7pp), (2008).

52. Dulin F. H. and Rase D. E., Phase Equilibria in the System ZnO-TiO$_2$, The American Ceramic Society, 125-131, (1960).

53. Bartram S.F. and Slepetys R. A., Compound Formation and Crystal Structure the System ZnO-TiO$_2$, Journal of The American Ceramic Society-Bwtram and Slepetys Vol. 44, No. 10, 493-499, (1961).

54. Ohring M, Material Science of thin films, , Academic Press, (1992).

55. Alexander A. Shklyaev, Motoshi Shibata, and Masakazu Ichikawa, Instability of two-dimensional layers in the Stranski-Krastanov growth mode of Ge on Si.111, Physical Reviews B, Volume 58, Number 23, 15647-15651, (1998).

56. Arvind Baskaran, Peter Smereka, Mechanisms of Stranski-Krastanov Growth, (2011).

57. Davidse PD, Theory and practice of RF sputtering, Symposium on the Deposition Thin Films by Ion Sputtering, Vacuum/volume 17/number 3, (1966).

58. Shinoki F, Itoh A, Mechanism of rf reactive sputtering, J. Appl. Phys. 46, Number 8, 3381-84, (1975).

59. Bashar SA, PhD thesis, Study of Indium Tin Oxide (ITO) for Novel Optoelectronic Devices, (1998).

60. Dangeti Siva Rama Krishna, Yong Sun, Zhong Chen, Magnetron sputtered TiO2 films on a stainless steel substrate: Selective rutile phase formation and its tribological and anti-corrosion performance, Thin Solid Films 519 4860–4864, (2011).

61. Doolittle A, Lecture 12, Physical Vapor Deposition: Evaporation and Sputtering, ECE 6450.

62. D.C. Carter, W.D. Sproul and D.J. Christie, Effective control for Reactive Sputtering Processes, Advanced Energy Industries Inc., Vacuum and coating, 1-9 (2006).

63. Lobl, M. Huppertz, D. Mergel, Nucleation and growth in TiO2 films prepared by sputtering and evaporation, Thin Solid Films, 251, 72-79, (1994).

64. D.C. Carter, W.D. Sproul and D.J. Christie, Control of reactive sputtering processes, Thin Solid Films 491, 1 – 17, (2005).

65. Callister WD., Materials Science and Engineering, 7 ed., John Wiley and Sons Inc, (2007).

66. Li C, Furuta M, Matsuda T, Hiramatsu T, Furuta H and Hirao T, RF Power and Thermal Annealing Effect on the Properties of Zinc Oxide Films Prepared by Radio Frequency Magnetron Sputtering, Research Letters in Materials Science, (2007).

67. Hull AW, A new method of Chemcial Analysis, J. Am. Chem. Soc., 41 (8), 1168–1175, (1919).

68. Cullity BD, Elements of X-Ray Diffraction, Addison Wesley Publishing Company, (1956).

69. Basics of X-Ray Diffraction, Scintag Inc., (1999).

70. Hayat MA, Principles and techniques of scanning electron microscopy. Biological applications. Volume 1, Cambridge University Press, (2000)

71. P.J. Goodhew, J. Humphreys, R. Beanland, Electron Microscopy and Analysis, third Edition, Taylor and Francis, (2001).

72. G. Binning, C. F. Quate, Ch. Gerber. Atomic force microscope. Phys. Rev. Lett. 56 (9), 930. (1986).

73. Arantxa Vilalta Clemente, Kathrin Gloystein. Principles of Atomic Force Microscopy (AFM). Physics of Advanced Materials Winter School (2008).

74. Fischione PA, Materials Specimen Preparation for Transmission Electron Microscopy, Fischione Instruments, Inc. Export, PA USA.

75. Thomas R., A beginners guide to ICP-MS, Spectroscopy 16(4), 38-42,(2001).

76. A 30 minute guide to ICP-MS, Perkin Elmer.

77. D.Y. Kwok A.W. Neumann, Contact angle measurement and contact angle interpretation, Advances in Colloid and Interface Science Volume 81, Issue 3, 167–249, (1999)

78. Woodward RP., Contact Angle Measurements Using the Drop Shape Method, First Ten Angstroms.

79. Kokubo T., Apatite Formation of surfaces of ceramics, metals and polymers in body environment, Acta mater. Vol. 46, No. I, 2519--2527, (1998).

80. Wei Xia, Carl Lindahl, Jukka Lausma and Håkan Engqvist, Biomimetic Hydroxyapatite Deposition on Titanium Oxide Surfaces for Biomedical Application, Chapter 20, Advances in Biomimetics.

81. Jalota S, Bharduri S, Tas A., Using a synthetic body fluid (SBF) solution of 27 mM HCO_3^- to make bone substitutes more osteointegrative., Mater Sci Eng C;28:129-140, (2008).

82. Kokubo T, Kushitani H, Sakka S, Kitsugi T, Yamamuro T., Solutions able to reproduce in vivo surface-structure change in bioactive glass-ceramic A–W. J Biomed Mater Res;24:721-734, (1990).

83. Pasinli A, Yuksel M, Celik E, Sener S, Tas AC, A new approach in biomimetic synthesis of calcium phosphate coatings using lactic acid–Na lactate buffered body fluid solution. Acta Biomaterialia, 6:2282-2288, (2010).

84. Lindgren M, Astrand M, Wiklund U, Engqvist H., Investigation of boundary conditions for biomimetic HA deposition on titanium oxide surfaces, J Mater Sci Mater Med, 20(7):1401-1408, (2009).

85. DeRenzis, F.A., Schechtman, A., Stainin, Stain Technol. 48, 135–136, (1973).

86. Crouch, S., Biocompatibility testing ATP bioluminescence, Med. Device Technol. 11, 12–15, (2000.).

87. Mosmann, Tim, Rapid colorimetric assay for cellular growth and survival: application to proliferation and cytotoxicity assays, Journal of Immunological Methods 65 (1–2): 55–63, (1983).

88. Horton T, ATCC MTT Cell Proliferation Assay Instructions,MTT Cell Assay Protocol, (1994).

89. W.H. Harris, C.B. Sledge, Total hip and total knee replacements, New Engl. J. Med. 323, 801, (1990).

90. V. Stranak, H. Wulff, H. Rebl, C. Zietz, K. Arndt, R. Bogdanowicz, B. Nebe, R. Bader, A. Podbielski, Z. Hubicka, R. Hippler, Deposition of thin titanium–copper films with antimicrobial effect by advanced magnetron sputtering methods, Materials Science and Engineering C 31, 1512–1519, (2011).

91. Japanase Industrial Standard, JIS Z 2801: 2000, Antimicrobial products-Test for antimicrobial activity and efficacy Japanase Standards Association.

92. MD/105c, Method for determining efficacy of antimicrobials incorporated into manufactured articles "Film Contact Method", Add Master.

93. Industrial Microbiological Services Ltd., V 1.0, (2005).

94. M. H. Mamat, M. Z. Sahdan, S. Amizam, H. A. Rafaie, Z. Khusaimi, A. Zain Ahmed, S. Abdullah, M. Rusop, The Effect ofAnnealing Temperatures on Zinc Oxide Thin Films Properties for Electronic Devices Application, IeSE Proc. (2008).

95. Ivan Hotov'y, Andrea Pullmannov'a, Martin Predanocy, Juraj Hotov'y, Vlastimil 'Reh'a'cek, Thomas Kups, Lothar Spiess, Structural and Morphological Investigations of TiO2 Sputtered Thin Films, Journal of Electrical Engineering, Vol. 60, No.6, 354–357, (2009).

96. Ye Q , Liu PY, Tang ZF, Zhai L, Hydrophilic properties of nano-TiO$_2$ thin films deposited by RF magnetron sputtering, Vacuum 81, 627–631, (2007).

97. Weiying Zhang, Jianguo Zhao, Zhenzhong Liu, Zhaojun Liu and Zhuxi Fu, Influence of TiO2 Buffer on Structure and Optical Properties of ZnO Film on Si(100) Substrate, Materials Transactions, Vol. 51, No. 6 , 1064 to 1066, (2010).

98. C.N. Ellas, D.C. Figueira, J.H.C. Lima, R.Bothomarco, G. Solorzomo, F.C. e Silva Filho, Hydrophillic properties of titanium dental implant surfaces, , Proceeding of the Materials and Processes for Medical Devices Conference, 433-437, (2004)

99. Hench LL, Paschall HA., Direct bonding of bioactive glass ceramics to bone and muscle. J Biomed Mater Res 4:25–42 (1977).

100. LeGeros RZ, Daculsi G, Orly I, et al., Substrate surface dissolution and interfacial biological mineralization. In: The Bone–Biomaterial Interface, Davies JE (ed). University of Toronto Press,Toronto,76–88,(1991).

101. LeGeros RZ, Orly I, Gregoire M, et al., Comparative properties and in vitro reactions of HA ceramic and coralline HA. Apatite 1:229–235, (1992).

102. Kokubo T, Kushitani H, Sakka S, et al., Solutions able to reproduce in vivo surface structure changes of bioactive glass ceramic. J Biomed Mater Res 24:721–734, (1990).

103. deOliveira PT, Nanci A., Nanotexturing of titanium based surfaces upregulates expression of bone sialoprotein and osteopontin by cultured osteogenic cells. Biomaterials 25:403–413, (2004.).

104. Masaki C, Schneider GB, Zaharias R, et al., Effects of implant surface microtopography on osteoblast gene expression, Clin Oral Implants Res 16:650–656, (2005).

105. Tabanella G, Nowzari H, Slots, J., Clinical and microbiological determinants of ailing dental implants. Clin Implant Dent Relat Res 11:24–36, (2009).

106. Shi ZL, Chua PH, Neoh KG, et al., Bioactive titanium implant surfaces with bacterial inhibition and osteoblast function enhancement properties. Int J Artif Organs 31:777–785. (2008).

107. Chuo AH, LeGeros RZ, Chen Z, et al., Antibacterial effect of zinc phosphate mineralized guided bone regeneration membranes. Implant Dent 16:89–100, (2007).

108. Chen H, Ding X, Maa S, Violet and blue-green luminescence from Ti-doped ZnO films deposited by RF reactive magnetron sputterin, Superlattices and Microstructures 49, 176–182, (2011).

109. F.H. Wang, H.P. Chang, J.C. Chao, Improved properties of Ti-doped ZnO thin films by hydrogen plasma treatment, Thin Solid Films 519, 5178–5182, (2011).

110. Jeng-Lin Chung, Jyh-Chen Chen, Chung-Jen Tseng, The influence of titanium on the properties of zinc oxide films deposited by radio frequency magnetron sputtering, Applied Surface Science 254, 2615–2620, (2008).

111. Jeng-Lin Chung, Jyh-Chen Chen, Chung-Jen Tseng, Electrical and optical properties of TiO2-doped ZnO films prepared by radio-frequency magnetron sputtering, Journal of Physics and Chemistry of Solids 69, 535–539, (2008).

112. Chun-Sen Wu, Bor-Tsuen Lin, Ru-Yuan Yang, Structural and optical properties of Ti-doped ZnO thin films prepared by the cathodic vacuum arc technique with different annealing processes, Thin Solid Films 519, 5106–5109, (2011).

113. Rajaram S. Mane, Won Joo Lee, Habib M. Pathan, and Sung-Hwan Han, Nanocrystalline TiO2/ZnO Thin Films:□ Fabrication and Application to Dye-Sensitized Solar Cells, J. Phys. Chem. B, 109 (51), (2005).

Internet links

i.   http://www.wtec.org/loyola/nano/usrnd/0604.htm

ii.   cmliris.harvard.edu/assets/082.pdf

iii.   http://en.wikipedia.org/wiki/Thin_film

iv.   http://www.azom.com/article.aspx?ArticleID=1558#_What_are_PVD

v.   http://www.ajaint.com/whatis.htm

vi.   http://ia.physik.rwth-aachen.de/research/sputtering/www-sputter-eng.pdf

vii.   http://www.uccs.edu/~tchriste/courses/PHYS549/549lectures/sputter.html

viii.   http://wwwold.ece.utep.edu/research/webedl/cdte/Fabrication/index.htm

ix.   http://www.umms.sav.sk/index.php?ID=415

x.   http://en.wikipedia.org/wiki/Annealing_(metallurgy)

xi.   http://web.pdx.edu/~pmoeck/phy381/Topic5a-XRD.pdf]

xii.   http://serc.carleton.edu/research_education/geochemsheets/techniques/SEM.html

xiii.   http://www.nobelprize.org/educational/physics/microscopes/tem/index.html

xiv.   ccber.ucsb.edu

xv.   http://minerals.cr.usgs.gov/icpms/intro.html

xvi.   http://web.natur.cuni.cz/ugmnz/icplab/icpm0.html

xvii.   http://www.face-kyowa.com/en/learning/learning1.html

xviii.   http://en.wikipedia.org/wiki/MTT_assay